Endovascular Coiling and its Influence on Intra-aneurysmal Hemodynamics by Image-based Modeling

Hernán G. Morales

PhD Thesis - UPF / 2012

Thesis submitted in partial fulfillment of the requirements
for the degree of Doctor of Philosophy.

Department of Information and Communication Technologies
Universitat Pompeu Fabra

Cover design by the author showing computational fluid dynamics (CFD) simulations of an image-based aneurysm model. CFD solutions were obtained with ANSYS CFX v12 and visualizations were performed with Blender v2.6.1. Cover page shows instantaneous streamlines color-coded according to the velocity magnitude in a virtually coiled aneurysm model. Back page depicts the uncoiled CFD simulation. The influence of coils on intra-aneurysmal hemodynamics is visualized by the blockage and redirection of streamlines inside the aneurysm cavity.

Endovascular Coiling and its Influence on Intra-aneurysmal Hemodynamics by Image-based Modeling

ISBN: 978-84-615-9824-3

Director

Prof. Alejandro F. Frangi
Department of Information and Communication Technologies,
Universitat Pompeu Fabra, Barcelona, Spain.
Department of Mechanical Engineering,
University of Sheffield, Sheffield, United Kingdom.

Co-director

Dr. Ignacio Larrabide
Department of Information and Communication Technologies,
Universitat Pompeu Fabra, Barcelona, Spain.
Centro de Investigación Biomédica en Red en Bioingeniería,
Biomateriales y Nanomedicina - CIBER-BBN, Barcelona, Spain.

Review Committee:

Prof. James V. Byrne
Nuffield Department of Surgical Sciences,
University of Oxford, Oxford, United Kingdom.

Prof. Giancarlo Pennati
Structural Engineering Department,
Politecnico di Milano, Milan, Italy.

Dr. Petia Radeva
Computer Science Department & Computer Vision Center,
Universitat Autònoma de Barcelona, Barcelona, Spain.

Prof. Vicent Caselles Costa
Department of Information and Communication Technologies,
Universitat Pompeu Fabra, Barcelona,Spain (reserve).

Prof. Vicente Riambau
Department of Vascular Surgery, Hospital Clinic,
University of Barcelona, Spain (reserve).

This work was carried out in the Center for Computational Imaging and Simulation Technologies in Biomedicine (CISTIB), at the Departament de Tecnologies de la Informació i les Comunicacions at the Universitat Pompeu Fabra, Barcelona, Spain. The research leading to these thesis has received funding from the European Union Seventh Framework Programme (FP7/2007-2013) under grant agreement number 223920, VPH-NoE project and has been funded by the Industrial and Technological Development Center (CDTI) under the CENIT-CDTEAM and CENIT-cvREMOD programs, by the European Commissions project @neurIST (IST-2005-027703) and by the Catalonian Department of Innovation, Universities and Enterprise (DIUE), through the EndoTreat project (exp. VALOR2010-00064). The company ANSYS Inc. provided us free software licenses for numeric simulation of flow dynamics.

To Issis, who has crossed oceans
and lands following my madness.
Thank you.

Abstract / Resumen / Resum

Abstract:

Technological advances in medical imaging and availability of cerebral angiographies have increased the detection of asymptomatic unruptured aneurysms. Although several physiological factors, including age, gender, hemodynamics and arterial wall properties, as well as living habits, have been associated with aneurysm rupture risk and subsequent subarachnoid hemorrhage, mechanisms for which the aneurysm wall fails remain incompletely known. These uncertainties have led to increasingly consider preventive treatments as an option. Nowadays, most frequent and popular therapies for cerebral aneurysms are Clipping and Coiling. Nonetheless, it is not easy to elucidate which therapeutic option is the most suitable, feasible and reliable for a patient-specific cerebral aneurysm.

To face and overcome this challenge, computational modeling arises as a powerful tool to support clinicians, thanks to their predictive capability. In the case of cerebral aneurysms and endovascular treatments, these techniques can help by understanding how inserted coils behave and alter intra-aneurysmal hemodynamics. In this research line, the presented thesis aims to enhance the general knowledge of endovascular coiling in cerebral aneurysms and its influence on intra-aneurysmal hemodynamics. This work has contributed in the following aspects: (1) To understand endovascular coil distribution for both clinical applications and validation of computational techniques, (2) To develop and to validate a virtual coiling technique for image-based aneurysm models and (3) To investigate intra-aneurysmal hemodynamic alterations induced by coils using computational fluid dynamics simulations. The ultimate vision behind this thesis is to provide a practical tool that can be used by physicians in the diagnosis, therapeutic planning, and post-operative monitoring of patients with cerebral aneurysms treated (or suitable to be treated) with endovascular coils.

Resumen:

Los avances tecnológicos en imagen médica y la disponibilidad de angiografías cerebrales, han aumentado la detección de aneurismas no rotos y asintomáticos. Aunque varios factores fisiológicos, como la edad, el género, la hemodinámica y las propiedades de la pared arterial, así como hábitos de vida, se han asociado con el riesgo de ruptura del aneurisma y posterior hemorragia subaracnoidea, los mecanismos de falla de la pared del aneurisma permanecen sin ser completamente conocidos. Estas incertidumbres han llevado a considerar cada vez más a los tratamientos preventivos como una opción. Hoy en día, los tratamientos más frecuentes y populares para los aneurismas cerebrales son Clipping y Coiling. Sin embargo, no es fácil aclarar qué opción terapéutica es la más adecuada, viable y confiable para un aneurisma cerebral específico.

Para enfrentar y superar este reto, los modelados computacionales surgen como una herramienta poderosa para apoyar a los clínicos, gracias a su capacidad de predicción. En el caso de aneurismas cerebrales y tratamientos endovasculares, estas técnicas pueden ayudar a entender cómo se comportan los coils y como modificar la hemodinámica dentro del aneurisma. En esta línea de investigación, la tesis presentada tiene como objetivo mejorar el conocimiento general de los coils endovasculares en aneurismas cerebrales y su influencia sobre la hemodinámica intraaneurismática. Este trabajo ha contribuido en los siguientes aspectos: (1) Entender la distribución de los coils endovasculares, tanto para aplicaciones clínicas, como para validación de técnicas computacionales, (2) Desarrollar y validar una técnica de coiling virtual para modelos de aneurismas basados en imágenes e (3) Investigar las alteraciones hemodinámicas producidas por los coils utilizando simulaciones computacionales de dinámica de fluidos. La visión futura detrás de esta tesis es proporcionar una herramienta práctica que pueda ser utilizada por médicos en el diagnóstico, la planificación terapéutica y el seguimiento postoperatorio de pacientes con aneurismas tratados (o factibles de tratar) con coils endovasculares.

Resum:

Els avanços tecnològics de la imatge mèdica i la disponibilitat d'angiografies cerebrals han augmentat la detecció d'aneurismes no trencats i asintomàtics. Encara que diversos factors fisiològics, com l'edat, el gènere, l'hemodinàmica i les propietats de la paret arterial, així com hàbits de vida, s'han associat amb el risc de ruptura de l'aneurisma i posterior hemorràgia subaracnoidea, els mecanismes de falla de la paret de l'aneurisma romanen sense ser completament coneguts. Aquestes incerteses ha conduït a considerar cada vegada més als tractaments preventius com una opció. Avui en dia, els tractaments més freqüents i populars per als aneurismes cerebrals són Clipping i Coiling. No obstant això, no és fàcil aclarir quina opció terapèutica és la més adient, viable i de confiança per a un aneurisma cerebral específic.

Per enfrontar i assolir aquest desafiament, els models computacionals sorgeixen com una eina poderosa per recolzar als clínics, gràcies a la seva capacitat de predicció. En el cas d'aneurismes cerebrals i tractaments endovasculars, aquestes tècniques poden ajudar a entendre com es comporten els coils i com modificar l'hemodinàmica a l'interior de l'aneurisma. En aquesta línia de recerca, la tesi presentada té com objectiu millorar el coneixement general dels coils endovasculars en aneurismes cerebrals i la seva influència sobre l'hemodinàmica intraaneurismàtica. Aquest treball ha contribut als segents aspectes: (1) Entendre la distribució dels coils endovasculars, tant per a aplicacions clíniques, com per a propòsits de va-lidació de tècniques computacionals, (2) Desenvolupar i validar una tècnica de coiling virtual per a models d'aneurismes basats en imatges, i (3) Investigar les alteracions hemodinàmiques produïdes per els coils utilitzant simulacions computacionals de dinàmica de fluids. La visió futura al darrere de aquesta tesi és proporcionar una eina pràctica que pugui ser utilitzada per metges en el diagnòstic, la planificació terapèutica i el seguiment postoperatori de pacients amb aneurismes tractats (o factibles de tractar) amb coils endovasculars.

Contents

Abstract / Resumen / Resum **i**

Acronyms **xiii**

Preface **xv**

1 General Introduction **1**
1.1 Cerebral Aneurysms . . . 3
1.2 Diagnostics of Aneurysms and SAH . . . 4
1.2.1 Clinical Symptoms of SAH: . . . 4
1.2.2 Medical Imaging . . . 5
1.3 Treatments . . . 6
1.3.1 Exovascular Treatments . . . 6
1.3.2 Endovascular Treatments . . . 7
1.4 The Importance of Hemodynamics . . . 9
1.5 Computational Approach . . . 9
1.5.1 From Medical Images to Computational Models . . . 10
1.5.2 Predicting Treatment Outcome . . . 11
1.6 Aim and Objectives of this Thesis . . . 14
1.7 Overview of the Thesis . . . 14

2 Insight into Endovascular Coiling **17**
2.1 Introduction . . . 20
2.2 Material and Method . . . 20
2.2.1 Aneurysm Creation and Embolization Procedure . . . 20
2.2.2 Tissue-Processing Procedure . . . 21
2.2.3 Image Processing . . . 21
2.3 Results . . . 23
2.3.1 Qualitative Evaluation . . . 23
2.3.2 Quantitative Evaluation . . . 23
2.3.3 Statistical Evaluation . . . 24
2.3.4 Intra- and Inter Observer Variability . . . 24
2.4 Discussion . . . 25
2.5 Conclusions . . . 27

3 The Virtual Coiling Technique **29**
3.1 Introduction . . . 32
3.2 Method: Virtual Coiling Technique . . . 32
3.2.1 Dynamic Path Planning Algorithm . . . 33
3.2.2 Algorithm Construction . . . 35
3.2.3 Sensitivity Analysis on Idealized Models . . . 35
3.2.4 Experiments on Image-Based Models . . . 38
3.3 Validation . . . 40
3.3.1 Clinical Assessment . . . 40
3.3.2 Validation of Intra-aneurysmal Coil Distribution . . . 42
3.4 Hemodynamics after Coiling . . . 48
3.4.1 Material . . . 48
3.4.2 Method . . . 48
3.4.3 Results . . . 49
3.5 Discussion . . . 50
3.6 Conclusions . . . 53

4 Validating Hemodynamic Modeling **55**
4.1 Introduction . . . 58
4.2 Material . . . 58
4.3 Method . . . 58
4.3.1 Vascular Models . . . 59
4.3.2 Computational Fluid Dynamics . . . 60
4.4 Results . . . 61
4.5 Discussion . . . 61
4.6 Conclusions . . . 62

5 Coil Configuration and Packing Density **63**
5.1 Introduction . . . 66
5.2 Material . . . 67
5.3 Method . . . 67
5.3.1 Virtual Coiling . . . 67
5.3.2 Hemodynamic Modeling . . . 67
5.3.3 Statistical Evaluation . . . 69
5.4 Results . . . 69
5.4.1 Qualitative Findings . . . 69
5.4.2 Quantitative Findings . . . 69
5.4.3 Analysis of Statistical Data . . . 71
5.5 Discussion . . . 72
5.6 Conclusions . . . 76

6 Conclusions and Outlook **77**
6.1 Conclusions . . . 79
6.2 Outlook and Future Work . . . 79
6.2.1 Where should we aim? . . . 81

Publications During PhD Thesis **xvii**
International Journal xvii
Book Chapter xvii
Peer-reviewed International Conference xvii
International Conference Abstract xviii

Curriculum Vitae **xxi**

List of Figures

1.1 Two types of cerebral aneurysm morphologies 3
1.2 Typical locations of cerebral aneurysms 4
1.3 Image modalities to visualize cerebral aneurysms 5
1.4 Aneurysm regions 6
1.5 Representation of endovascular treatments 8

2.1 Photomicrographs showing aneurysms with removed coils 21
2.2 Processing of a histological image 22
2.3 Color maps of normalized coil densities 23
2.4 Peripheral-core density ratio versus total in-slice coil density 24
2.5 Boxplots of normalized densities per region of histological images . 25

3.1 Schematic description of potential fields 35
3.2 Tests of the coiling technique on a sphere 37
3.3 Tests of the coiling technique on a sphere with bleb 38
3.4 Coiling technique on sixteen image-based aneurysm models 40
3.5 Comparison between DSA and angiographic-like images 43
3.6 Six coil configurations applied on case P3 44
3.7 Histology-like image generation and processing 45
3.8 Periphery-core density ratio versus total in-slice coil density 46
3.9 Boxplots of coil densities per region of aneurysm models 47
3.10 Spatial averaged WSS and blood flow velocity magnitude 49
3.11 Contrast concentration inside the aneurysm 50

4.1 Pipeline for CFD setup 59
4.2 Coiled aneurysm 60
4.3 DSA image with the control regions for TIC measurements 61
4.4 Visualization of DSA sequence and virtual angiography images . . 62

5.1 Results of virtual coiling in three cases 68
5.2 Blood flow velocity magnitudes for an aneurysm-cross section . . . 70
5.3 WSS distributions for the untreated and several treated models . . 70
5.4 Time-averaged mean flow velocity magnitude and WSS 71
5.5 Variation of aneurysm areas with low and high WSS 72

List of Tables

1.1 Virtual coiling techniques 12
1.2 Virtual stenting techniques 13

2.1 Intra- and inter-observer variations of manual image processing . . 25

3.1 Sensitivity analysis of virtual coil parameters 37
3.2 Tests on image-based aneurysm models 39
3.3 Summary of the real treatment information 41
3.4 Comparison of the theoretical and the virtual packing density . . . 42

5.1 Design parameters of virtual coiling experiments 68
5.2 p-values of ANOVA tests 73

Acronyms

3D	Three-dimensional
3DRA	Three-dimensional rotational angiography
ACom	Anterior communicating artery
ANOVA	Analysis of variance
CFD	Computational fluid dynamics
CTA	Computed tomography angiography
DSA	Digital subtraction angiography
FEM	Finite element method
ICA	Internal carotid artery
MCA	Middle cerebral artery
MRA	Magnetic resonance angiography
PCom	Posterior communicating artery
PICA	Posterior inferior cerebellar artery
PIV	Particle image velocimetry
SAH	Subarachnoid hemorrhage
TIC	Time-intensity curve
WSS	Wall shear stress

Preface

This thesis and my life as PhD student would not be the same without the support and contribution of several people.

First, I would like to thank Dr. Alejandro F. Frangi, who created the research environment CISTIB, in which I grew up as scientist, advised me during my PhD and financially supported my studies. To Ignacio Larrabide, who supervised my day-to-day work. Thanks to be there as a friend and colleague when things were difficult.

I appreciate the support of the co-authors of my projects during this PhD, Ignacio Larrabide, Arjan J. Geers, Minsuok Kim, Maria-Cruz Villa-Uriol, Elio E. Vivas, Juan M. Macho, Luis San Roman, Jordi Blasco, David D. Kallmes and Daying Dai, with whom I had constructive discussions and learned how to do research. Thanks to the PMO and SSD teams, and to my past and present colleagues at CISTIB. I would love to name and acknowledge all of you in particular but the list is huge.

Then to my friend Minsuok Kim for his advices about research and life. Thanks to my Dutch friends, Arjan and Corné, and to the members of the four guys, Hrvoje, Tristan and Rubén, who made my stay enjoyable.

Special thanks to my Chilean non-blood family Catalina and Matías, and my exceptional friends Chiara, Martha, Valeria and Nicolas, whose shoulders were always there to support me and my beloved's.

I am grateful to my family in-law Rosa, Ricardo, Dafne and Felipe, I will never have enough words to thanks your support, and to be with us in this adventure away from home. To Beatrice and Hector, whose eyes, cares and generosity were with us since first day in foreign lands.

My infinite gratitude to my family in Chile. To my father for his unconditional support and friendship and to be proud of me. To Nelson for his advices and Carolina for her love and smiles. I thank my mother for her life lessons and love. I know you will be proud of me.

Finally, I am tremendously grateful to my wife Issis, who encouraged and unconditionally supported me in this adventure even before starting. You know that all this work was done with your selfless effort and love.

1

General Introduction

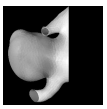

1.1 Cerebral Aneurysms

Cerebral aneurysms are a cardiovascular disease consisting in an abnormal deformation of the arterial wall. According to their morphology, cerebral aneurysms can be classified intro: sacculars, which are pouch- or balloon-like protrusions that arise from artery (Fig. 1.1a); fusiforms which are vessel wall dilatations that do not lead to formation of a separate saccular pouch (Fig. 1.1b); dolichoectasias that are tortuous, elongated, and some times dilated vessel segments; or dissecting which are originated from acute dissection or tearing of the arterial wall layers.

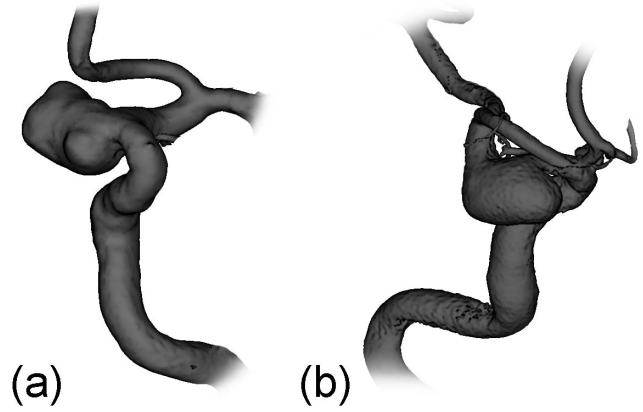

Figure 1.1: Two types of cerebral aneurysm morphologies. (a) Saccular aneurysm. (b) Fusiform aneurysm.

Cerebral aneurysms are mostly found at or in proximal arterial bifurcations, in areas where arterial walls are weak [1]. A common place in the vascular system where cerebral aneurysms could form is the Circle of Willis, which is located at the skull base and irrigates blood to the brain (Fig. 1.2).

It has been estimated that around 2% of human population harbors cerebral aneurysms [2]. This estimation is based on angiography studies and prospective autopsy series. Many of those aneurysms never rupture during lifetime of their carriers (between 50% and 80% [1]). However, an spontaneous aneurysm rupture is the main cause (in 85%) of the non-traumatic subarachnoid hemorrhage (SAH) [3], which is fatal between 25% and 50% of the times [3, 4]. Moreover, aneurysm can rupture directly to the brain parenchyma causing intracerebral hemorrhage, or through it towards the lateral ventricles, causing intraventricular hemorrhage [5,6].

Aneurysm rupture produces a temporal increase in the intracranial pressure due to the blood leakage in the subarachnoid space. The blood leakage may cause impact injury on the brain parenchyma [7] and can obstruct and stagnate the physiological circulation of the cerebrospinal fluid, producing hydrocephalia [3]. Moreover after one or two weeks, SAH can also induce vasospasm on the affected arteries that might lead to critical ischemia in the supplied brain regions [3].

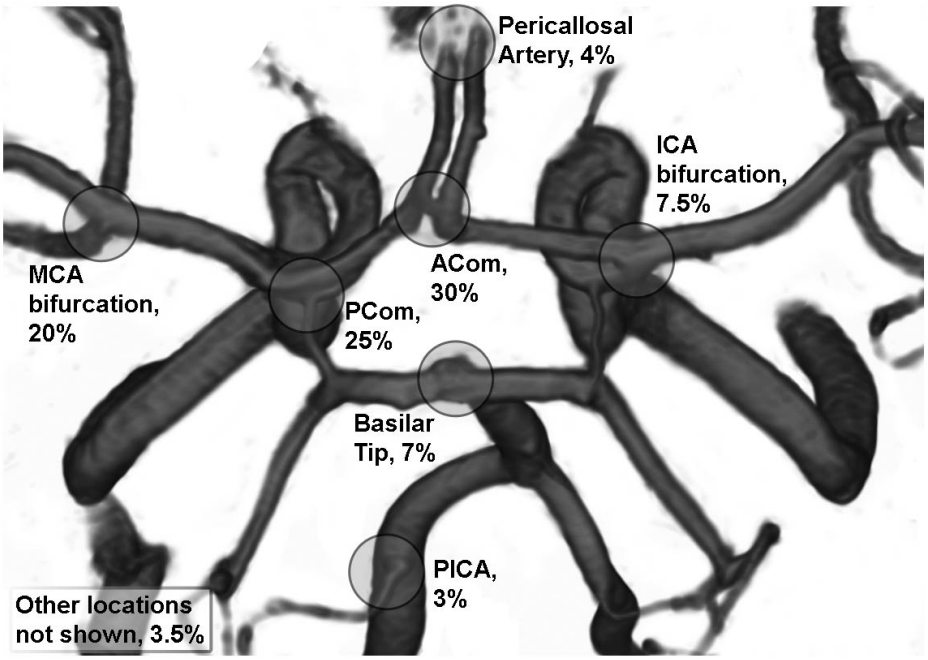

Figure 1.2: Cerebral vasculature and typical locations of aneurysms. Percentages indicate the incidence of cerebral aneurysms [1]. ICA: internal carotid artery. MCA: middle cerebral artery. Pica: posterior inferior cerebellar artery. PCom: posterior communicating artery. ACom: anterior communicating artery.

1.2 Diagnostics of Aneurysms and SAH

There are two main ways to diagnose cerebral aneurysms and SAH: by symptoms or by imaging.

1.2.1 Clinical Symptoms of SAH:

The most common symptom of SAH is a sudden explosive and constant headache, which has been described by the affected as the worst in his/her lifetime. If this headache is developed in seconds, then the SAH is normally attributed to an aneurysm rupture. This unusual and severe headache is often followed by a decrease in consciousness and other neurological symptoms, such as paresis, vomiting or neck stiffness [3, 6]. Some cases are almost symptom free or with a minor headache, and can be misdiagnosed. Nonetheless, the most unfortunate cases are those manifesting a sudden death.

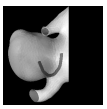

1.2.2 Medical Imaging

Three types of imaging modalities are commonly used for cerebral angiographic diagnostics. Depending on the aneurysm stage as well as the purpose, accuracy and cost of the modality, a cerebral aneurysm can be either diagnosed or monitored with these modalities:

Magnetic Resonance Angiography (MRA): It is the least invasive imaging modality of cerebral angiography. MRA produces a magnetic field and a frequency radio wave to acquire computerized images. With MRA, it is possible to visualize rough flow patterns with low temporal and spatial resolution, which may produce false negative findings. It is used for diagnosis, specially for SAH, and to monitor the patient after treatment.

Computed Tomography Angiography (CTA): This modality uses a special X-ray equipment to visualize an iodinated contrast material, inserted through the peripheral vein system of the patient. CTA is frequently used for diagnoses and gives more precise anatomical detail of blood vessels than MRA. The presence of bones in the CTA images produces problems for image post-processing. However, this feature is beneficial for surgical planning.

Digital Subtraction Angiography (DSA): This modality is considered as the gold-standard angiography for aneurysm detection and visualization due to its ample temporal and spatial resolution [1]. It is used for diagnosis and support of endovascular treatments. Moreover, it is more reliable than CTA to find small aneurysms (<5 mm) [8]. However, DSA is the most invasive modality since a contrast agent is injected in the arterial blood circulation and required a small dose of ionizing radiation (X-rays).

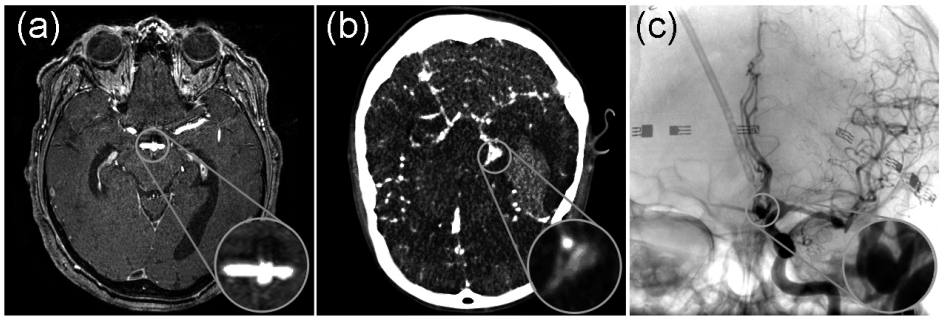

Figure 1.3: Image modalities to visualize cerebral aneurysms. (a) MRA, (b) CTA. (c) DSA. Aneurysm location was amplified to enhance the visualization.

1.3 Treatments

Once a cerebral aneurysm is diagnosed, the next step is to decide whether or not it has to be treated. The aneurysm will be treated if its rupture risk is higher than the risk of treatment. Nonetheless, there is not a clear and strict guidance for clinicians that accurately assesses both risks.

To evaluate aneurysm rupture risk, several factors are taken into account including: patient age, gender, living habits, tendency for multiple aneurysms, family history carrying aneurysms, hemodynamics, aneurysm morphological descriptors and location, among others [9,10]. Moreover, aneurysms previously ruptured, have higher change of rebleeding with an even more often fatal outcome than the first SAH [9, 11], and thereby, their treatment is unquestionable.

The risk of aneurysm treatment depends on the expertise of the clinician and the selected approach. All treatment have an associated risk of mortality and morbidity, both during intervention and at short/long-term conditions, even though treatments have been developed as minimally invasive, safest and reliable as possible.

If the decision is to treat, no matter the selected therapy, the common goal of all aneurysm therapies is to prevent SAH by exclusion of the aneurysm from blood circulation. Aneurysm exclusion can be performed through exovascular or endovascular techniques. Most common and popular treatments are clipping and coiling, which have been extensively compared and evaluated [9, 12–15].

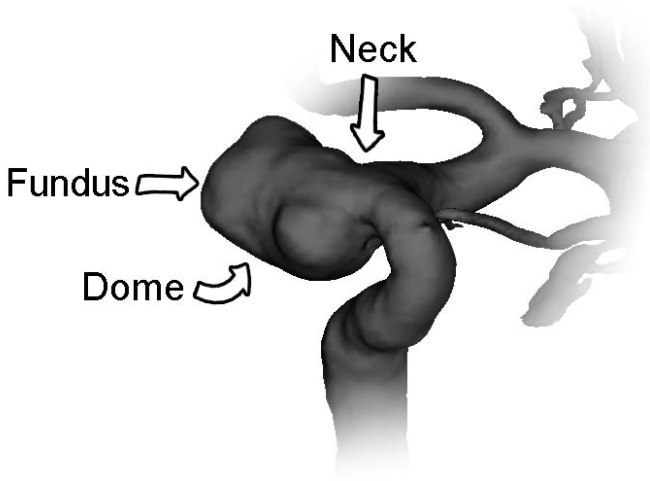

Figure 1.4: Aneurysm regions.

1.3.1 Exovascular Treatments

Exovascular approaches access the aneurysm region through a craniotomy, i. e. removal of a skull section. Afterwards, brain tissue is spread to have visual and

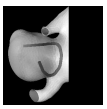

tactile access to the aneurysm and surrounding arteries. After surgery, the bone is secured in its original place, and the wound is closed. Exovascular treatments require longer time-recovery and hospitalization, and are more invasive than endovascular approaches due to the craniotomy. Nevertheless, their have been associated with a higher long-term efficacy compared to endovascular treatments [9, 12].

Clipping: the Classical Approach

Clipping is the traditional treatment for cerebral aneurysms. It has been worldwide used for more than 50 years [9]. It consists in the placement of a tiny metal clip across the aneurysm neck, which is the zone that divides the aneurysm from its parent artery (Fig. 1.4). Mortality and morbidity risk rates during clipping are 2.8% and 10.9%, respectively [16]. If an aneurysm is not completely clipped, meaning that a remnant neck is left, a new aneurysm could arise from the neck region and bleed. It has been estimated that around 5% of the clipped aneurysm have a remnant neck [17].

Other Exovascular Treatments:

Although clipping is the most important treatment for cerebral aneurysms, there are other exovascular techniques for otherwise incurable cases.

Trapping: It is the sacrifice of the aneurysm feeding arteries by microsurgical ligation [18]. The ligation may need an adequate by-pass to warranty blood supply to the brain regions downstream the ligation.

Wrapping: It is the reinforcement of the aneurysm wall by muscle fascia or fat grafts wrapped around it [19]. Wrapping is performed in cases in which the aneurysm could no be completely isolated from circulation.

1.3.2 Endovascular Treatments

Endovascular treatments are so called minimally invasive when compared to exovascular ones. They consist in the deployment of biocompatible devices aiming to completely block and redirect the flow inside the aneurysm by triggering flow stagnation, thrombogenesis inside the aneurysm and endothelialization of the aneurysm neck [12, 13, 20–22]. To deploy the devices, a X-ray guided microcatheter is used, often from the femoral artery to the aneurysm location.

Coiling

Coiling is the most common and popular endovascular treatment, introduced by Dr. Guglielmi in 1990 [23]. It consists in a partial filling of the aneurysm cavity by the insertion of small and thin biocompatible metal wires (Fig. 1.5a). Compared to clipping, it has been accepted with better outcomes [13], and it is effective for prevention of early recurrence of bleeding [24]. Furthermore, coiling allows to

treat aneurysms that were considerable inoperable with the traditional surgery and carries lower risk of procedural complications (1% and 4% of mortality and morbidity, respectively [9]). Additionally, coiling reduces hospital stay, and patients recover faster than through clipping [13, 20, 21, 25].

In spite of its benefits, the most important drawback of endovascular coiling is aneurysm recanalization, which means reopening of aneurysmal lumen. Aneurysm recanalization increases the risk of delayed bleeding and SAH. It has been reported that around 15% and 25% of the coiled aneurysms recanalize and require re-treatment [22, 26]. Recanalization is caused by aneurysm regrowth or coil compaction [22, 27, 28], which have been associated with hemodynamic forces acting on both aneurysm wall and coils over time [1, 20].

Stent-assisted coiling: Wide-neck cerebral aneurysms are challenging for coiling since the devices might migrate and compromise the parent artery. To overcome migration, coils can be supported by the deployment of a high-porosity stent in the parent artery [29]. This stent acts as an intraluminal scaffold, reducing the risk of coil migration (Fig. 1.5b). This technique was adapted from the balloon-remodeling technique [30] and was available only after stents were sufficiently flexible to navigate through the tortuous cerebral vasculature.

Flow Diverters

Flow diverters are low-porosity stents deployed in the aneurysm parent artery (Fig. 1.5c). They are meant to redirect the blood circulation and to induce flow cessation inside the aneurysm. Although it is a relatively new treatment (2001), flow diverters have become a promising alternative to coils. They are applied in aneurysms that are not suitable for coiling, such as fusiform or wide-neck [31, 32]. Another advantages is that flow diverters do not produce mass effect symptoms. However, since this therapy is relatively new, its outcomes in humans are still controversial [33]. The results of ongoing studies may resolve whether flow diverters can be a reliable alternative for treating aneurysms [31].

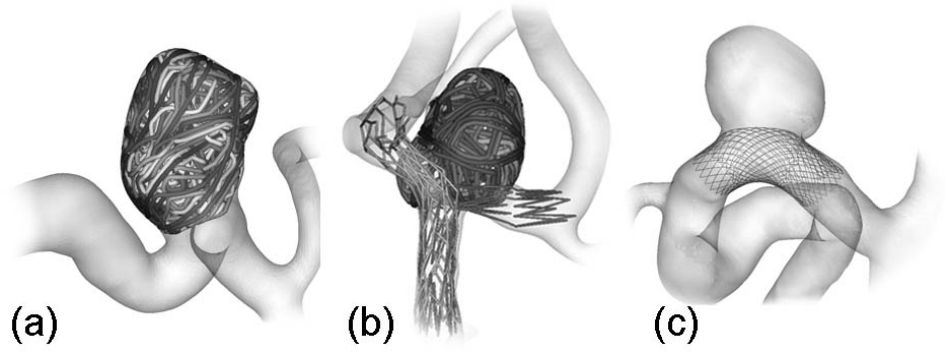

Figure 1.5: Representation of endovascular treatments for cerebral aneurysms. (a) Endovascular coiling, (b) Stent-assisted coiling, (c) Flow diverter stent.

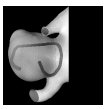

Other Endovascular Treatments:

Besides coils and flow diverters, which nowadays have most of the attention and technological development, there are other endovascular alternatives. Two examples are cited here:

Liquid Embolic Agents: It is the filling of the the aneurysm cavity by injecting a liquid solution that solidifies afterwards. The catheter is located inside the aneurysm and before injection, an inflated balloon is placed at the parent artery to completely seal the aneurysm cavity. Although liquid injection has better aneurysm conformability than coiling, it has been associated with difficulties during procedure including aneurysm rupture, parent vessel compromise and leakage during injection [29].

The Woven EndoBridge Recently, a new endovascular device, called Woven EndoBridge, has been proposed [34]. The Woven EndoBridge is a ellipsoid braided-wire embolization device designed to provide flow disruption along the aneurysm neck. Currently, it is under evaluation using in vivo aneurysm models.

1.4 The Importance of Hemodynamics

Hemodynamics plays a key role in blood rheology and vascular remodeling [35, 36], and it influences the intravascular coagulation process [37]. In the case of cerebral aneurysms, hemodynamics has been associated with aneurysm genesis [1], aneurysm wall response, inflammation and muscle cell degeneration, and to the endothelial cell alignment and disorder [38].

For treated aneurysms, specially those through endovascular means, hemodynamics is crucial since determines the success (or failure) of the therapy by triggering (or not) intra-aneurysmal thrombosis. Moreover in case of endovascular coiling, pulsatile blood flow can compress and compact coils within the aneurysm over time [1, 20].

To study such postoperative hemodynamics, several approaches have been used, including ex- and in-vivo experiments, as well as in-vitro and in-silico models through computational fluid dynamics (CFD).

1.5 Computational Approach

CFD techniques provide a third approach to understand the physics of flow dynamics after pure theory and experiments. In particular, CFD has been applied to investigate hemodynamics in cerebral vasculature. A variety of reasons can be cited to use CFD either to reconstruct or to predict a physical situation under assumed or measured boundary conditions:

- *Predicting performance*: The ability to test a new prototype of an endovascular device before manufacturing.

- *Cost of experiments*: CFD simulations are cheaper in terms of time and instrumentation than experiments with in-vivo or in-vitro models.

- *Control*: CFD simulations offer full control of their experimental setup (fluid properties, boundary conditions, etc.).

- *Impossibility of experiments by other means*: To test an endovascular device (or several devices) in a patient without endangering his/her life.

- *Insight*: CFD offers much higher temporal and spatial resolutions compared to experiments with imaging or measuring devices.

- *Enhanced visualization*: The higher resolution of CFD simulations compared to experiments provides enhanced visualizations to understand the involved phenomena.

- *Computer speed and Memory*: The development of new technologies increases computational speed and memory capacity, facilitating CFD calculations.

- *Portability*: CFD solvers generate digital data, which is easy to transport and transfer.

1.5.1 From Medical Images to Computational Models

To define a CFD simulation, two elements are essential: the geometry and boundary conditions. In the case of hemodynamic simulation in image-based models a pipeline, starting from medical images to personalized hemodynamic assessment, was defined in 2005 [39]. Nowadays, this pipeline has been extended to include morphological, morphodynamics, hemodynamics and structural analyses to extract image-based models and the information from which diagnostic and prognostic descriptors can be obtained [40]. This pipeline is briefly explained here:

Image Segmentation

After image acquisition of the region of interest, it is necessary to subtract a meaningful representation of the aneurysm and surrounding arteries. This process is called segmentation and consists in the assignment of labels at each image pixel to split it into coherent 'objects'. Some computed properties that can determine these objects are the color, intensity or texture of the pixels. In the medical image context, these object are typically lines or curves, which define boundaries of organs, arteries or bones in the image. There are three main areas of practical applications for image segmentation: (1) Diagnosis by identifying sclerosis lesions or tumors for example; (2) Treatment by monitoring the images; and (3) Visualization for surgical planning, simulation, teaching, and research for example.

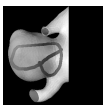

Volumetric Mesh Generation

Once the geometry is defined, either by an idealized model or after segmentation of medical images, it is necessary to discretize the working domain by computing a volumetric mesh. This mesh is used to solve the governing equations of fluid flow, usually called Navier-Stoke equations.

Idealized models are easier to mesh in general, since structured regular grids can be used. On contrary, image-based anatomies require unstructured meshes, which are often conformed by tetrahedral elements.

Computational Fluid Dynamic (CFD) Simulations

CFD is the use of numerical methods and algorithms to solve and analyze problems that involve fluid flows. CFD solves the Navier-Stokes equations on the volumetric mesh previously generated by using discretization methods. Most common methods that solve Navier-Stokes equations are finite volumes, finite elements and finite differences methods [41]. In computational simulations of the hemodynamics in cerebral vasculature, the Navier-Stokes equations assume blood as an incompressible fluid in a transient laminar flow regime, as well as adiabatic without energy transfer. These conditions make the mathematical formulation of the equations as follows:

Mass conservation equation.

$$\nabla \cdot v = 0, \tag{1.1}$$

and Momentum conservation equation

$$\rho(\frac{\partial v}{\partial t} + v \cdot \nabla v) = -\nabla p + \nabla \mu \cdot \nabla v, \tag{1.2}$$

where v and p are the unknowns velocity and pressure fields respectively. The density ρ is constant and the dynamic viscosity, μ, might vary depending on the imposed viscous model. The time is represented by t.

Cerebral arteries are generally assumed as rigid walls with no-slip boundary condition. This assumption is based on that the arterial dilatation is very small compared to its diameter; they are stiffer than other vessels closer to the heart, and that hemodynamics is strongly driven by vascular morphology [39]. Outlet boundary conditions are usually set with pressure values, while flow rates or velocity conditions are imposed at inlets. These boundary conditions can be derived from studies that measure the physiological blood flow [42], one-dimensional models [43] or can be taken from the patient itself, which occurs in quite unique situations.

1.5.2 Predicting Treatment Outcome

One of the big advantages of CFD simulations is the capability to test endovascular devices and to predict the postoperative hemodynamics without risking patient's life. In the case of cardiovascular interventions of cerebral aneurysms, stenting and coiling have been computationally modeled during last decade. Tables 1.1 and 1.2 summarize publications that developed computational techniques for these two endovascular therapies, without considering the contributions of this thesis.

Table 1.1: Publications reporting virtual coiling techniques to treat cerebral aneurysm models.

Authors/Year	Aneurysm model	Coil models	Hemodynamic assessment	Purpose	Validated
Groden et al. [44] / 2001	Idealized	Porous medium	Yes	To evaluate the effect of different percentages of inserted coils on intra-aneurysmal hemodynamics	No
Jou et al. [45] / 2004	Idealized	Porous medium	Yes	To predict hemodynamic forces acting on coils	No
Byun et al. [46] / 2004	Idealized	Spheres	Yes	To investigate the influence of coils location on intra-aneurysmal hemodynamics	No
Narracott et al. [47] / 2005	Idealized	Tubes	Yes	To evaluate a coagulation model in coiled aneurysms	No
Cebral et al. [48] / 2005	Image-based	Randomly generated arc segments	Yes	To show a meshing technique and CFD simulations in complex geometries	No
Cha et al. [49] / 2007	Idealize	Porous medium	Yes	To evaluate the influence of permeability in porous models of coiled aneurysms	No
Kakalis et al. [50] / 2008	Image-based	Porous medium	Yes	To propose a novel technique of coil simulation using a porous medium model	No
Dequidt et al. [51] / 2008	Idealized	Explicit physic-based	No	To show an interactive simulation of coil embolization	Yes, under idealized conditions
Schirmer et al. [52] / 2010	Idealized	Idealized helical coil	Yes	To investigate the influence of coil framing orientation on intra-aneurysm hemodynamics	No
Wei et al. [53] / 2011	Image-based	Explicit [50]	Yes	To show an interactive blood-coil simulation in real-time	No

Table 1.2: Some publications reporting virtual stenting techniques to treat cerebral aneurysm models. PIV: particle image velocimetry. FEM: finite element method

Authors/Year	Aneurysm model	Stent deployment	Hemodynamic assessment	Purpose	Validated
Stuhne and Steinman [54] / 2004	Idealized	Manual	Yes	To evaluate CFD mesh requirements	No
Otha et al. [55] / 2005	2D, Idealized	Manual	Yes	To study the influence of stent on Non-Newtonian fluid flow	No
Kim et al. [56] / 2007	Image-based	Manual	Yes	To study the influence of stent design on intra-aneurysmal hemodynamics	No
Liou and Li [57] / 2008	Idealized	Manual	Yes	To study the effect of stent porosity on intra-aneurysmal hemodynamics	Yes, using PIV
Appanaboyina et al. [58] / 2009	Image-based	Automatic	Yes	To describe a virtual stenting technique and to study CFD challenges	No
Fu et al. [59] / 2010	Image-based	Manual	Yes	To study the influence of five stent designs on intra-aneurysmal hemodynamics	No
Larrabide et al. [60] / 2010	Image-based	Automatic	No	To describe a virtual stenting technique	Yes, using CFD
Austburger et al. [61] / 2011	Image-based	Manual	Yes	Modeling stents as porous medium	No
Bernardini et al. [62] / 2011	Idealized	Automatic [60] and using FEM	Yes	To evaluate different stent deployment techniques	No
Babiker et al. [63] / 2012	Image-based	Manual	Yes	To study the influence of stent configuration on intra-aneurysmal hemodynamics	No

1.6 Aim and Objectives of this Thesis

This thesis is framed in the context of endovascular treatments of cerebral aneurysm and their influence on intravascular hemodynamics. The overall aim of this thesis was to enhance the general knowledge of endovascular coiling in cerebral aneurysms and its influence on intra-aneurysmal hemodynamics by clinical and computational means. On the clinical side, the analysis of coil density and distribution inside the aneurysm cavity, as well as the exploration of uncertainties about hemodynamic alterations induced by coils were done. On the technical side, the development and validation of a methodology to explicitly model endovascular coils and CFD simulations in complex geometries were tackled. Moreover, the ultimate goal and vision behind this thesis was to make use of the predictive capability and possibility to perform experiments of computational techniques to support physicians in their decision-making during planning and treatment without risking the patient's life.

Concretely, this aim has been transcribed in following objectives:

- To understand endovascular coil distribution for both clinical applications and validation of computational techniques,
- To develop and to validate a virtual coiling technique for image-based aneurysm models,
- To investigate intra-aneurysmal hemodynamic alterations induced by coils using CFD simulations.

1.7 Overview of the Thesis

In this thesis, geometrical features of endovascular coils were obtained by observing and measuring the devices and their complex structure after insertion. These observations allow us to develop and to validate a virtual coiling technique for image-based aneurysm models. Finally, CFD simulations were performed to show a practical application and potential capabilities of the developed computational techniques in clinical procedures. This overview is explained in four chapters:

Chapter 2 presents observations and the quantitative analysis of coil shape, density and distribution inside real aneurysms. This chapter enhances the understanding of the intra-aneurysmal coil structure, and provides data for validation of computational techniques.

Afterwards, chapter 3 introduces the development of a virtual coiling technique for treating aneurysm models. A parametric study of the technique was performed on both idealized and image-based aneurysm models. Then, the virtual coiling technique was validated in two ways: through a clinical perspective and by geometrical features of coil structure. CFD simulations were performed to show a practical application of the technique.

To demonstrate that the intravascular hemodynamics is properly captured by the computational modeling, chapter 4 introduces the validation of a CFD simulation in a coiled aneurysm. The geometry and flow boundary conditions were

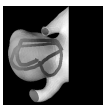

taken from patient images. The validation was done by comparing the time-intensity curves extracted from a simulated bolus injection and from a DSA image sequence.

Finally, chapter 5 presents a clinical application of the virtual coiling technique for hemodynamic assessment. In this chapter, one concrete relevant question was investigated, How do coil configuration and packing density influence intra-aneurysmal hemodynamics?

Each chapter is self-contained and their contents are based on journal or conference publications, either in accepted or submitted status. Thereby, some concepts might be repeated and reformulated according to the specific and particular interests of each chapter.

2

Insight into Endovascular Coiling

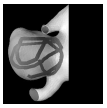

Endovascular coiling is often performed first by placing coils along the aneurysm wall to create a frame and then by filling up the aneurysm core. However, little attention has been paid to quantify this filling strategy and to see how it changes for different packing densities. The purpose of this chapter is to analyze and quantify endovascular coil distribution inside aneurysms based on serial histological images of experimental aneurysms.

Seventeen histological images from ten elastase-induced saccular aneurysms in rabbits treated with coils were studied. In-slice coil density, defined as the area taken up by coil winds, was calculated on each histological image. Images were analyzed by partitioning the aneurysm along its longitudinal and radial axis. Coil distribution was quantified by measuring and comparing the in-slice coil density of each partition.

Mean total in-slice coil density was 22.0% 6.2% (range 10.1% to 30.2%). The density was non-significantly different (p=0. 465) along the longitudinal axis. A significant difference (p <0.001) between peripheral and core densities was found. Additionally, peripheral-core density ratio was observed to be inversely proportional to the total in-slice coil density (R^2=0.57, p <0.001). This ratio was near unity for high in-slice coil density (around 30%).

Our findings demonstrate and confirm that coils tend to be located near the aneurysm periphery when few are inserted. However, when more coils are added, the radial distribution becomes more homogeneous. Coils are homogeneously distributed along the longitudinal axis.

The content of this chapter is adapted from the following publication:

H.G. Morales, I. Larrabide, A.J. Geers, D. Dai, D.F. Kallmes, A.F. Frangi. Analysis and Quantification of Endovascular Coils Distribution Inside Saccular Aneurysms Using Histological Images. Journal of NeuroInterventional Surgery. *In press.* 2012.

2.1 Introduction

Endovascular coiling is often performed first by placing coils along the aneurysm wall to create a frame for succeeding coils that fill the aneurysm core [64–68]. This aneurysm filling approach from the aneurysm periphery to its core is called by some clinicians as 'cocooning' occlusion technique [64]. Although this filling approach is a common clinical practice, little attention has been paid to corroborate the actual distribution of inserted coils, but most importantly, to quantify it and to see how it changes when different amount of coils are added.

The importance of studying and understanding coil distribution has to do with the post-treatment hemodynamics inside the aneurysm and ultimately in the treatment success. Previous studies reported that the hemodynamic changes after endovascular coiling depend on coil distribution inside the aneurysm [46, 52, 69, 70]. Moreover, computational models of fluid flow with coils, which can predict the post-treatment hemodynamics, require this information to properly and accurately model the presence of the devices [49, 50, 71].

The use of current clinical imaging techniques, such as magnetic resonance, computer tomography or digital subtracted angiography, is limited to study coil distribution. These modalities are only used to evaluate the level of aneurysm occlusion [25], but cannot discriminate the location of individual coils inside the aneurysm. However, histological images of coiled aneurysms can provide this information. The use of induced aneurysms in animals is a feasible option to obtain such images, since they overcome the difficulties of having access to ex-vivo human aneurysm samples and, when adequately processed, distortion or destruction of the sliced tissue can be prevented [72–74]. Additionally, induced aneurysms in rabbits are similar in morphology and hemodynamic conditions to saccular cerebral aneurysms in humans, which allow us to extrapolate our findings to human aneurysm cases [75].

The purpose of the chapter was to analyze and quantify coil distribution inside aneurysms using histological images of experimental coiled aneurysms. For this evaluation, the aneurysm cavity was partitioned in the longitudinal and radial orientation.

2.2 Material and Method

2.2.1 Aneurysm Creation and Embolization Procedure

Aneurysm Creation and Embolization Procedure Ten New Zealand White rabbits went through a protocol approved by the animal institutional review committee at the Mayo Clinic, Rochester, Minnesota for creation of elastase-induced aneurysms followed by coil embolization. Aneurysms were created by ligation of the stump of the right common carotid artery [73]. They were allowed to mature for at least three weeks prior to embolization [76]. Aneurysms were treated with standard platinum coils as dense as possible. Animals were kept alive for more than two weeks after coiling before sacrifice.

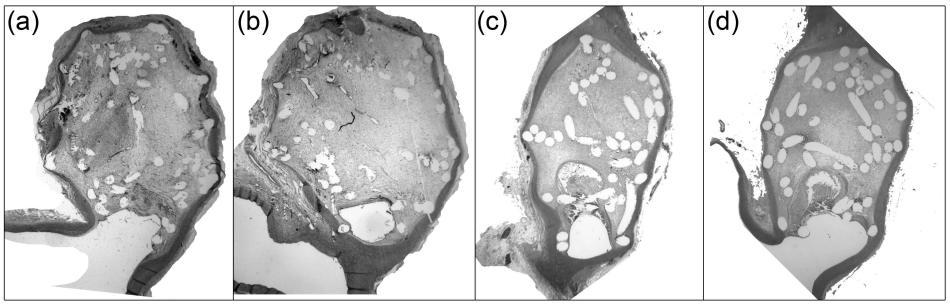

Figure 2.1: Photomicrographs showing aneurysms with removed coils. (a) and (b) correspond to case #4 (hematoxylin and eosin, original magnification, 15×), and (c)and (d) to case #5 (hematoxylin and eosin, original magnification, 20×).

2.2.2 Tissue-Processing Procedure

Animals were deeply anesthetized and sacrificed to get access by surgery to the coiled aneurysms. Specimens were removed and immediately fixed in 10% neutral-buffered formalin for at least 24 hrs. They were then dehydrated in an ascending series of ethanol, cleared in xylene, and embedded in paraffin. Using a slow-speed diamond saw (Isomet, Beuhler, IL), 1000μm-thickness sections of the aneurysms were extracted. These sections were oriented according to the aneurysm longitudinal axis and perpendicular to the neck. Afterwards, coils were manually removed and aneurysm sections were sliced at 7μm-thickness intervals following previous cut plane. This procedure has been previously implemented and guarantees little or no distortion of the samples [74]. Details of this process can be found elsewhere [72–74].

A total of 17 histological images were used in this study (Fig. 2.1). For nine cases, a histological image crossing the aneurysm center was available. For six of them, a total of seven additional images away from the center were included. For last case, only an image away from the aneurysm center was available. These additional images away from the aneurysm center were included to analyze if coil density and distribution change between cut planes of the same aneurysm.

2.2.3 Image Processing

To evaluate coil distribution, qualitative observations and quantitative measurements were performed. For qualitative assessment, the images were visually inspected. For quantitative evaluation, the images were processed as follows.

Each image was manually processed to characterize and quantify its coil distribution. The images were processed in three steps. First, coils were manually segmented (Fig. 2.2b). Second, the aneurysm region containing the coils was delineated creating a closed area (blue contour in Fig. 2.2c). We refer to this region as the total aneurysm area, A_T. Finally, the aneurysm longitudinal axis (green line in Fig. 2.2c) was created by identifying the aneurysm fundus (point f) and neck (point n) on the delineated contour.

After manual processing, coil density in A_T was measured and denoted as total in-slice coil density ρ_T. Coil density is defined as the ratio between the area occupied by coils and the total area of the region:

$$\rho_x = \frac{\text{area occupied by coils in region } x}{\text{total area of the region x}} \times 100\% \tag{2.1}$$

The aneurysm cavity was partitioned and evaluated in two ways: along its longitudinal axis, from aneurysm neck to fundus, and along its radial axis, from aneurysm periphery to its core. Both partitions generated independent regions, which were defined as follow:

Longitudinal partition: It divides the aneurysm cavity into three regions along the longitudinal axis. These regions were constructed by dividing equally the longitudinal axis and were called fundus, dome and neck (Fig. 2.2d). The in-slice coil density of each region was calculated using equation 2.1 and normalized by ρ_T. The normalized densities of fundus, dome and neck were denoted as ρ_F, ρ_D and ρ_N, respectively.

Radial partition: It separates the aneurysm cavity into its periphery and core. The region within one coil diameter from the aneurysm contour was considered as the periphery, and the remaining area as the core (Fig. 2.2d). In-slice coil densities at peripheral and core regions were calculated using equation 2.1 and normalized with ρ_T. These normalized densities were denoted as ρ_P and ρ_C for peripheral and core region, respectively.

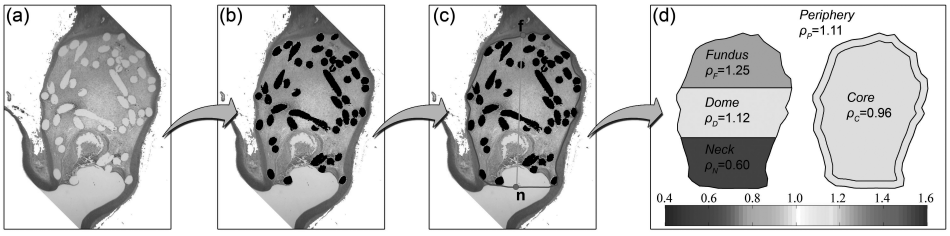

Figure 2.2: Processing of a histological image. (a) Original histological image. (b) Coil segmentation. (c) Aneurysm wall and neck delineation (blue contour) and longitudinal axis (green line) defined by f and n (red dots). (d) Automatic partitioning and calculation of normalized densities. Colored version on page xxiii.

Differences between regions were assessed with statistical tests. A Friedman's 2-way ANOVA by rank test was used to compare ρ_F, ρ_D and ρ_N, while a Wilcoxon matched-pair signed-rank test was performed to compare ρ_P and ρ_C.

Intra- and inter-observer variability on ρ_T was quantified for both coil segmentation and aneurysm delineation. For this quantification, one observer segmented and delineated all images twice to assess intra-observer variability. Inter-observer variability was evaluated by comparing the segmentation and delineation performed by two observers of all images. The manual processing was performed independently.

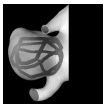

2.3 Results

2.3.1 Qualitative Evaluation

From the visual inspection of the histological images (Fig. 2.3), three aspects can be highlighted. First, the aneurysm core presented large voids in some cases and coils were usually touching the aneurysm wall. Second, most coils were transversely cut resulting in circular or nearly-circular shapes. Few elongated shapes (partially longitudinal coil cuts) were visible, especially in histological samples taken from the aneurysm center. Third, from aneurysms with multiple images, it was observed that coil distribution can change from one cut plane to another.

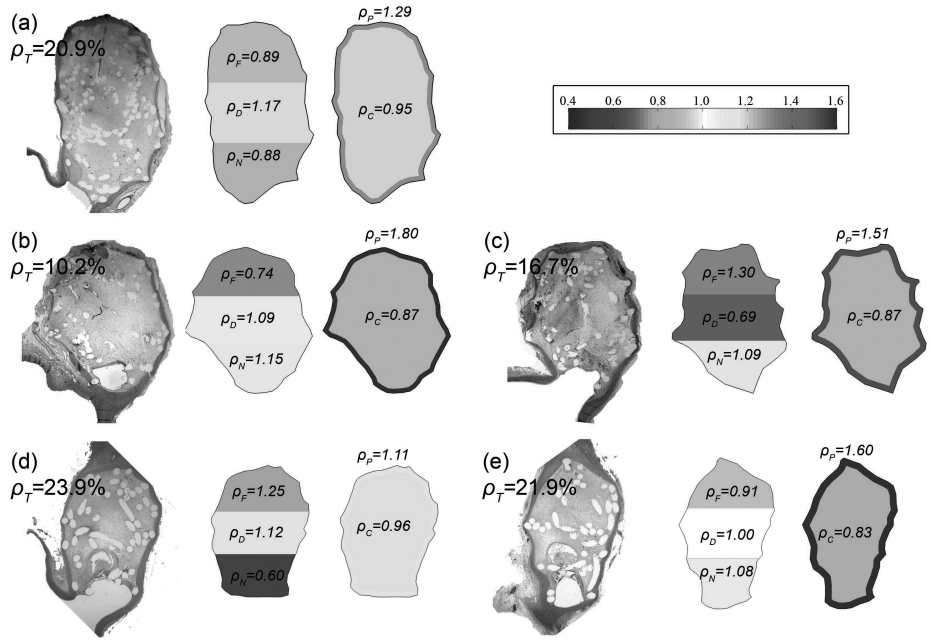

Figure 2.3: Color maps of normalized coil densities for five histological images (three aneurysms). Colored version on page xxiii.

2.3.2 Quantitative Evaluation

After analyzing all histological images, a mean ρ_T of 22.0% ± 6.2% was found, with a minimum of 10.1% and maximum of 30.2%.

Fig. 2.3 shows color maps of in-slice coil densities for the regions in both partitions of five images (three aneurysms). All images presented a higher ρ_P than ρ_C. Additionally, Fig. 2.3a and 2.3e show a homogeneous distribution of the coils (near one) along longitudinal axis with high ρ_T (>20%). Fig. 2.3d has a heterogeneous distribution (low ρ_N), even though it has high ρ_T. When comparing images

of same aneurysm, we observed that ρ_T can be very similar between cut planes (case #5 in Figs. 2.3d and 2.3e) or can change (case #4 in Figs. 2.3b and 2.3c).

Fig. 2.4 shows the relationship between peripheral-core density ratio and ρ_T. This ratio was inversely proportional to ρ_T (R^2=0.57, p <0.001). For low ρ_T (<15%), the peripheral-core density ratio tends to be greater than 2.0 while for ρ_T around 30%, the ratio is close to 1.0.

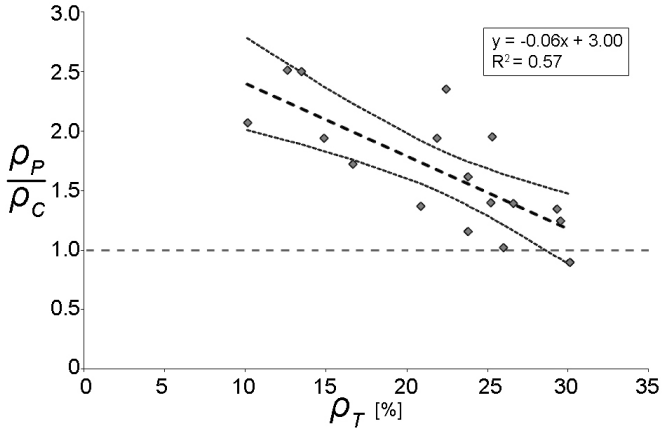

Figure 2.4: Peripheral-core density ratio versus total in-slice coil density. Linear regression of the results is represented by the dashed line. Dotted curves are the lower and upper limits of the 95% confidence intervals.

Fig. 2.5 is a box plot of the normalized densities per each region. Each histological image was considered to be independent from the rest of the samples as the density depends on both coil configuration and choice of cut location.

2.3.3 Statistical Evaluation

The Friedman's 2-way ANOVA test showed that the differences among ρ_F, ρ_D and ρ_N were not statistically significant (p=0.465). Wilcoxon matched-pair signed-rank test reported that the difference between ρ_P and ρ_C was significant (p <0.001).

2.3.4 Intra- and Inter Observer Variability

Table 2.1 presents the intra- and inter-observer variation of manual coil segmentation and aneurysm delineation.

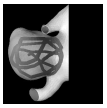

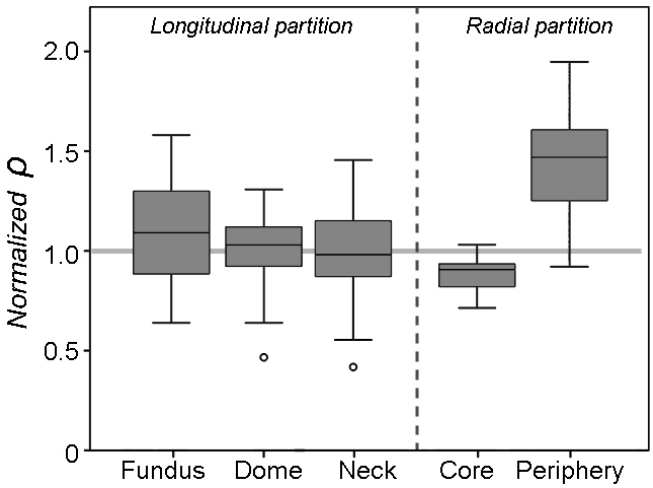

Figure 2.5: Boxplots of normalized densities per aneurysm region of histological images.

Table 2.1: Intra- and inter-observer variation of coil segmentation and aneurysm delineation.

Evaluation	Measurement	ρ_T [%]			
		Mean	Std	Min	Max
Intra-observer	#1	22.00	6.27	10.16	30.23
	#2	21.77	6.18	10.44	31.63
	difference	0.96	1.16	0.28	1.40
Inter-observer	#1	22.00	6.27	10.16	30.23
	#2	21.68	6.18	10.11	30.64
	difference	1.01	1.00	0.05	0.41

2.4 Discussion

In this chapter, we analyze and quantify coil distribution in saccular aneurysms using histological images to better understand this endovascular treatment. Images were obtained from elastase-induced saccular aneurysms in rabbits. These images were analyzed by partitioning the aneurysm along its longitudinal and radial axis and comparing the in-slice coil density at each region. There are three main findings.

First, coils tend to be located near aneurysm periphery when ρ_T is low (<20%). This finding confirms that the first coils produce a frame (or basket) attached to the aneurysm wall, and coils added later fill the aneurysm core [64–66]. As ρ_T increases, the peripheral-core density ratio decreases until it is close to one (Fig. 2.4). This means that when more coils are added, the radial distribution tends to be more homogeneous.

Previous studies have shown that high packing density leads to better aneurysm stability after endovascular coiling [77–80]. These results could be explained by the homogeneous coil distribution that was found at high ρ_T (>25%) in this chapter.

A homogeneous distribution might create a stable mechanical structure inside the aneurysm that successfully blocks and redirects the blood flow towards the parent artery. On the contrary, for low packing densities, where coils mainly lay on the aneurysm wall, leaving a hollow core, the coil structure may forms a weak block against the blood flow. This hollow core at low packing densities cannot be visualized with current modalities of medical imaging. Still, it is necessary to confirm this statement with studies that consider long-term results.

Second, densities on the longitudinal axis (fundus, dome and neck regions) were not found to be significantly different (p-value=0.465, Friedman's test), indicating that coils are homogeneously distributed along the aneurysm main axis.

Third, we observed that different histological images of the same aneurysm do not necessarily show similar ρ_T and coil distributions. This suggests that the characterization of in-slice coil density and distribution of a sole aneurysm should not rely on a single slide of histology, as it has been previously proposed and implemented [81].

It has been indicated that the coil distribution inside aneurysms is random due to the limited control that clinicians have on coil deployment, and also that the distribution could be more homogeneous or uniform for certain coil shapes [66–68]. Although this "randomness" during coil deployment, our findings demonstrate that first the aneurysm periphery is filled up with coils and then its core, and also we provide evidence that coils tend to be equally distributed in the longitudinal orientation. These results clarify how coil are distributed inside the aneurysm in both axes, but most importantly, a quantification of in-slice coil density and distributions was provided.

This quantification is valuable to understand the differences that can occur among regions inside the aneurysm cavity but also it can be used to validate computational models of coils and blood flow [49, 50, 71]. The computational models need to know how coils are distributed to properly simulate the post-treatment hemodynamics inside the aneurysm. Similarly, the use of histological images and the followed methodology can be adapted to assess the porosity and strut distribution of both stents and flow diverters, and to compare it with their effect on thrombotic occlusion [82, 83].

Recently, in-slice coil density was calculated to assess coil distribution is a similar way but in silicone coiled aneurysm models [84]. There, the authors used slices of the aneurysm dome and neck that were partitioned in angular regions to assess coil distribution. A coil uniformity index was implemented and defined as inversely proportional to the standard deviation of the in-slice coil density at each angular region. They found that a particular coil shape design has a significant higher uniformity index than the other two tested coil designs. Our results confirm this finding, since they also reported that the highest packing densities were achieved with that particular coil design. Nonetheless, this uniformity index is a relative measurement among tested coil designs and may not be suitable to quantify coil distribution, which was the purpose of our study.

Two main limitations of this chapter can be mentioned. First, the proposed methodology includes manual image processing (coil segmentation and aneurysm delineation), which might introduce some intra- and inter-observer variability in

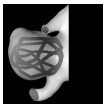

our results (table 2.1). However, we assessed this variability and we found that was not enough to alter our main findings and conclusions. Second, coils were removed from the samples for cutting purposes, and the cast of the coils induced uncertainties in some location during coil segmentation. To overcome this issue and thereby to avoid the inclusion of false-positive segmented coils, the images with doubtful coil locations were discarded from our analysis.

2.5 Conclusions

In this chapter, the coil density and distribution inside the aneurysm were analyzed and quantitative evaluated using histological images of elastase-induced saccular aneurysms in rabbits treated with endovascular coils. We observed that coils are homogeneously distributed along the aneurysm longitudinal axis. Additionally, the results show that coils tend to be located near aneurysm periphery when in-slice coil density is low (<20%). As in-slice density increases, the peripheral-core density ratio decreases until it is close to one for high in-slice coil density (around 30%). This finding confirms that first coils produce a frame for succeeding coils, but also it shows that as the packing density increases, the radial coil distribution tends to be homogeneous.

3

The Virtual Coiling Technique

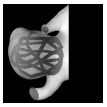

Computational algorithms modeling the insertion of endovascular devices, such as coil or stents, have gained an increasing interest in recent years. This scientific enthusiasm is due to the potential impact that these techniques have to support clinicians by understanding the intravascular hemodynamics and predicting treatment outcomes. In this chapter, a virtual coiling technique for treating image-based aneurysm models is proposed. A dynamic path planning was used to mimic the structure and distribution of the coils inside aneurysm cavities, and to reach high packing densities, which is desirable by clinicians when treating with coils. Several test were done to see the performance on idealized and image-based aneurysm models. Afterwards, the proposed technique was validated using clinical information of real coiled aneurysms. The virtual coiling technique reproduces the macroscopic behavior of inserted coils and properly captures the densities, shapes and coil distributions inside aneurysm cavities. A practical application was performed by assessing the local hemodynamic after coiling using computational fluid dynamics. Wall shear stress and intra-aneurysmal velocities were reduced after coiling. Additionally, CFD simulations show that coils decrease the amount of contrast entering the aneurysm and increase its residence time.

The content of this chapter is adapted from the following publication:

H.G. Morales, I. Larrabide, M. Kim, M.-C. Villa-Uriol, J.M. Macho, J. Blasco, L. San Roman, A.F. Frangi. Virtual Coiling of Intracranial Aneurysms Based on Dynamic Path Planning. In *International Conference on Medical Image Computing and Computer Assisted Intervention (MICCAI). Toronto, Canada.* pp. 355-362, 2011. Winner of a Student Travel Award.

H.G. Morales, I. Larrabide, A.J. Geers, L. San Roman, J. Blasco, J.M. Macho and A.F. Frangi. A Virtual Coiling Technique for Image-Based Aneurysm Models by Dynamic Path Planning. Submitted 2012 - Under review.

3.1 Introduction

Coiling is the most important and popular endovascular therapy to treat cerebral aneurysms since their invention in early nineties [23]. It consists in the insertion of small and thin biocompatible metal wires that partially fill the aneurysm cavity. Coils alter intra-aneurysmal hemodynamics by reducing flow velocities and increasing blood residence times, which may trigger thrombus formation [37]. Nonetheless, around 15% to 25% of aneurysms treated with coils recanalize [22,26], which means reestablishment of blood flow in the aneurysm lumen. Recanalization can be caused by either coil compaction or aneurysm regrowth [22, 27, 28], both associated to the hemodynamic forces acting on coils and the aneurysm wall over time [1,20]. Moreover, little is known about reliable predictors that identify which aneurysms are prone to recanalize due to hemodynamics and what coiling strategy carries a lower risk for the patient.

Clinical reports suggest that packing density, which expresses the percentage of the aneurysm volume that is occupied by coils, is a good predictor of coiling success. The higher the packing density, the better the output [64, 78, 79]. Another clinical predictor of coiling performance is the aneurysm occlusion rate [64, 85]. This indicator classifies how obliterated the aneurysm is by coils using two-dimensional medical images such digital subtraction angiography (DSA). Still, none of these indicators are neither fully reliable, nor accurately measured nor considered the postoperative hemodynamics [24, 79].

To study endovascular coiling and its effect on local hemodynamics, several computational techniques have been implemented. These techniques can be clustered according to how coils are modeled. The first group implicitly represents the coils by adapting the governing equations of fluid flow in the coiled region [44, 45, 49, 50, 53]. The second group, explicitly represents the coils and solves the incompressible Navier-Stokes equations in the fluid domain [46–48, 52].

In this chapter, we propose a virtual coiling technique for treating image-based aneurysm models that explicitly represents endovascular coils. The goal is to create a computational tool that provides accurate information to support clinicians in the treatment optimization and the assessment of both coil geometrical features, coil packing density and hemodynamic alterations induced after coiling. For that, the virtual coiling technique aims to capture the macroscopic structure of the coils, to keep the particular features of each device, and to reproduce the coil densities and distributions inside aneurysm cavities. Additionally, it is meant to achieve high packing densities (around 30% [77, 79]) and to obtain different coil configurations as happen in reality.

3.2 Method: Virtual Coiling Technique

The proposed virtual coiling technique uses a dynamic path planning algorithm to mimic coil insertion and to obtain a similar distribution and structure of endovascular coils inside image-based aneurysm models. The explanation of the algorithm is presented in the following section. A previous description of the technique and

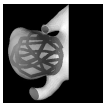

results, which include a test in a sphere, an hexahedron and in image-based aneurysm models, can be found elsewhere [86].

The virtual coiling technique inserts one by one the desired coils inside the aneurysm model as happens in reality. It uses as treatment input both, the aneurysm model and coils to be inserted. Moreover, the virtual coiling technique has its own parameters, which are evaluated in the following sections. Any change in either treatment inputs or parameters will affect the results.

3.2.1 Dynamic Path Planning Algorithm

A virtual coil model, from here on called a *coil* is a three-dimensional (3D) tubular structure with a fixed radius r_j and length L_j. A coil is defined from a group of ordered points that are consecutively added in a set C_j. This set is define as:

$$\mathrm{C}_j \equiv \{\mathbf{p}_j^i \in \mathbb{R}^3 : ||\mathbf{p}_j^i - \mathbf{p}_j^{i+1}|| = r_j, \text{ for } i = 0...n_j\}, \tag{3.1}$$

where j denotes the coil currently being inserted, which ranges from 1 to the total number of coils J. The index i indicates the points of coil j and n_j the number of its segments. The integer n_j is defined as $\lfloor (L_j/r_j) \rfloor$, where L_j and r_j are provided as treatment inputs.

To add a new point $\mathbf{p}_j^{i+1}$ in C_j, a set of candidate locations H_j^i is created around the latest inserted coil point $\mathbf{p}_j^i$, called *coil tip*. This set is defined as $\mathrm{H}_j^i \equiv \{\mathbf{h}_j^{i,q} \in \mathbb{R}^3 : ||\mathbf{p}_j^i - \mathbf{h}_j^{i,q}|| = r_j, \text{ for } q = 0...Q\}$ (Fig. 3.1a). The parameter of the technique, Q determines the number of candidate locations around the coil tip. The element $\mathbf{h}_j^{i,q'}$ that satisfies equation 3.2 is selected as $\mathbf{p}_j^{i+1}$.

$$\mathbf{h}_j^{i,q'} = \underset{\mathbf{h}_j^{i,q} \in \mathrm{H}_j^i}{\operatorname{argmin}}(\phi). \tag{3.2}$$

The potential field ϕ was established on basis observations of coil behavior during real interventions. These observations included the facts that coils would neither cross the aneurysm wall nor protrude outside the aneurysm, they change its direction in the presence of an obstacle and coils are pulled back by the clinician if no more available space inside the aneurysm is found. These observations lead to three rules that are evaluated on each candidate location $\mathbf{h}_j^{i,q}$, namely: coiling domain, coil flexibility and coil pull-back, which mathematically define the potential field ϕ as follows.

$$\phi(\mathbf{h}_j^{i,q}) = \phi_D(\mathbf{h}_j^{i,q}) + \phi_F(\mathbf{h}_j^{i,q}) + \phi_{PB}(\mathbf{h}_j^{i,q}). \tag{3.3}$$

Coiling Domain

It represents the region where a coil is allowed to move and is defined as the sum of two potential fields.

$$\phi_D(\mathbf{h}_j^{i,q}) = \phi_A(\mathbf{h}_j^{i,q}) + \phi_C(\mathbf{h}_j^{i,q}). \tag{3.4}$$

the first term, $\phi_A(\mathbf{h}_j^{i,q}) : \mathbb{R}^3 \rightarrow \{0,1\}$, is defined by the aneurysm model to be filled with coils. The aneurysm model is a treatment input and needs to be a close volume. If the candidate location $\mathbf{h}_j^{i,q}$ is inside the aneurysm model, $\phi_A(\mathbf{h}_j^{i,q})$ is zero, otherwise is one (Fig. 3.1a). The second term, $\phi_C(\mathbf{h}_j^{i,q}) : \mathbb{R}^3 \rightarrow \{[0, \frac{1}{2}), 1\}$, avoids coil crossings. It also accounts for the distance between coils such that the newly inserted coil avoids dense areas. The field $\phi_C(\mathbf{h}_j^{i,q})$ is defined as follows:

$$\phi_C(\mathbf{h}_j^{i,q}) = \begin{cases} 1, & \text{if } \exists\ \mathbf{m}_j^{i,t} \text{ satisfying} \\ & ||\mathbf{h}_j^{i,q} - \mathbf{m}_j^{i,t}|| \leq 2 \cdot r_j \\ \dfrac{r_j}{|\mathrm{M}_j^i|} \cdot \displaystyle\sum_{|\mathrm{M}_j^i|} \dfrac{1}{||\mathbf{h}_j^{i,q} - \mathbf{m}_j^{i,t}||}, & \text{otherwise,} \end{cases} \tag{3.5}$$

where $\mathbf{m}_j^{i,t} \in \mathrm{M}_j^i$. The set M_j^i (see equation 3.6) is a subset of all neighbor coil points around the coil tip within a distance $\alpha \cdot r_j$ (Fig. 3.1b).

$$\mathrm{M}_j^i \equiv \{\mathbf{m}_j^{i,t} \in \bigcup_{j'} \mathrm{C}_{j'} : ||\mathbf{p}_j^i - \mathbf{m}_j^{i,t}|| \leq \alpha \cdot r_j, \text{ for } j' = 1...j\}, \tag{3.6}$$

The distance, $\alpha \cdot r_j$ limits the size of M_j^i. By setting α >4, we take into account the closest coil points that could potentially produce coil crossings. Fig. 3.1c shows a schematic representation of how $\phi_C(\mathbf{h}_j^{i,q})$ is evaluated.

Coil Flexibility

It considers the local deformation of the coil during insertion by comparing the angle $\theta_j^{i,q}$ of a candidate location $\mathbf{h}_j^{i,q}$ and coil tip with respect to the coil direction. The coil direction is defined as $\mathbf{p}_j^i - \mathbf{p}_j^{i-1}$ (Fig. 3.1d). The potential field $\phi_F(\mathbf{h}_j^{i,q}) : \mathbb{R}^3 \rightarrow [0, \frac{1}{2}]$ is formulated as:

$$\phi_F(\mathbf{h}_j^{i,q}) = \frac{\theta_j^{i,q}}{2 \cdot \pi}, \tag{3.7}$$

where $\theta_j^{i,q} = \arccos[(\mathbf{h}_j^{i,q} - \mathbf{p}_j^i) \cdot (\mathbf{p}_j^i - \mathbf{p}_j^{i-1})/r_j^2]$.

Coil Pull-Back

It is meant to solve the situation when the coil advance is blocked by either others coils or the aneurysm wall, i. e. $\phi(\mathbf{h}_j^{i,q}) \geq 1$, $\forall\ \mathbf{h}_j^{i,q} \in \mathrm{H}_j^i$ (becoming a dead-end). In such situation, the algorithm pulls back and relocates the coil tip to the position $\mathbf{p}_j^{i-(k+1)}$, being k the number of consecutive dead-ends. Then a potential field, $\phi_{PB} = 1$ is assigned to the candidate location previously selected for $\mathbf{p}_j^{i-k}$ (blocking this position for selection). An schematic representation of the coil pull back is presented in Fig. 3.1e.

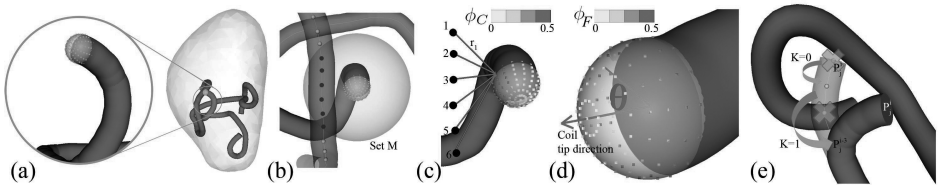

Figure 3.1: Schematic description of potential fields. (a) Coil being inserted (blue), candidate locations (green dots) at coil tip and the coiling domain, which is represented by the aneurysm model (close volume) and an inserted coil (red). (b) The set M_j^i (black dots) defined by the yellow sphere of radius $\alpha \cdot r_j$ around the coil tip. (c). Representation of the field ϕ_C for one of the candidate locations. (d) Representation of the field ϕ_F and coil tip direction (red arrow). (e) An scheme of coil pull-back field ϕ_{PB}. Colored version on page xxiv.

To initialize C_j, a particular set S_j of initial candidate locations is required. This set is defined as $S_j \equiv \{\mathbf{s}_j^q \in \mathbb{R}^3 : ||\mathbf{o} - \mathbf{s}_j^q|| = \beta \cdot r_j \text{ for } q = 0...Q_0\}$, where $\mathbf{o}$ is the center of the aneurysm bounding box and $\beta > 1$. The number of elements in S_j is defined by Q_0. The initial candidate location that satisfies equation 3.2 in S_j is selected as $\mathbf{p}_j^0$.

To evaluate $\phi_F(\mathbf{s}_j^q)$ of the first coil, one extra parameter is required. This parameter corresponds to a user-defined initial direction, for instance $\hat{x}$. After this iteration, the coil direction is updated to $\mathbf{p}_j^0 - \mathbf{o}$. Note that the fist coil follows the user-defined direction, and thereby if this direction changes, then a new coil configuration will be obtained.

3.2.2 Algorithm Construction

The sets H_j^i and S_j were created from the nodes of a hemi- and a complete sphere, respectively. The hemisphere of H_j^i is always oriented to the coil direction (Fig. 3.1d), while the complete sphere of S_j is $\hat{z}$-axis.

Finally to generate a volumetric representation of the coils, a 3D tubular structure, which centerline corresponds to the connected elements of the set C_j is created. The sequence of point insertion in C_j is very important to ensure a proper representation of coils as a tube without coil crossing or migrations outside the aneurysm model.

The algorithm pseudocode 1 describes the sequence of steps followed to generate the virtual coils.

3.2.3 Sensitivity Analysis on Idealized Models

To assess the results of the virtual coiling technique and its parameters, two experiments were done in idealized geometries. The experiment #1 aims to understand the influence of the paraments of the technique using a sphere as the aneurysm model. The experiment #2 was performed to see the behavior of coils when the aneurysm has a bleb. For latest experiment, a small spherical protrusion was added to the sphere used in the first experiment.

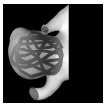

Algorithm 1: Virtual coiling

Treatment inputs: Aneurysm model, Number of coils (J), coil radii (r_j) and lengths (L_j).
Parameters of the technique: Initial coil direction, number of candidate locations (Q), number of initial candidate locations (Q_0), ×radius of the neighbor set M_j^i (α) and ×radius of the initial set S_j (β).
Output: Virtual coil models.

begin

for $j = 1$ **to** J **do**
  $n_j = \lfloor (\frac{L_j}{r_j}) \rfloor$;
  Create S_j;
  for $q = 0$ **to** $q = Q_0$ **do**
    Find $\mathbf{s}_j^{q'} = \underset{\mathbf{s}_j^q \in \mathrm{S}_j}{\mathrm{argmin}}(\phi)$
    $(\mathbf{p}_j^0 = \mathbf{s}_j^{q'}) \rightarrow \mathrm{C}_j$;
  for $i = 0$ **to** $i = n_j$ **do**
    Create H_j^i and M_j^i;
    for $q = 0$ **to** $q = Q$ **do**
      Find $\mathbf{h}_j^{i,q'} = \underset{\mathbf{h}_j^{i,q} \in \mathrm{H}_j^i}{\mathrm{argmin}}(\phi)$
    if $\phi(\boldsymbol{h}_j^{i,q'}) < 1$ **then**
      $(\mathbf{p}_j^{i+1} = \mathbf{h}_j^{i,q'}) \rightarrow \mathrm{C}_j$.
      i = i+1;
      k=0
    else
      if *there are consecutive dead-ends* **then**
        k = k+1;
      i = i-(k+1);
      $\phi_{PB} = 1$ at $\mathbf{p}_j^{i+k}$;
  Create a tube with C_j;
  $j = j+1$;

end

In both experiments, treatment inputs were four 0.254 mm-diameter coils, each of them with a length of 100 mm. These coils provided a packing density of approximately 30%. A summary of the experiments is presented in table 3.1.

Experiments were done in a Intel(R) Core(TM)2 Quad CPU Q6600 @2.40GHz, 2.40GHz, 8.00GB of RAM.

Experiment #1

Four tests were performed (S1 to S4) to evaluate the parameters of the technique. A 5mm-radius sphere was used as the aneurysm model. The size of the sphere corresponds to a typical mean aneurysm size found in literature [67]. In this experiment, only the number of candidate locations Q, and α, which controls the size of M_j^i were studied. Table 3.1 shows the values imposed for these parameters. The initial coil direction was $\hat{x}$ and was not changed due to the symmetry of the

Table 3.1: Sensitivity analysis of virtual coil parameters on idealized aneurysm models

Experiment #	Aneurysm Model	Test	Q	α	Computed time [s]
1	Sphere	S1	33	4	57
		S2	193	4	206
		S3	481	4	451
		S4	193	6	304
2	Sphere with bleb	S5	33	4	57
		S6	193	4	206
		S7	481	4	451

idealized aneurysm model. Additionally, the parameters β and Q_0, which control S_j, were kept equal to 10 and 342, respectively. These two parameters were not modified since they just affect the initial candidate locations.

Fig. 3.2 shows the results of three tests in the sphere: S1, S2 and S3. It is noticeable that, when Q (the number of candidate locations) is increased, the coil bends became smoother and were better adapted to follow the aneurysm surface. However, more candidate locations also increased the required computational time (table 3.1). Test S4 provided a different coil configuration and a higher computational time compared to S2, which has the same Q but with a reduced α.

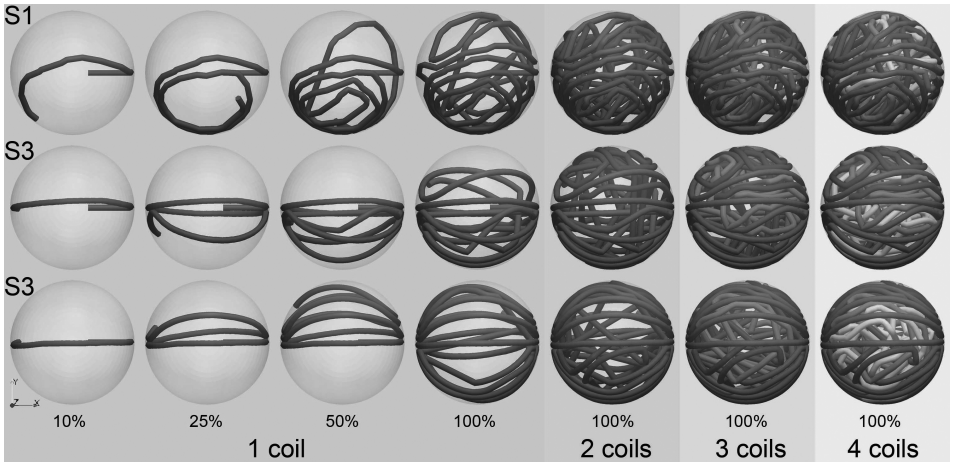

Figure 3.2: Three tests performed on the sphere increasing number of candidates from S1 to S3. Columns present the percentage of insertion for each coil. Colored version on page xxiv.

Experiment #2

Three tests were performed here (S5 to S7) to evaluate the behavior of the parameters when the aneurysm model has a bleb. A 5 mm-radius sphere with a 0.5 mm-radius bleb was used here as the aneurysm model. The center of the bleb was located in the intersection between the sphere and the $\hat{y}$-axis. In this

experiment, only Q was evaluated (see table 3.1). The initial coil direction was $\hat{x}$.

Fig. 3.3 depicts the final results of experiment #2. It is noticeable that there are always coils inside the bleb, no matter Q, even though the initial direction was not pointing to the bleb.

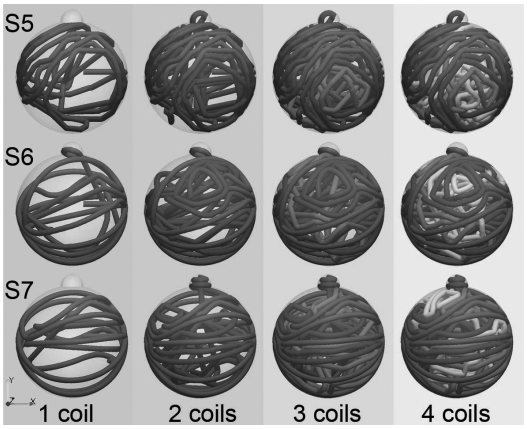

Figure 3.3: Three tests performed in a sphere with a bleb. Here, the number candidates was incremented from S5 to S7. Initial coil direction was $\hat{x}$. Colored version on page xxiv.

3.2.4 Experiments on Image-Based Models

Sixteen image-based aneurysm model were considered to evaluate the algorithm performance in complex morphologies with different sizes and volumes. All aneurysms were suitable for coil embolization. To extract the aneurysm models, a three-dimensional rotational angiography (3DRA) image of the aneurysm was acquired with a AXIOM Artis (Siemens Medical Solutions, Erlangen, Germany). The images were segmented with a geodesic active region algorithm [87]. The aneurysm sac was isolated by manually defining the neck and placing a surface at the aneurysm ostium. To quantify the variability of size and shape in this aneurysm population, the volume and the non-sphericity index (NSI) were calculated [88]. NSI characterizes the deviation of the aneurysm shape from that of a perfect hemisphere, and it is calculated according to [88] as:

$$\mathrm{NSI} = 1 - \frac{(18\pi)^{1/3} \cdot \mathit{Volume}^{2/3}}{\mathit{Surface}} \tag{3.8}$$

Aneurysm models were virtually coiled with treatment inputs presented in table 3.2. A packing density of around 30% was aimed for all cases, which is considered high in clinical practice [77, 79]. In aneurysms with a volume higher than 500 mm^3, 0.355 mm-diameter coils were used, otherwise 0.254 mm-diameter coils were imposed. Both coil diameters are currently manufactured and used in clinical proceedings. The number of coils per case was arbitrary designated. To simplify the virtual treatments, the coil lengths was imposed to be same in

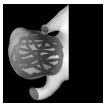

Table 3.2: Tests on image-based aneurysm models.

Case #	Aneurysm volume [mm^3]	Number of Coils	Coil length [mm]	Coil diameter [mm]	Packing density [%]
P1	108	8	81	0.254	29.4
P2	53	5	64	0.254	29.4
P3	32	3	64	0.254	29.5
P4	66	5	79	0.254	29.2
P5	12	2	36	0.254	28.9
P6	101	8	75	0.254	29.2
P7	689	20	273	0.355	27.8
P8	524	15	259	0.355	29.1
P9	14	2	41	0.254	29.0
P10	255	10	151	0.254	28.5
P11	60	5	76	0.254	29.1
P12	605	12	153	0.355	27.1
P13	73	5	88	0.254	29.4
P14	71	5	85	0.254	29.3
P15	20	2	60	0.254	29.2
P16	280	10	166	0.254	27.0

each case and it was calculated using the aimed packing density, the coil diameter and number of coils. This decision produced that coil lengths do not necessarily correspond to the ones available in the market. Different coil lengths and diameters currently manufactured, are later evaluated in the clinical assessment section.

The parameters of the technique were set for all cases to Q=97, α=4, β=10 and Q_0=342, and the initial coil direction was $\hat{x}$.

As results, mean aneurysm volume was 186 mm^3 $\pm$224 mm^3, in a range from 12 mm^3 to 689 mm^3. These values cover a wider range of aneurysm volumes compared to a previous report with a larger population [89]. Regarding the aneurysm shape, mean NSI was 0.166 $\pm$0.057, sweeping from 0.035 to 0.248. These values are similar to published data in larger aneurysm databases [88, 89].

Fig. 3.4 shows the results of the virtual coiling technique in sixteen image-based aneurysm models. It is visualized an homogeneous filling and a good compliance of the coils in all models, independently of either aneurysm volume, or morphology, or the presence of blebs. In all cases, a packing density of approximately 30% was achieved (table 3.2).

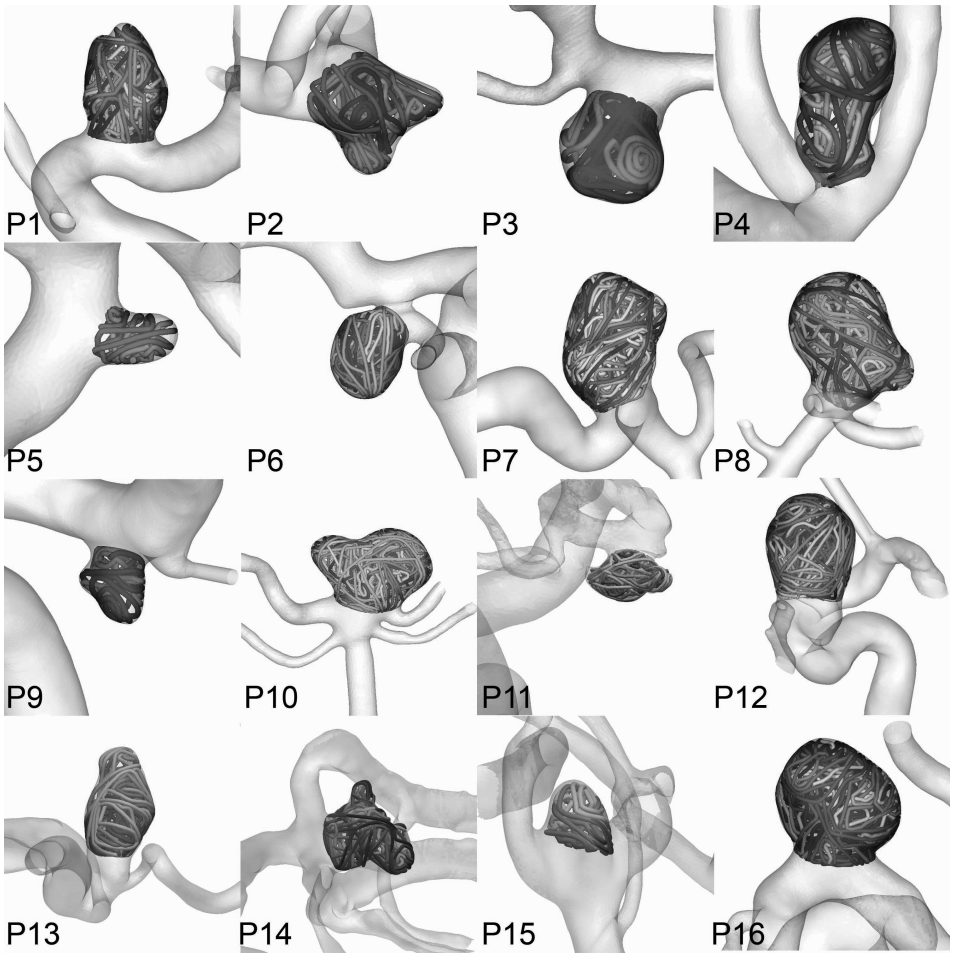

Figure 3.4: Virtual coiling technique applied on sixteen image-based aneurysm models. Coils were colored to differentiate them from each other. Colored version on page xxv.

3.3 Validation

Two evaluations were performed to validate our virtual coiling technique. First, a clinical assessment of the technique and an overall impression of the results were carried out using real coiling data. Second, an incisive validation was performed by looking at the intra-aneurysmal coil density and distribution in the same way as was done with histological images of real coiled aneurysms [90].

3.3.1 Clinical Assessment

In this section, the technique was evaluated when clinical scenarios of endovascular coiling were imposed as input. This mean that for each image-based aneurysm

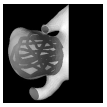

model under evaluation, the geometrical specifications of virtual coils corresponded exactly to the ones used in the real aneurysm. Additionally, the macroscopic behavior of the virtual coiling technique was tested by presenting the results in an angiogaphic fashion, which helped to compare the results with DSA images of these aneurysms. This comparison provides an angiographic-like assessment of the results as clinicians are used to visualize and evaluate the performance of coiling and other endovascular therapies.

Material

Five image-based aneurysm models were used here, corresponding to cases P11 to P15 presented in subsection 3.2.4. The aneurysms were densely packed by clinicians using coils summarized in table 3.3. This information is the real treatment performed in these aneurysms. Case P12 is an exception, since its available data corresponds to an incomplete stage of coiling. Once the coils were inserted in the aneurysm, a DSA image sequence was captured with a biplane equipment. This image acquisition provided two view points of the coils and the vasculature.

Table 3.3: Summary of the real treatment information performed in five aneurysm.

Case #	Number of coils	Coil diameters [mm]	Coil lengths [mm]	Total coil length [mm]
P11	6	0.254 to 0.292	20 to 80	240
P12	4	0.254 to 0.355	300	1200
P13	7	0.254 to 0.292	40 to 100	380
P14	3	0.254 to 0.292	40 to 100	200
P15	3	0.254 to 0.292	20 to 60	120

Method

Aneurysm models were virtually coiled following the real treatment data described in table 3.3. The parameters of the technique were same than before (subsection 3.2.4).

After virtual coiling, the 3DRA images and virtual coils were manually registered on the DSA images to get similar points of view for qualitative assessment. Both, vasculature and virtual coils, were visualized together using volume rendering to generate angiographic-like images of both arteries and virtual coils. Additionally, the theoretical and the virtual packing density were measured for each case. The theoretical packing density was calculated by considering coils as a straight cylinders, while the virtual one uses the volume of inserted coils.

Results

Cases P11 to P15 were successfully coiled with the virtual coiling technique using the real treatment input, which included different diameters and lengths. Fig. 3.5 depicts the results of the virtual coiling in these cases. Projections in two directions were compared between the DSA image of the real coiled aneurysm and the generated angiographic-like image containing the virtual coils.

The theoretical and the virtual packing density results are presented in table 3.4. Virtual coiling underestimates the theoretical values. The mean percentage of differences between packing densities was less than 3.7%.

Table 3.4: Comparison of the theoretical and the virtual packing density for clinical assessment.

Case	Packing density [%]		Differences
#	Theoretical	Virtual	[%]
P11	19.99	19.40	2.95
P12	12.81	12.20	4.76
P13	31.07	30.00	3.44
P14	17.42	16.90	2.98
P15	34.99	33.60	3.99

3.3.2 Validation of Intra-aneurysmal Coil Distribution

This validation used previous findings of the coil shape, density and distribution reported from histological images of real coiled aneurysms [90]. There, authors found that most of the coil cuts were transversal than longitudinal. Additionally, by defining several regions inside the aneurysm cavity, they demonstrated that coils tend to be located near the aneurysm periphery when few are inserted. Moreover, when more coils are added, the radial coil distribution becomes more homogeneous. They reported that coils were equally distributed along the aneurysm longitudinal axis (neck to fundus).

Material

Six image-based aneurysm models of our population were used. The cases corresponded to P1, P2, P3, P4, P5 and P9 and were selected considering their different morphologies and volumes. Cases with same number of coils such as P2 and P4, treated with 2 coils; and P5 and P9, treated with 5 coils were evaluated to see results under different aneurysm morphologies.

Method

Each of the selected aneurysm models was virtually treated with 6 coil configurations. Same treatment inputs and parameters of the technique presented in

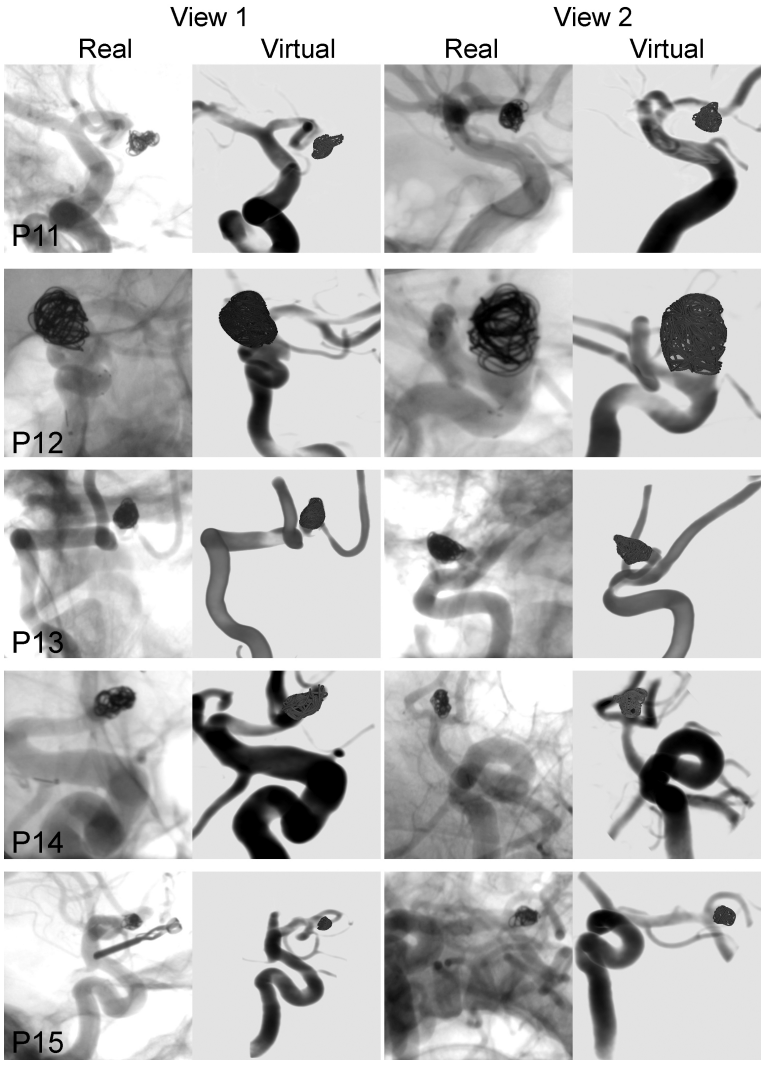

Figure 3.5: Comparison between DSA and angiographic-like images containing the virtual coils for cases P11 to P15.

subsection 3.2.4 were used here, with the exception of the initial coil direction that was modified to generate different coil configurations. Fig. 3.6 shows coil configurations generated for case P3.

To get histology-like images from the 3D geometries, the aneurysm model and coils where cut with a plane. The cut plane was placed at the aneurysm center and oriented along the longitudinal direction of the parent artery (Fig. 3.7a). Histology-like images were generated after the insertion of each coil and for all coil configurations, leading to a total of $6 \times$ *number-of-coils* images per each case.

Figure 3.6: Six coil configurations applied on case P3, made of three 0.254 mm-diameter coils of 64 mm of length. A Packing density of 29% was obtained for all configurations.

Fig. 3.7 shows the resulting histology-like images of case P3 for one to three inserted coils in one configuration.

An automatic image processing was done as performed in the followed histology-based study. Briefly, the aneurysm cavity was partitioned and evaluated in two ways. The first partition divides the aneurysm cavity along its longitudinal axis into three regions called fundus, dome and neck (Fig. 3.7c). This partition was done by equally dividing in three the longitudinal axis. The second partition splits the aneurysm cavity into two regions by defining the periphery and aneurysm core. The region within one coil diameter from the aneurysm contour was considered as the periphery and the remaining area as the core (Fig. 3.7c). Aneurysm contour was defined as the intersection of the aneurysm model and the cut plane.

The in-slice coil density of each region (fundus, dome, neck, periphery and core), and the total coil density, denotes as ρ_T, were calculated as follow:

$$\rho_x = \frac{\text{Area occupied by coils in region } x}{\text{Area of the region } x} \times 100 \tag{3.9}$$

The densities of fundus, dome, neck, peripheral and core regions were normalized by ρ_T and denotes as ρ_F, ρ_D, ρ_N, ρ_P and ρ_C, respectively.

Statistical tests were done to analyze the level of significance of differences in the densities among regions for each partition. A Friedman's 2-way ANOVA by rank test was done using ρ_F, ρ_D and ρ_N, while a Wilcoxon matched-pair signed-rank test was performed using ρ_P and ρ_C.

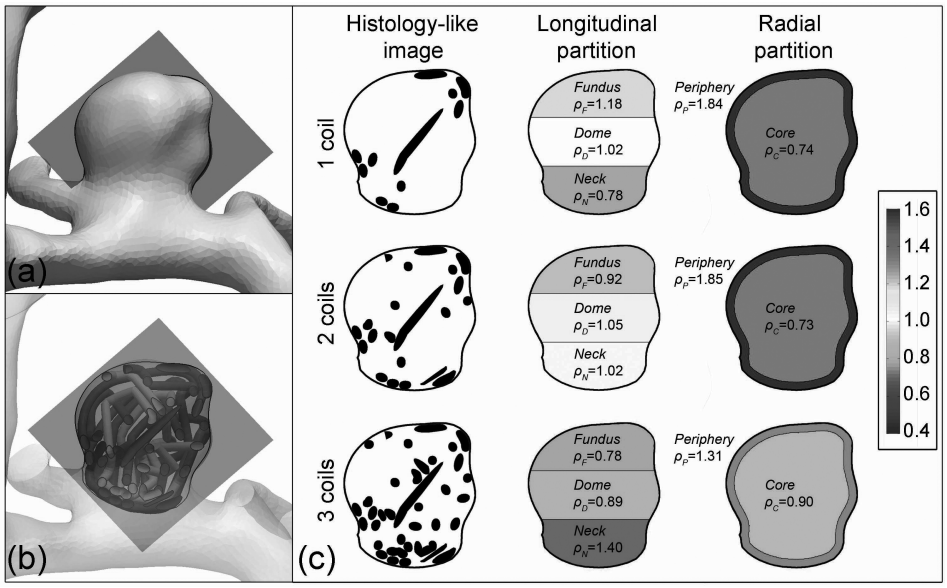

Figure 3.7: Histology-like image generation and processing for three coils inserted in case P3, produced with initial direction $\hat{x}$. (a) Definition of the cut plane. (b) Intersection of the cut plane and the aneurysm model and coils. (c) Histology-like image with one to three coils, with their partitions and calculated normalized in-slice densities at each region. Colored version on page xxvi.

Results

From visual inspection of the histology-like images, two aspects can be highlighted. First, the aneurysm core presents large voids in some cases and coils are usually touching the aneurysm wall. However, as more coils were added, the aneurysm core was progressively filled (Fig. 3.7c). Second, most of the coils cross sections were circular or nearly-circular (transverse coil cuts) and very few were elongated shapes (partially longitudinal coil cuts).

Fig. 3.8 shows the relationship between peripheral-core density ratio (ρ_P/ρ_C) and ρ_T. In general, this ratio was inversely proportional to ρ_T and tended to one for all coiled aneurysm models, meaning that when more coils were added, the radial distribution becomes more homogeneous. the ration ρ_P/ρ_C was near one for ρ_T around 30%. A linear function (dashed line in plots of Fig. 3.8), fitted from data of real coiled aneurysms was included to compare our results. This function is described by the equation 3.10.

$$\frac{\rho_P}{\rho_C} = A \times \rho_T + B, \tag{3.10}$$

where, A=-0.06 and B=3.0. These values were taken from the followed histology-based study [90].

Fig. 3.9 presents coil density for each region considering all inserted coils (around 30% of packing density). It was found that coils tend to be located near

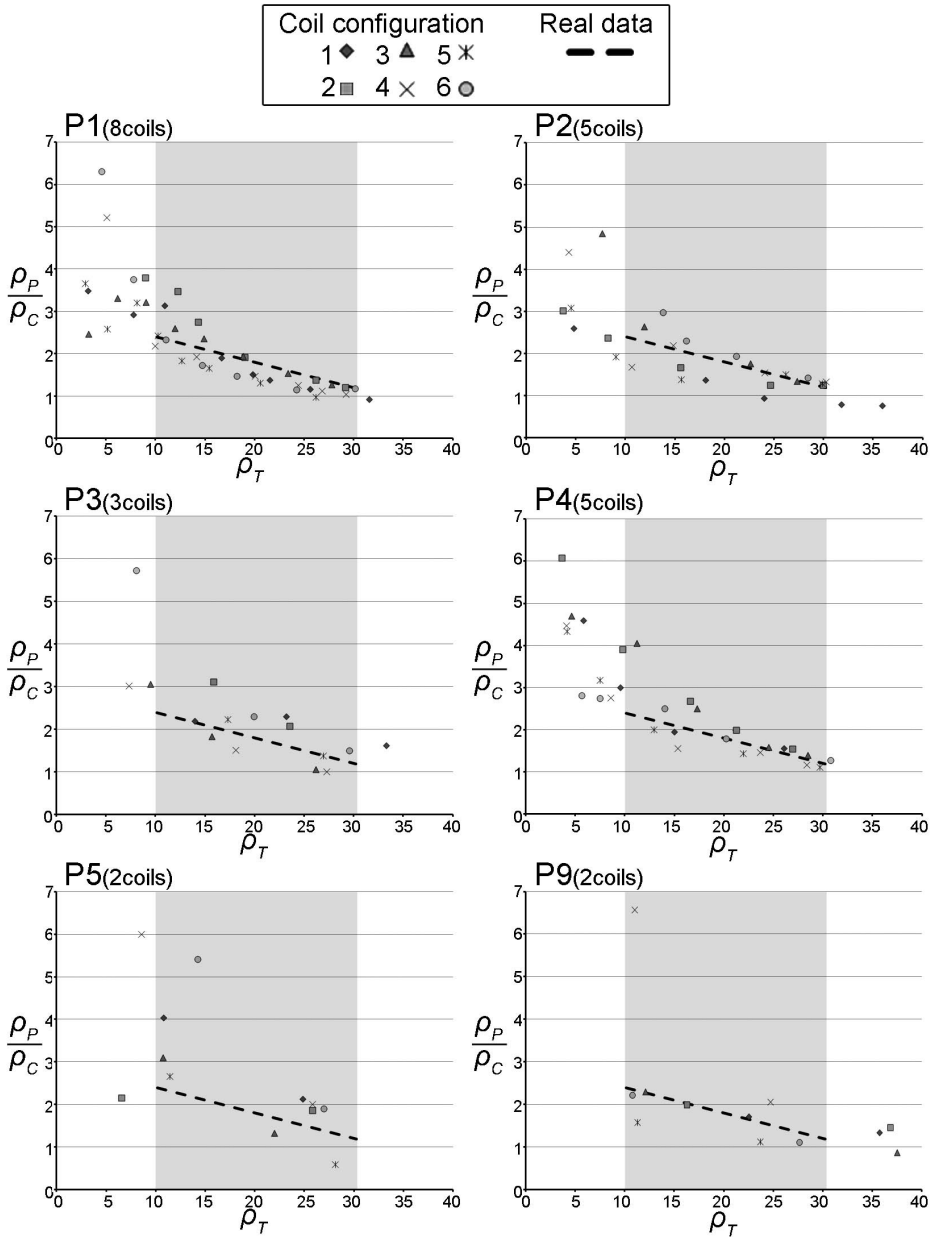

Figure 3.8: Periphery-core density ratio (ρ_P/ρ_C) versus total in-slice coil density (ρ_T). Dashed line comes from a fitted linear function of data extracted of real coiled aneurysms, of which valid interval is highlighted.

the peripheral region instead of the core region. Along the longitudinal axis, coils were equally distributed. Statistical results were presented in Fig. 3.9 (p-values).

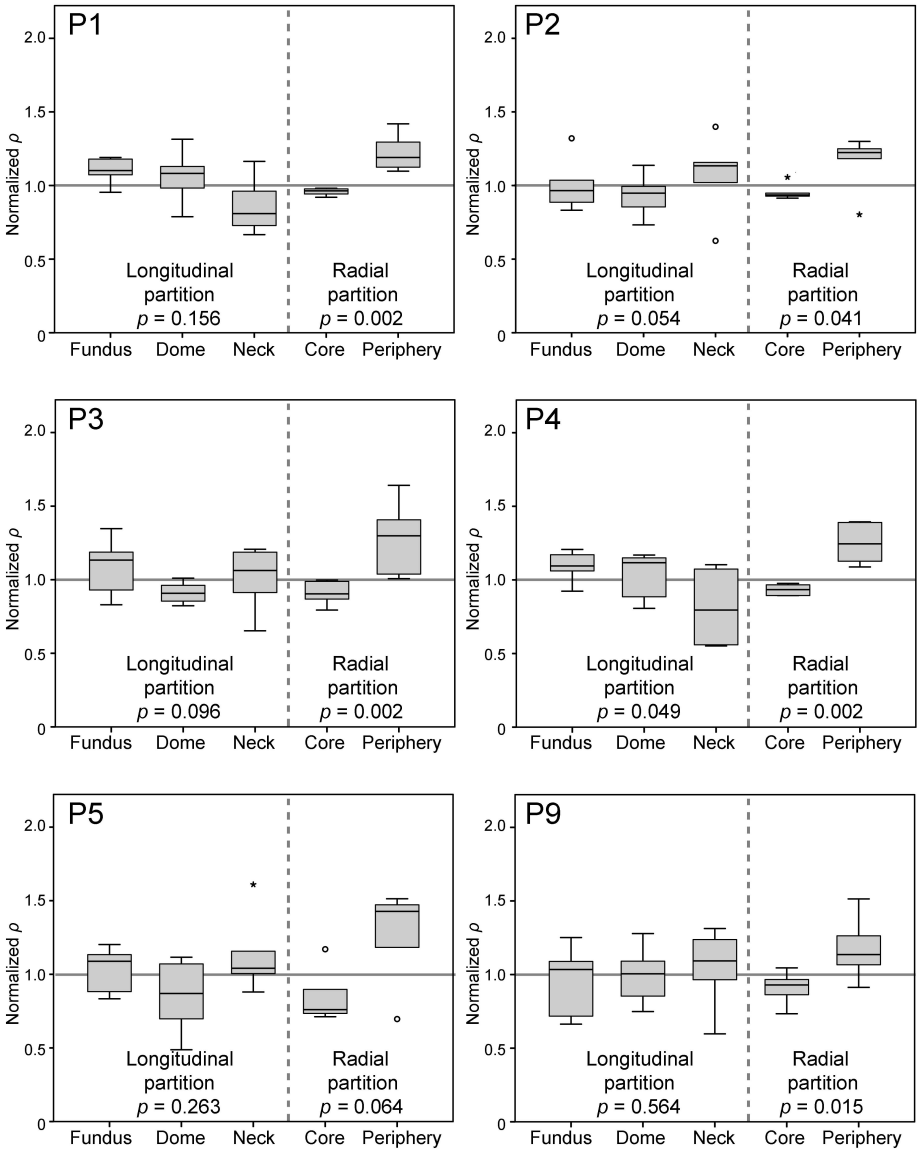

Figure 3.9: Boxplots of coil densities per region of aneurysm models treated with 6 coil configurations. p-values were calculated for each partition. Vertical dashed line separates the partitions, while the horizonal line corresponds to the normalized density at one.

3.4 Hemodynamics after Coiling

The success of coiling is intimately related to the hemodynamic alterations that the devices induce and whether or not the aneurysm is isolated from blood circulation. Such hemodynamic conditions include low flow velocities and high blood residence times [37]. Moreover, hemodynamic forces acting on coils may compact them over time, causing aneurysm recanalization [1,20]. Using CFD solvers and the proposed virtual coiling technique, it is possible to evaluate postoperative intra-aneurysmal hemodynamics to predict the output of a particular coiling scenario before the real intervention takes place.

In this section, CFD simulations were performed in image-based aneurysm models treated with our virtual coils. These simulations rely on the fact that the mechanical resistance of coils has a strong influence on intra-aneurysmal blood flow [91].

3.4.1 Material

Cases P3, P9 and P16 were used in this section. Cases were selected for their differences in volume and shape and to be located in the the internal carotid artery. Sharing parent vessel facilitates the CFD setup and analysis, since same flow boundary conditions were imposed in all of the simulations.

3.4.2 Method

Cases were virtually treated with a packing density of 33% using 0.254 mm-diameter coils. This high packing density was used to ensure homogeneity of the coil distribution but also to neglect the influence of coil configuration on hemodynamics [69].

To solve the governing equations of fluid flow in the untreated and coiled models, the fluid domain was discretized using the commercial software ANSYS ICEM CFD v12 (Ansys Inc., Canonsburg, PA). The volumetric meshes of the treated models requires small elements around the coils to obtain mesh-independent CFD calculations. About 12 elements around coils was sufficient to reach independence of the volumetric meshes on flow calculations. As a result, the meshes of the coiled models were approximately an order of magnitude larger than meshes of the geometries without coils.

The commercial software ANSYS CFX v12 was used for CFD simulations. Blood was considered an incompressible Newtonian fluid with a density of 1066 kg/m^3 and a viscosity of 0.0035 Pa·s. The flow regime was laminar. Coils, vessel and aneurysm surfaces have no-slip boundary conditions. A time-dependent physiological flow waveform was imposed at the inlet and pressure waveforms were imposed at outlets. The inlet and outlet conditions were taken from a one-dimensional model [43].

Two CFD simulations, untreated and coiled, were performed per case. In each one, three cardiac cycles of 0.8s, discretized in time steps of 0.005s, were

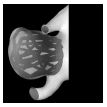

computed and the first cycle was discarded to remove numerical errors due to the initial transient conditions.

At the beginning of the second cycle, the passive transport equation of a massless scalar was solved. This was done to simulate the injection and propagation of a contrast material through the vasculature. The injection was performed during the whole second cycle at a constant value equal to one. The third cardiac cycle was considered to visualize the washout phase of the contrast. This modeling approach of a contrast injection and propagation has been previously validated by virtual angiographies and time-density curves [60, 92].

Wall shear stress (WSS) at the aneurysm, spatial-averaged velocity and contrast concentration inside the aneurysm were calculated during the last two cardiac cycles.

3.4.3 Results

Fig. 3.10 shows the spatial-averaged WSS at the aneurysm (first row) and the intra-aneurysmal velocity (second row) for studied cases. All coiled models reduced both hemodynamic variables. Case P3 (first column) has higher WSS and velocities inside the aneurysm than other two cases.

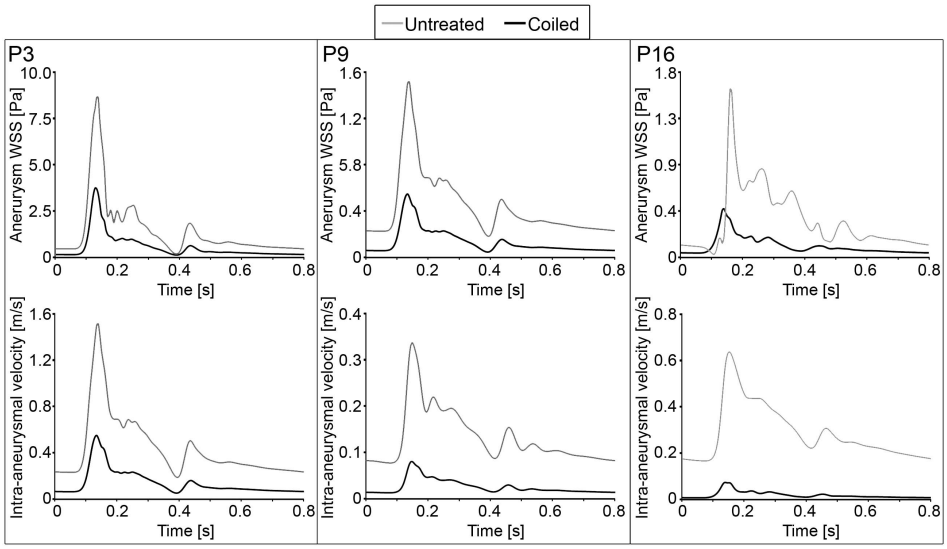

Figure 3.10: Spatial averaged WSS and intra-aneurysmal blood flow velocity magnitude during one cardiac cycle for case P3, P9 and P16.

Fig. 3.11 presents the contrast concentration inside the aneurysm along time for studied cases. Besides, some time points during filling and washout phases were depicted. A reduction in the amount of contrast concentration entering the aneurysm and an increment in its residence time was observed for all cases. These

phenomena were especially well captured in case P16 since after 2.4s of computation (end of the third cardiac cycle), there was still contrast inside the aneurysm fundus.

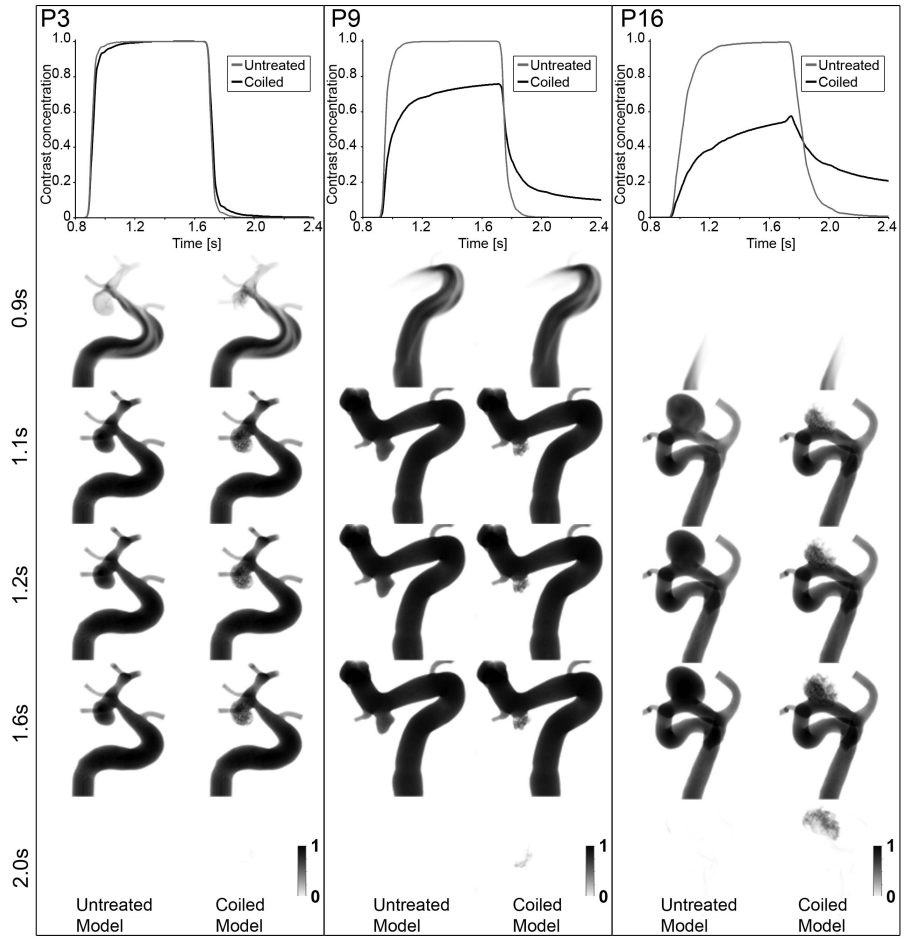

Figure 3.11: Contrast concentration inside the aneurysm during two cardiac cycles (first row) and visualization of the contrast in some time steps during filling and wash-out phases of cases P3, P9 and P16. Coils were hidden to enhance the visualization of the contrast inside the coiled aneurysms.

3.5 Discussion

In this chapter, a virtual coiling technique was presented, tested, validated and applied in combination with CFD, in image-based aneurysm models. The technique is a clinic-oriented tool for understanding endovascular coiling and its effects on intra-aneurysmal hemodynamics.

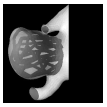

The proposed technique uses dynamic path planning to mimic the coil structure and their distribution inside aneurysms as happen in reality [90, 93]. Reproducing the position and orientation of a sole coil exactly as it happens inside a real aneurysm is challenging. This is due to the limited control that clinicians have during coil deployment, but also to the unrepeatable position and shape that coils adapt when real aneurysms are treated.

The proposed technique aims to understand the macroscopic behavior of the coil, but considering the geometrical features of each device such the diameter. The simplicity of our technique, in term of concepts and development, allows reproducing realistic inserted coils and their distribution inside the aneurysm cavity under real treatment scenarios. This technique is has not been designed for training, where physics-based coiling models are essential [51].

The implementation of the technique can be done within minutes (table 3.1). The number of candidate locations is the most important parameter that impact the computational time. Elevating the number of candidate locations increases the computational time but also enhances the smoothness of the coils and allows a better compliance of coils at the aneurysm wall. A better compliance produces higher densities at the aneurysm periphery for few inserted coils. However, later coils will fill the aneurysm core.

An experiment in sixteen image-based aneurysm models was done to show the capability and reliability of the technique to reach realistic high packing densities in complex morphologies. The descriptive statistics of both volume and NSI, show that our aneurysm models covers a wide range of sizes and shapes compared with other studies with larger aneurysm populations [88, 89]. As a result of this experiment, all aneurysm models including their blebs were successfully coiled, independently of their volume or superficial irregularities. Such aneurysm occlusion is visualized with DSA images (Fig. 3.5) and observed in dissected aneurysms [93].

After testing, the technique was validated in two ways. First, an overall impression of the macroscopic coil behavior was evaluated using clinical data of endovascular coiling performed in five aneurysms. With this validation, we proved that the technique is able to work with real inputs and achieves the highest packing densities obtained by clinicians (excepting case P12 of which data corresponds to a partial status during coiling). The results show that some particular wires can be found due to the unique and unrepeatable coil disposition of both real and virtual treatments as it is expected. Nevertheless, similar occlusion rates as well as remand necks can be visualized on Fig. 3.5. Virtual coiling underestimates the theoretical packing densities, which is due to the assumption of straight tubes in the theoretical evaluation. Still, the mean percentage difference between packing densities was small ($<$3.7%).

The second validation was more incisive and demonstrates that the coil shape, density and distribution inside the aneurysm cavity correspond to what it has been found in histological images of real coiled aneurysms [90]. When few coils are inserted, a higher coil density was found at the aneurysm periphery than at the core region. Then, when more coils were added, ρ_P/ρ_C decreases till it gets close to one (for ρ_T=30%). This aneurysm filling by coils was recently confirmed to occur in real cases [90]. The first coils generate a frame near aneurysm wall,

while coils added later fill the aneurysm core as it was speculated [64, 65].

As in reality, virtual coils are evenly distributed along the longitudinal axis. Moreover, we found more circular than longitudinal coil cut in our histology-like images as it has been visualized in real coiled aneurysms [90].

When the technique is combined with a CFD solver, the intra-aneurysmal hemodynamic alteration induced after coiling can be investigated. Here, CFD simulations in three aneurysms showed that WSS and intra-aneurysmal velocities are reduced after coiling (Fig. 3.10) as it has been reported in coiled aneurysm phantoms [94]. Additionally, it has been observed in phantoms that coils decrease the amount of contrast entering the aneurysm and increase its residence time [95, 96]. Both phenomena were well captured by our CFD simulations, specially in case P16.

Previous computational models that explicitly simulate coils for further CFD analysis, are fully-user dependent and limited to idealized geometries of either the aneurysm or coils [46,47,52]. Moreover, the use of randomly distributed coils does not guarantee to reach high packing densities and a good compliance of the coils with the aneurysm wall [48].

In contrast with the explicit coils in our CFD simulations, an implicit approach using a porous medium can be considered to assess the postoperative hemodynamics [44, 45, 49, 50]. The required spatial discretization in the coiling domain of these models is simpler than ours, and thereby, CFD solutions are faster to compute. However, the main limitations of these models are the isotropy and homogeneity of the medium, as well as the assumed permeability and pressure loss. Our technique does not have such limitations, since it is explicit and model real coil distributions. Moreover, there is no need to solve additional equations or to assume certain parameters to estimate flow motion in the coiled region. Our technique can be used to parameterize those implicit models in the lack of experiments.

The proposed technique neglects both coil mechanical properties and preshape for deployment, which are important limitations to properly understand coils during their insertion. Nevertheless, the macroscopic coil behavior was reproduced and coil density and distribution inside aneurysm cavities were properly validated. Additionally, the interaction of the coils with the aneurysm wall was not considered. The definition of a surface to keep the coils inside the aneurysm also constrains our technique. However, other computational approaches that models coils as the porous medium, also require the neck definition to separate the porous and non-porous domains.

Although higher packing densities are achievable with our technique compared to real coiled aneurysms, the implemented dynamic path planning also has an upper limit. In general, packing densities over 40% are difficult to obtain with our technique unless the parameters are particularly modified for the aneurysm model under evaluation.

Limitations of the CFD simulations are related to the assumption of rigid wall, Newtonian viscosity of the blood, and constraints in the coil motion (solid and rigid obstacles). The last issue is an interesting topic for future work, since a fluid-structure interaction model of coils and blood flow can help to understand the mechanisms of coil compaction.

3.6 Conclusions

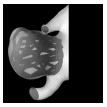

In this chapter, a virtual coiling technique for treating image-based aneurysm models was proposed. The technique uses dynamic path planning to mimic the coil structure and distribution inside aneurysm cavities and to reach high packing densities. The technique was tested and validated using information from the literature and clinical data. We found that our virtual coiling technique reproduces the macroscopic behavior of the coils by occluding completely the aneurysm model, independently of aneurysm volumes, morphologies or the presence of blebs. Besides, coil distribution, shape and density inside the aneurysm were properly captured with the technique. Finally, a practical application of the proposed technique was shown by assessing the local hemodynamic changes due to coils using CFD. Coils reduced both WSS and intra-aneurysmal velocity. Moreover, coils decrease the amount of contrast entering the aneurysm and increase its residence time.

4

Validating Hemodynamic Modeling

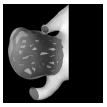

Endovascular coiling is a well-established therapy to treat cerebral aneurysms. However, its outcome is not always predictable. The purpose of this chapter is to present the validation of the proposed virtual coiling technique and computational fluid dynamic (CFD) simulation based on the comparison with *in vivo* medical images. For this, a patient harboring a coiled aneurysm was selected. A three-dimensional vascular geometry derived from medical image was used. The aneurysm geometry was virtually coiled. Afterwards, a CFD model was constructed simulating the bolus injection of a contrast material. The injection was done using time-intensity curves (TIC) obtained from a digital subtracted angiography (DSA) image sequence. A qualitative comparison between real and virtual angiographic images, and the quantitative differences between TICs were assessed. As a result, the CFD model properly reproduced the global aspects of the injected contrast agent along the vascular model, including the branches downstream the coiled aneurysm.

The content of this chapter is adapted from the following publication:

H.G. Morales, I. Larrabide, M.-C. Villa-Uriol, A.J. Geers, A.F. Frangi. Towards the validation of a virtual coiling technique using a real versus simulated bolus injection. In *2nd International Conference on Mathematical and Computational Biomedical Engineering (CMBE), Washington, USA*. pp. 513–515, 2011.

4.1 Introduction

Cerebral aneurysms are arterial dilatations often occurring at branching points in the circle of Willis [1]. One of their treatment options is endovascular coiling [23]. This minimally invasive therapy tries to prevent aneurysm rupture and further subarachnoid hemorrhage (SAH) by inserting biocompatible metal wires inside the aneurysm cavity. Hemodynamics plays a crucial role in the success of endovascular coiling by triggering (or not) intra-aneurysmal thrombosis. Moreover, pulsatile blood flow can compress and compact coils within the aneurysm over time and cause aneurysm recanalization [1, 20], which could leads to a delayed SAH.

To study hemodynamic alterations induced after coiling, computational fluid dynamics (CFD) has grown as a valuable tool due to its predictive capability and possibility to evaluate treatments when it is not feasible by other means without endanger patient's life. These features provide a potential clinical impact of CFD, especially at pre-operative planning and post-treatment diagnosis. Nonetheless, to evaluate the reliability and accuracy of numerical approaches, a proper validation is mandatory. To validate CFD simulations of hemodynamics in cerebral vasculature, virtual angiographies has been proposed as a means [97]. This validation approach has been used by several publications with promising results [60, 98].

The purpose of this chapter was to validate a CFD simulation in a virtually coiled aneurysm model by the virtual angiographic approach. The CFD model was geometrically and hemodynamically constructed from medical images of the patient.

4.2 Material

A 37-years old female harboring a right middle cerebral artery bifurcation aneurysm was selected for this study. One three-dimensional rotational angiography (3DRA) image before and another after endovascular coiling were acquired using a Philips Integris System (Philips Healthcare, Best, The Netherlands). A digital subtraction angiography (DSA) image sequence was also acquired and was synchronized with the bolus injection of a contrast agent during 2.5 s at 4 ml/s. DSA images were acquired at 60 frames per second for a period of 7.8 s. Treatment information, i. e. number of coils, diameters and lengths was also recorded.

4.3 Method

To simulate the blood flow in this image-based vascular model with a bolus injection, geometrical and hemodynamic information was extracted from the medical images. Fig. 4.1 shows the pipeline that was used to obtain the vascular geometry and flow boundary conditions to properly construct the CFD simulation.

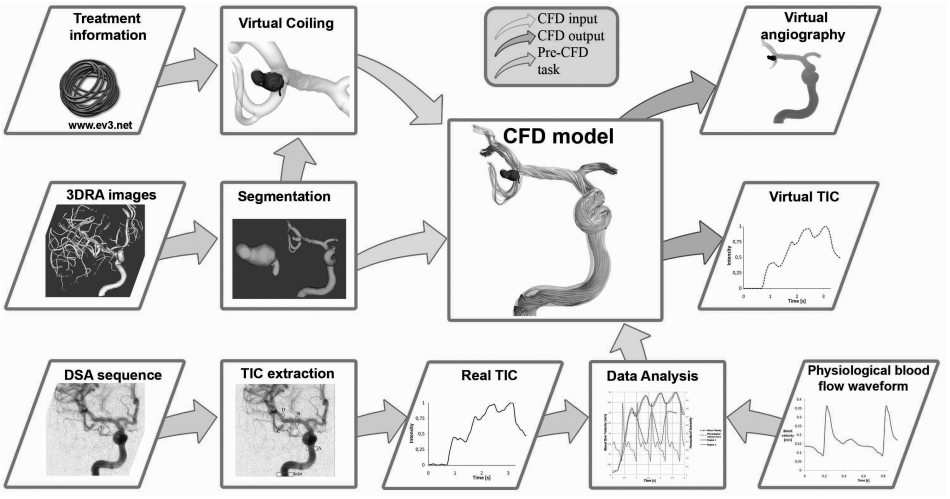

Figure 4.1: Pipeline for CFD setup using geometrical and flow information from medical images. Colored version on page xxvi.

4.3.1 Vascular Models

A three-dimensional (3D) representation of the vascular luminal surface was extracted from the region of interest of the acquired 3DRA image before coiling. The vascular surface was obtained using a geodesic active region method combined with an image intensity standardization technique [87]. Then, the resulting 3D geometry was cropped, cleaned and smoothed using the in-house software, GIMIAS [99].

The same method was applied on the 3DRA image after coiling without contrast and the resulting 3D geometry was combined with the aneurysm surface previously created to extract a similar volume where the coils were actually inserted. This new volume was called coiled region. Afterwards, the virtual coiling technique was applied on the coiled region [86, 100], using as input the diameters and lengths of the real inserted coils.

The virtual coiling technique sequentially inserts the coils by advancing its tip through a planned path, starting from an initial position and direction inside the coiled region. To build the path, the coiling technique avoids coil migration outside the coiled region and the collisions between coils by smoothly changing the advancing tip direction. If the coil tip is trapped by other coils, the technique retreats the coil tip and redirects its advance. As a result, the virtual coiling produced a similar representation of the real inserted coils, including the small coil segment protruding in the parent artery of this specific aneurysm (Fig. 4.2). The generated packing density, defined as the ratio between the coils and coiled region volumes, was 43%.

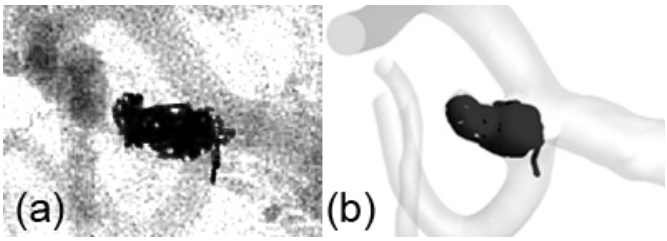

Figure 4.2: Coiled aneurysm. (a) DSA image. (b) Virtual image.

4.3.2 Computational Fluid Dynamics

Once the geometric models were obtained, a volumetric mesh was created. The mesh was generated using the commercial software ANSYS ICEM-CFD v11 (Ansys Inc., Canonsburg, PA). This volumetric mesh was exported in the CFD solver package, ANSYS CFX v11, to compute the fluid flow governing equations.

Blood was modeled as a Newtonian incompressible fluid with viscosity and density of 0.00375 Pa·s and 1060 kg/m^3, respectively. Flow was assumed to be laminar. Vessel wall and coil surfaces were imposed as rigid with no-slip boundary condition. At the outlets, a traction-free boundary condition was applied. For the inlet flow boundary condition, a physiological blood flow waveform from a validated one-dimensional model was used [43], but a modified version was imposed in the model. This modification was done as follows.

The flow waveform at the inlet was scaled based on the estimation of the mean flow velocity, calculated with time-intensity curve (TIC) approach [101] at different locations in the vasculature. Besides, the increase of flow rate due to the bolus injection was considered using the information of the real contrast injection (see plot at inlet region in Fig. 4.3). The cardiac period was 0.6 s, and it was derived from the averaged time differences between consecutive peaks or valleys presented in the TIC.

To compute the contrast propagation through the vasculature, a scalar field of its concentration was solved from a transport equation following the strategy of a previous validated CFD study [98].

The TIC at the inlet region of the DSA images was imposed as boundary condition for the contrast concentration at the inlet of the CFD model (Fig. 4.3) with a homogeneous distribution. The TICs computed from the CFD simulation were calculated using the contrast concentration at the control regions defined in the medical images (Fig. 4.3). Each TIC was normalized based on the highest value of each curve. The visualization of the virtual angiography images were done by volume rendering as was previously performed [102].

Four seconds were computed in total, which was divided in time-steps of 0.0005 s. The first cardiac cycle (from 0 to 0.6 s) was discarded to remove transient effects of the initial flow conditions. The CFD results were taken every 0.005 s.

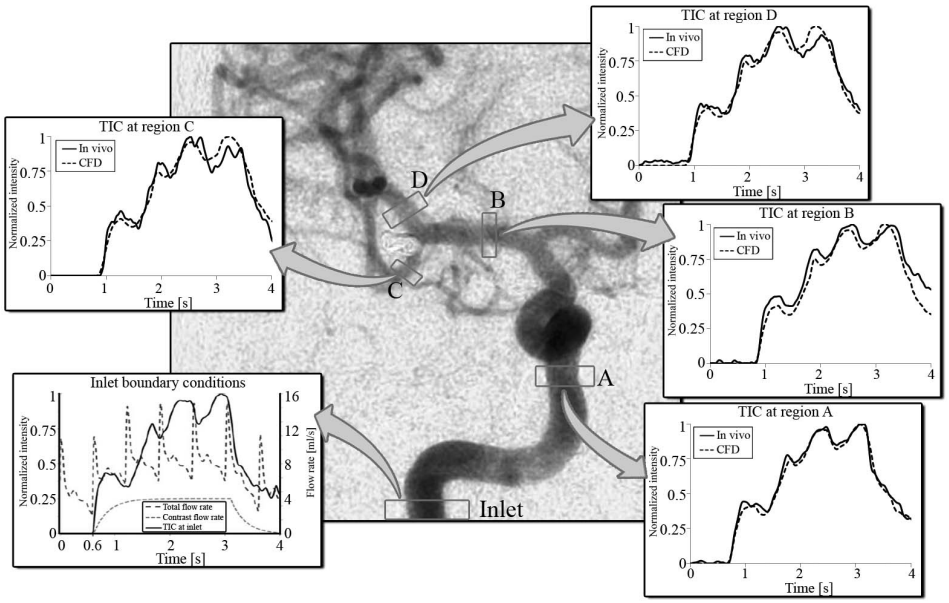

Figure 4.3: DSA image with the control regions for TIC measurements. Plots present the measured and simulated TIC.

4.4 Results

In Fig. 4.3, the TICs of the DSA sequence and CFD simulation are presented at the four control regions in the vasculature. The plots show 4 s in total, including the initial part of the wash-out phase.

For qualitative assessment, Fig. 4.4 depicts DSA sequence with the corresponding virtual angiography obtained from the CFD simulation at different time instants during the contrast filling phase. Once the vasculature was full of contrast, TIC oscillations (Fig. 4.3) were not visible.

4.5 Discussion

In this chapter, the validation of a CFD simulation in a coiled aneurysm was done using one image-based model. The CFD simulation was constructed based on geometric and hemodynamic information extracted from the patient medical images (3DRA and DSA sequence). To validate the CFD simulation, a virtual angiography that models the transport and propagation of an injected contrast material was used.

Figs. 4.4 and 4.3 show the qualitative and quantitative comparison between DSA sequence and CFD simulation, respectively. Qualitatively, the intensity of the contrast shows a good correspondence between the DSA sequence and the virtual angiography (Fig. 4.4). Quantitatively, all control regions present similar

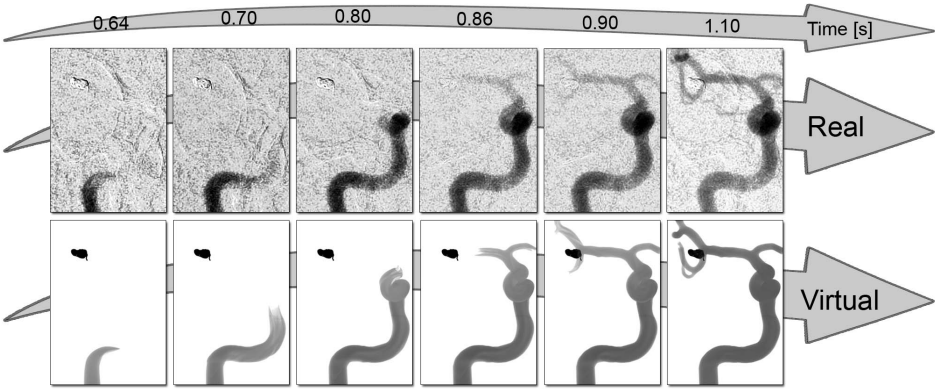

Figure 4.4: Visualization of DSA sequence and virtual angiography images at some time instances.

TIC for both DSA sequence and CFD simulation.

The CFD model was able to capture the global flow characteristics obtained from the intensity of the contrast injection, including the regions downstream the aneurysm (control regions C and D in Fig. 4.3). A good agreement between the TICs was observed, especially when the contrast arrived at the control regions, peaks and valleys of the TIC and the intensity gradient during the filling and wash-out phases.

With this study, we also show that it is feasible to obtain both geometry and flow boundary conditions to construct and to validate an image-based CFD simulation. However, a high-frequency DSA sequence is required to capture the peaks valleys and arrival times of the TIC. A lower resolution increases the deviation of the measurements and might produce inaccuracies in the estimation of the mean flow velocity and cardiac frequency.

Finally, TICs of Fig. 4.3 show only 4 s, even though 7.8 s were available from the DSA sequence. This was done since the superposition of the arteries of interest with other vessels and veins downstream in the DSA sequence, introduces important changes in the background of the medical images, generating an overestimation of the TIC after the fourth second. This changes in the background only allows the inclusion of the initial part of the wash-out phase.

4.6 Conclusions

In this chapter, we have validated a CFD simulation of a image-based coiled aneurysm. The geometry and flow boundary conditions were taken from the patient medical images. Good agreement was found between the DSA sequence and virtual angiography results, as well as between the TICs along the vasculature including downstream the coiled aneurysm.

5

Coil Configuration and Packing Density

Although coiling is a well-established therapy for treating cerebral aneurysms, its postoperative hemodynamic changes induced by this therapy remain not fully understood. In this chapter, the influence of coil configuration and packing density on intra-aneurysmal hemodynamics was assessed.

Three-dimensional rotational angiography images of three cerebral aneurysms before and after endovascular coiling were used. For each aneurysm, a three-dimensional representation of the vasculature was obtained after image segmentation. Afterward, a virtual coiling technique was used to treat the aneurysm geometries with coil models. The aneurysms were coiled with five packing densities, and each was generated by using three coil configurations. Computational fluid dynamics analyses were carried out in both untreated and treated aneurysm geometries. Statistical tests were performed to evaluate the relative effect of coil configuration on local hemodynamics.

The intra-aneurysmal blood flow velocity and wall shear stress were diminished as packing density increased. Aneurysmal flow velocity was reduced>50% due to the first inserted coils (packing density <12%) but with a high dependency on coil configuration. Nonsignificant differences (p >0.01) were found in the hemodynamics due to coil configuration for high packing densities (near 30%). A damping effect was observed on the intra-aneurysmal blood flow waveform after coiling.

Intra-aneurysmal hemodynamics are altered by coils. Coil configuration might reduce its influence on intra-aneurysmal hemodynamics as the packing density increases until an insignificant influence could be achieved for high packing densities.

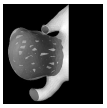

The content of this chapter is adapted from the following publication:

H.G. Morales, M. Kim, E.E. Vivas, M.-C. Villa-Uriol, I. Larrabide, T. Sola L. Guimaraens, A.F. Frangi. How Do Coil Configuration and Packing Density Influence Intra-Aneurysmal Hemodynamics? AJNR Am J Neuroradiol. 32(10):1935-1941, 2011.

H.G. Morales, M. Kim, E.E. Vivas, A.F. Frangi. Influence of Coil Packing Rate and Configuration on Intracranial Aneurysm Hemodynamics. In *World Congress on Medical Physics and Biomedical Engineering, 11th International Congress of the IUPESM. Munich, Germany.* pp. 2291-2294. 2009.

5.1 Introduction

Cerebral aneurysms are balloon-like dilatations of arteries often occurring at branching points in the circle of Willis. In most cases, they stay asymptomatic and are only diagnosed through medical imaging or after their spontaneous rupture. Aneurysm rupture typically leads to subarachnoid hemorrhage producing rates of mortality of about 50% [3]. The existing therapeutic options seek isolating the aneurysm from the blood stream and preventing its rupture. The most important therapies are surgical clipping and endovascular interventions [13], such as coiling and stenting.

Coiling has been the most popular endovascular option for the last fifteen years [3, 13, 25]. This minimally invasive treatment consists in the placement of biocompatible metal alloy coils flow to block the blood into the aneurysm and to prevent the rupture. Although coiling is associated to lower mortality and morbidity rates compared to surgical clipping [13], its outcome is not always predictable [3, 13, 25, 78, 103]. Packing density is thought to have a strong influence in post-coiling outcome, and usually the aneurysms are packed as dense as possible [77–79]. Packing density is defined as the ratio between the inserted coils and aneurysm volume.

Moreover, the success of coiling is intimately related to the biological responses to hemodynamics inside the aneurysm [37]. Certainly, computational fluid dynamics (CFD) is an effective and well-accepted technique to investigate the intravascular hemodynamics in silico [104]. However, the use of this technique in the presence of endovascular coils is still challenging, due to the geometrical complexity of the devices, their small size (diameters of 0.010 to 0.015 inch [105]) and their unpredictable distribution inside the aneurysm.

To simulate the hemodynamics in coiled aneurysm geometries, researchers have modeled explicitly the coils, including straight [47] or helical cylinders [52], big hollow spheres [46] or small overlapping spheres along the axis of curved filaments [48]. Other approaches assume that coils act as a porous medium inside the aneurysm [44, 45, 49, 50]. Most of these studies have taken into account the influence of packing density on the hemodynamics. However, little is known about how coil configuration, i.e., the arrangement of coils inside the aneurysm, could affect the blood flow. Recently, an in vitro experiment has studied qualitatively the influence of both coil configuration and packing density, but only on near-wall flow [70]. Additionally, a CFD-based study on an idealized sidewall aneurysm geometry found that the orientation of helical coils has influence on intra-aneurysmal hemodynamics [52].

The purpose of this chapter is to qualitatively and quantitatively assess the influence of coil configuration and packing density on intra-aneurysmal hemodynamics. Three image-based aneurysm geometries were virtually treated with coils, and CFD simulations were performed in both untreated and treated geometries. The main hypothesis behind our CFD experiments was that intra-aneurysmal hemodynamics strongly depends on the mechanical resistance produced by the coils as it was previously reported in the literature [91].

5.2 Material

Three aneurysms at different locations in the human brain vasculature were chosen. The locations for cases 1, 2 and 3 were respectively left internal carotid sinus, right middle cerebral artery bifurcation and basilar tip. All three cases were selected for treatment with endovascular coils. Three-dimensional rotational angiography (3DRA) images of the aneurysms were obtained using a Philips Integris System (Philips Healthcare, Best, The Netherlands). The size of the images in voxels was 256x256x256, with a field of view of 134.95 mm. A three-dimensional (3D) representation of the luminal surfaces of the vessels and aneurysms were obtained after segmentation of the medical images using an iso-intensity surface extraction approach. Afterwards, the extracted 3D geometries were cleaned, cropped and smoothed [99].

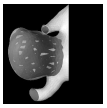

5.3 Method

5.3.1 Virtual Coiling

Cases were treated using a virtual coiling technique [86, 100, 106]. This technique was designed to place coil models inside image-based aneurysm geometries. Coils are characterized by their geometry, namely wire diameter and length.

Each coil is progressively placed by advancing its tip, which starts from an initial position inside the aneurysm. The coil tip motion is constrained by the aneurysm dome and its ostium. If the tip of the coil is close to either the surface of the aneurysm or another coil previously inserted, the tip smoothly changes its direction to remain inside the aneurysm and to avoid collision with the other coils. When the coil tip cannot move further because it is blocked by other coils previously placed, the virtual coiling technique partially retracts and redirects the tip towards another region.

The technique sequentially places the coils inside the aneurysms until the desired packing density is achieved. As a result, a plausible representation of the distribution of the coils is produced as it could be obtained after a real intervention (see Fig. 5.1).

This virtual coiling technique was used in our three cases. Five coil packing densities were produced (table 5.1). Packing densities were calculated from the volumes of the 3D geometries. Besides, for each packing density, three coil configurations were generated and labeled as I, II and III. In this way, the influence of geometrical dissimilarities due to the coil configuration on intra-aneurysmal hemodynamics could be evaluated.

5.3.2 Hemodynamic Modeling

To solve the governing equations of fluid flow, body-fitted unstructured tetrahedral meshes were generated with the vascular geometries and coils using the commercial

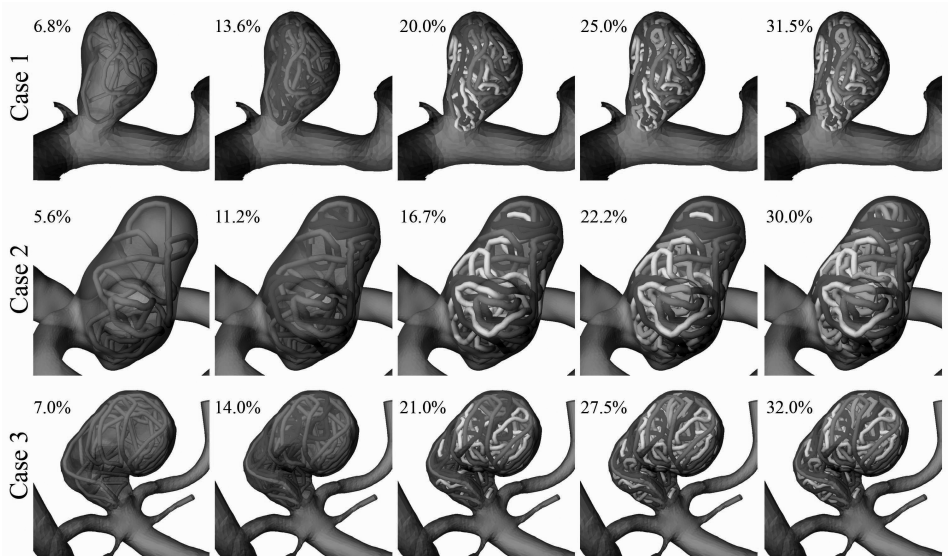

Figure 5.1: Results of virtual coiling in all cases. Percentages indicate coil packing densities. Colored version on page xxviii.

Table 5.1: Design parameters of virtual coiling experiments

Case #	Aneurysm Volume [mm^3]	Coil Diameter [mm]	Coil Length [cm]	Packing Densities [%]
1	107	0.304	5 to 30	6.8, 13.6, 20.0, 25.0, 31.5
2	423	0.457	4 to 30	5.6, 11.2, 16.7, 22.2, 30.0
3	635	0.457	4 to 30	7.0, 14.0, 21.0, 27.5, 32.0

software ANSYS ICEM-CFD v11 (Ansys Inc., Canonsburg, PA). In the treated models, the volumetric mesh near the coils was refined, and a convergence test was performed to obtain mesh-independent CFD simulations. The test criterion was set to be below 5% of differences of the averaged wall shear stress (WSS) at the aneurysm between consecutive mesh refinements. Average WSS was found to fulfill this criterion when the coil cross section perimeter was enclosed with approximately 10 mesh elements.

These volumetric meshes were exported in ANSYS CFX v11 (Ansys Inc., Canonsburg, PA) for the CFD simulations. Blood was modeled as a Newtonian fluid with viscosity of 0.00375 Pa· s. Flow was assumed to be laminar and incompressible (blood density of 1060 kg/m^3). Vessel wall and coil surfaces were imposed to be rigid with no-slip boundary condition on the flow. At the inlet of the models, a parabolic velocity profile (spatial condition) was imposed as well as a physiological blood flow waveform (temporal condition) from a normal individual. These flow waveforms were scaled to ensure a time-averaged Reynolds number of 300 at the inlet of each model. At the outlets, a traction-free boundary condition

was applied.

Two entire cardiac cycles were simulated and the results from the second one were analyzed as time-averaged, and at peak systole and end-diastole. The blood flow velocity, the average WSS, and the areas of low (<0.4 Pa) and high WSS (>1.5 Pa) were evaluated in the aneurysm. These WSS thresholds were selected because of their association with pathologic states of the arterial wall [35].

5.3.3 Statistical Evaluation

Analysis of variance (ANOVA) tests were performed to evaluate the relative effect of the coil configuration on the intra-aneurysmal hemodynamics at different packing densities. The results for an entire cardiac cycle were taken into account as samples for the tests. Before applying the tests, the hypotheses of normal distribution, homogeneity of the variance and independence were confirmed for each sample.

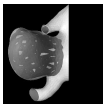

5.4 Results

5.4.1 Qualitative Findings

Fig. 5.2 depicts velocity magnitudes at peak systole on a fixed aneurysm cross section for all cases. changes in packing densities are shown in Fig. 5.2a-c, while Fig. 5.2d compares different coil configurations for case 2. The untreated aneurysms showed high-velocity regions with strong flow impingement on the distal wall and a vortical flow structure inside the aneurysm. For packing densities below 11.2%, inflow was disturbed and aneurysmal flow velocity was decreased, especially at the aneurysm fundus. As the number of coils increased, a progressive reduction in the flow velocity inside the aneurysm was observed. Nonetheless, small additional velocity reductions were associated for coil packing densities above 22.2%. Furthermore, Fig. 5.2d shows how two coil configurations for case 2 were able to visually induce substantial differences on the flow fields at a low packing density, such as 11.2%.

Visualization of WSS distributions at peak systole and end-diastole are respectively presented in Fig. 5.3a and 5.3b. Here, simulations for case 2 are showed with and without coils. A reduction of WSS was already observed for a low packing density 5.6%, while above 16.7%, a stable low WSS throughout the cardiac cycle was found at the aneurysm dome. A remarkably high WSS at peak systole near the aneurysm neck were also observed. Similar WSS distributions, as well as flow structures and velocity reduction trends were visualized for cases 1 and 3.

5.4.2 Quantitative Findings

Time-averaged velocity reduction inside the aneurysm based on the untreated model was computed for the different coil configurations and packing densities (see Fig. 5.4a). The velocity reduction was almost independent of the coil configuration

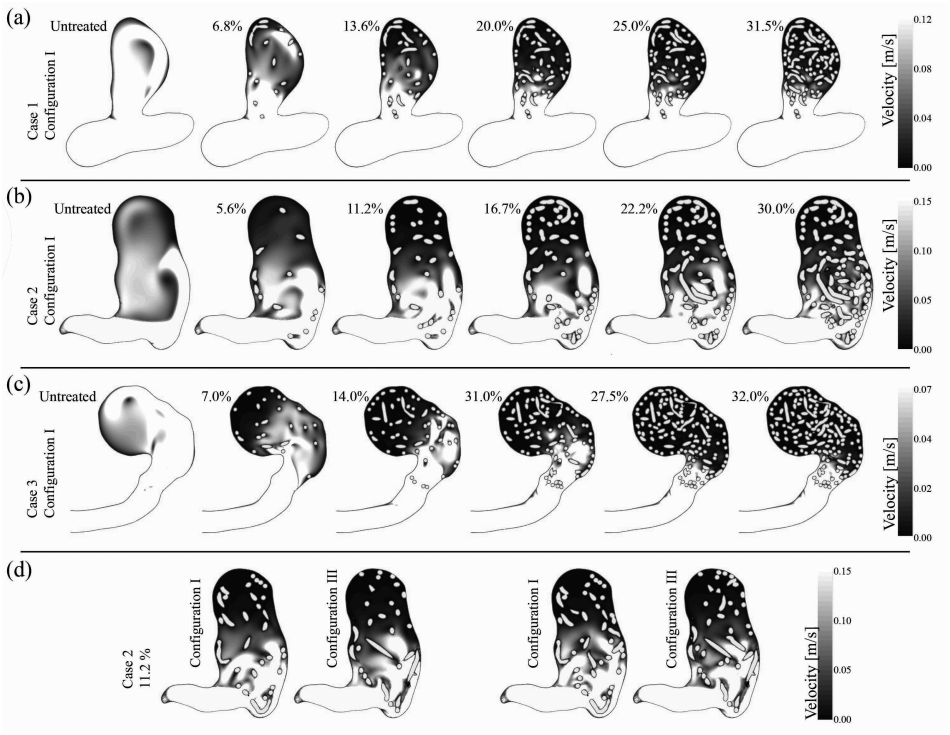

Figure 5.2: Blood flow velocity magnitudes in grayscale for an aneurysm-cross section at peak systole for all cases. (a-c) Changes in the velocity are presented with a fixed coil configuration and increasing packing density for all cases. In (d) two coil configurations are compared for packing densities of 11.2% and 16.7% of case 2. The coils are presented in yellow and the percentages represent the packing densities achieved for each model. Colored version on page xxvii.

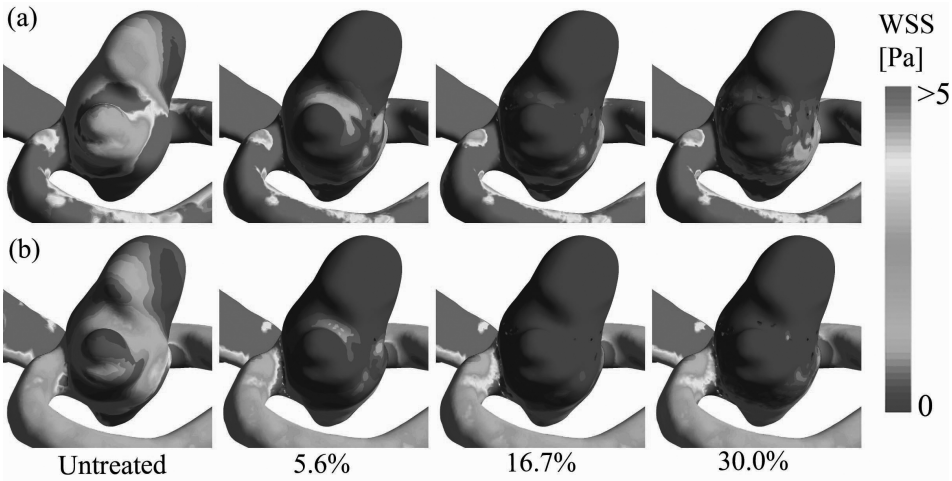

Figure 5.3: WSS distributions for the untreated and several treated models for case 2, calculated at peak systole (a) and end-diastole (b). Colored version on page xxviii.

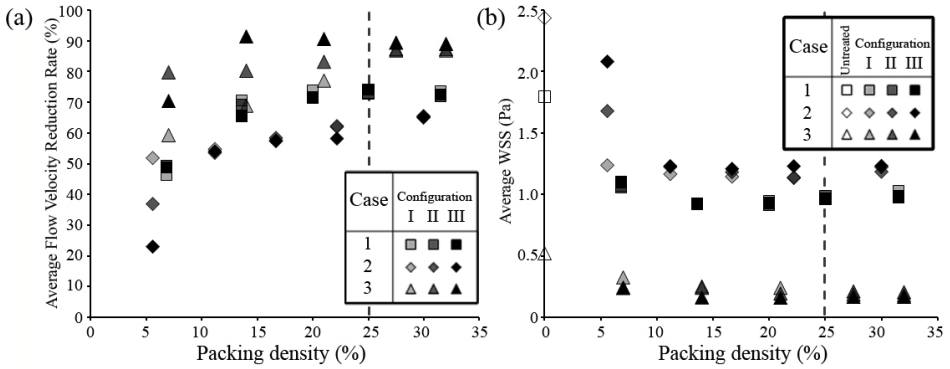

Figure 5.4: (a) Time-averaged intra-aneurysmal mean flow velocity reduction rate. (b) Time-averaged WSS at the aneurysm dome.

for packing densities above 25%. In general, velocity reduction increased as packing density rose. For high packing densities (near 30%), the coils induced a maximum velocity reduction of approximately 70% for case 1, 65% for case 2 and almost 90% for case 3.

Fig. 5.4b shows time-averaged aneurysmal WSS. For all cases, a reduction in WSS was found after coiling, even for those with lower packing densities. A progressive decrease of the average WSS was observed as packing density increased. For low packing densities (<10%), a large variability in the average WSS was induced by the coil configuration, especially for case 2 with 5.6% of packing density (mean WSS of 1.65 Pa and standard deviation of 0.4 Pa).

To analyze the evolution of the WSS in a cardiac cycle, the areas of low (<0.4 Pa) and high (>1.5 Pa) WSS were computed for each aneurysm. In Fig. 5.5, these areas were presented for three CFD models of all cases, including the untreated simulation. A clear difference on these areas is visualized among simulations with and without coils. After coiling, low WSS areas increased and reached values of around 75% for case 1, 60% for case 2 and 95% for case 3. High WSS areas decreased and were around 20% for cases 1 and 2, and below 10% for case 3. Besides, there were noticeable differences in the WSS areas due to the coil configuration for packing densities below 27.5% in all cases, especially near peak systole. However, these differences were less evident as packing density increased.

5.4.3 Analysis of Statistical Data

The ANOVA test results (table 5.2) showed that there were non-significant differences (p>0.01) on the average WSS and high WSS areas due to the coil configuration when packing density was over 20%. However, there were significant differences (p<0.01) in the velocity reduction and low WSS areas when the packing density was below 22.2% in all three cases (case 2 had the highest packing density). The only exception to this result was for the low WSS areas in case 1, in which the differences induced by the coil configuration were negligible. Table 5.2

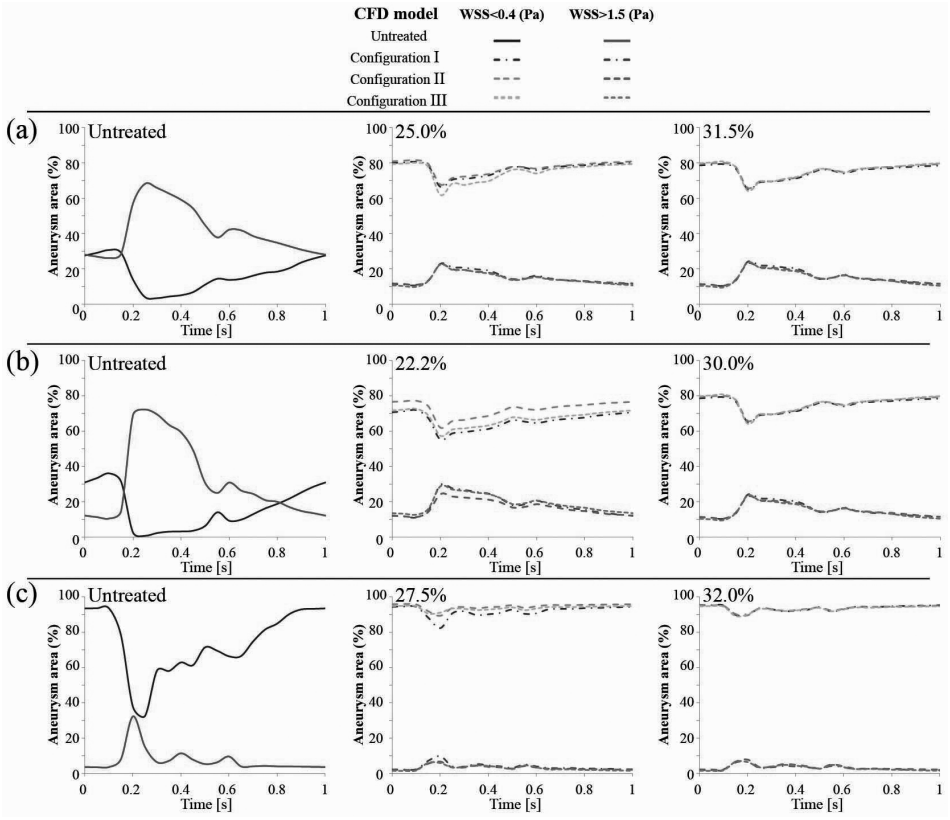

Figure 5.5: Variation of aneurysm areas with low and high WSS expressed as a percentage of the whole aneurysm dome (%) during one cardiac cycle for all cases. (a) case 1, (b) case 2 and (c) case 3. Colored version on page xxviii.

also shows that, for the studied cases, the hemodynamic variables derived from different coil configurations were non-significant for packing densities about 30%.

5.5 Discussion

The present study aims at elucidating how packing density and coil configuration might influence the intra-aneurysmal hemodynamics. Four main findings were obtained from our numerical modeling and data analyses. First, the intra-aneurysmal velocity and WSS decreased as packing density increased. Second, the influence of coil configuration on intra-aneurysmal hemodynamics showed to be negligible for elevated packing densities (near 30%). However for lower packing densities, this influence was larger and statistically significant. Third, aneurysmal flow velocity was reduced by more than a 50% after the insertion of the first coils (packing den-

Table 5.2: *p*-values of ANOVA tests performed for each of the cases at different packing densities.

Case #	Packing density [%]	p-values obtained from ANOVA tests for			
		Velocity Reduction Rate	Average WSS	Low WSS Area	High WSS Area
1	20.0	0.001∗	0.981	0.245	0.834
	25.0	0.064	0.988	0.533	0.886
	31.5	0.127	0.914	0.269	0.723
2	22.2	0.000∗	0.927	0.000∗	0.309
	30.0	0.869	0.981	0.181	0.956
3	21.0	0.000∗	0.373	0.002∗	0.163
	27.5	0.077	0.601	0.757	0.583
	32.0	0.155	0.655	0.760	0.552

∗ Means significant difference due to coil configuration ($p<0.01$)

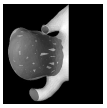

sity <12%). Fourth, evidence was found that the blood flow waveform is damped near the aneurysm wall as packing density increases, which was reflected in the flattening of the areas with low and high WSS.

These findings were obtained by qualitative observations, analyses of quantitative data, and statistical evaluations of our CFD simulations. The first hemodynamic variable analyzed was blood flow velocity inside the aneurysm. In Fig. 5.2, a progressive reduction of the velocity inside the aneurysm was observed as packing density increased. This finding is consistent with previous CFD-based studies and in-vitro experiments [48, 50, 52, 70, 94]. Particular flow patterns were visualized due to the coil configuration (see Fig. 5.2d), which are associated to the special location of the coils at the aneurysm ostium. Specific flow characteristics were also reported by an in vivo study, in which short and disturbed streamlines were found near the aneurysm wall [70].

The second evaluated hemodynamic variable was average WSS. In Fig. 5.3, a stable (systole and diastole) low WSS distribution (blue area) was found as packing densities were above 16.7%. This was mainly observed in the aneurysm fundus. Furthermore, high WSS (red areas) were localized at the aneurysm neck, which is associated to the blockage and reflection of the flow stream due to the coils. These WSS distributions were previously observed in a CFD-based study modeling the coils as a porous medium [45]. Besides, the reduction of average WSS as packing density increased was noticeable in Fig. 5.3 by the increment of the blue area.

The third hemodynamic variable was the intra-aneurysmal velocity reduction. In Fig. 5.4a, the previous qualitative observations were confirmed as for the influence of packing density and coil configuration on the local hemodynamics. The efficiency of the coils reducing the intra-aneurysmal flow velocity depends on coil configuration and packing density as is visualized among cases. Furthermore, the dependency of the velocity reduction on coil configuration was lower for high packing densities (>25%).

For our three cases, the insertion of the first coils (packing densities <12%) produced the most important velocity reduction (over 50%) inside the aneurysm.

However, more variability of the velocity reduction was induced by low packing densities (see cases 2 in Figs. 5.3 and 5.4). In general, an asymptotic trend of the velocity reduction was observed as packing density increased. In other words, the last coils have a smaller role in the velocity reduction inside the aneurysm. Additionally, the maximum velocity reduction observed in Fig. 5.4a for our cases (for 70% to 90%), corresponds well to previous CFD-based studies [45] and in vivo animal experiments [107].

The last hemodynamic variables studied were the aneurysmal areas of low (<0.4 Pa) and high (>1.5 Pa) WSS, presented in Fig. 5.5. Here, the high/low WSS areas were damped by the coils, suggesting that the hemodynamics near the wall tends to be steady as packing density increases. However, the damping was strongly related to packing density. Furthermore, most of the variations in WSS areas happened near the aneurysm neck (see Fig. 5.3), and thereby, WSS at the aneurysm dome was almost time-invariant. This steady hemodynamic condition at the aneurysm wall combined with the previously mentioned low-shear stresses and low velocity flow might be favorable hemodynamic conditions to isolate the aneurysm from blood stream [37,108]. Additionally, it was observed how coil configuration reduces its influence on hemodynamics when packing density increases (Fig. 5.5).

The statistical tests were performed to study the variability induced by the coil configuration as packing density increased on the studied hemodynamic variables. We found that coil configuration has an influence on intra-aneurysmal hemodynamics when packing density is low. However, the hemodynamic dependence on coil configuration was reduced as packing density increased. This dependence was statistically non-significant ($p>0.01$) for packing densities about 30%.

From our results, we observe that intra-aneurysmal hemodynamics tends to stabilize as packing density increases and becomes independent of coil configuration. However, the reported packing densities do not ensure the success of coiling, mainly because the required hemodynamic conditions to warranty aneurysm occlusion by coiling are unknown. Besides, the presented results are based on the flow waveforms imposed as boundary conditions, which were physiologic and measured under rest condition but neither patient-specific nor general. As it has been found that local hemodynamic forces are associated with heart rate and aneurysm geometry [109], further investigation is required to generalize and/or extrapolate our findings to other physiological flow waveforms (different heart rate, flow rate, or waveform shape) and different vascular morphologies.

Our results have shown to be comparable to previous CFD-based studies with coils, but our virtual coiling technique presents some advantages over them. The first advantage is that our technique has the potential of becoming relevant in clinical practice. It is able to reproduce the wide range of packing densities as it is obtained in real interventions [77–79] and in vitro experiments with coils [110]. Furthermore, it considers the geometrical specifications of coils, such as wire diameter and length, and can be used in image-based geometries. The technique uses medical images before treatment to extract the 3D representation of the vasculature, and the manual definition of the ostium to constrain the space occupied by the coil models provides a tool for preoperative hemodynamic assessment. Addi-

tionally, the use of images after treatment allows us to extract similar regions to insert the coils as the ones visualized with medical images, which provides post-operative hemodynamic assessment.

The other advantage is the explicit modeling of the coils, which allowed us to investigate the influence of coil configuration and packing density on the intra-aneurysmal hemodynamics. Certainly, packing density can be modeled with a porous medium approach by setting the porosity [45, 49, 50] but the simulation of different coil configurations is not trivial due to the assumptions of homogeneity and isotropy of the medium. On the other hand, in the study of Cebral and Löhner [48] it was proposed an explicit modeling of the coils for further CFD analysis. However, it is not clear the packing densities that can be achieved with the generation of arbitrary objects and more specifically, the coil distribution near the aneurysm walls. Finally, the helical coils presented by Schirmer and Malek [52] in an idealized aneurysm geometry are fully user-dependent and did not achieve high packing densities.

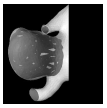

Despite these advantages and our interesting findings, this chapter has some limitations. One is that the coils were assumed as rigid bodies and their motion was not allowed in our CFD simulations, which means that the coils were not affected by the flow. Although this assumption considerably simplifies the numerical solution, coil deformation as well as a more precise interaction with the flow should be taken into account to investigate other relevant issues related to this therapy, such as coil compaction. Also, another limitation is that the vessel and aneurysm walls were considered as rigid bodies due to the lack of information regarding wall thickness and mechanical properties of the tissue. Nevertheless, such choice is supported by several CFD-based studies that assumed the rigid wall condition and claimed that this effect is minor when compared to others, such as lumen morphology [39, 45, 48–50].

A CFD simulation able to assess the success or failure of coiling an aneurysm should consider the thrombus formation inside the aneurysm. In this chapter, thrombus formation was not tackled since efforts were mainly focused on evaluating the hemodynamic resistance of the coils as these have been found to be relevant experimentally [91]. Additionally, thrombus formation has been related to hemodynamics and blood viscosity [37]. Our study was limited to the use of a Newtonian model for blood viscosity and further investigation is required to establish the influence of the non-Newtonian behavior of blood on the hemodynamics of coiled aneurysms. On the one hand, the assumption of Newtonian flow is justified since it has been reported to be as good as non-Newtonian models in similar studies in arteries with aneurysms when compared to the uncertainties introduced by geometrical models [39]. This aspect has also been recently used to assess the effect of flow diverters on intra-aneurysmal hemodynamics [111]. On the other hand, the consideration of a non-Newtonian model opens questions such as which non-Newtonian model (e.g. Casson, Herschel-Bulkley or Power law) represents more accurately the behavior of blood and why, which are the differences and similarities when compared to a Newtonian model, and are if these differences are meaningful.

5.6 Conclusions

We have studied the influence of coiling treatment on intra-aneurysmal hemodynamics in three image-based aneurysm geometries using a virtual coiling technique and CFD modeling. Four main findings were extracted from our results. First, coils attenuate blood flow velocity and WSS with increasing packing density. Second, the influence of coil configuration on intra-aneurysmal hemodynamics is reduced with increasing packing density, such that no significant influence ($p>0.01$) is found for packing densities of 30%. Third, the first inserted coils (packing density <12%) cause more than 50% of the velocity reduction inside the aneurysm. Finally, a damping effect is observed on WSS areas due to the coils, which creates a stable hemodynamic condition inside the aneurysm.

6

Conclusions and Outlook

6.1 Conclusions

The overall aim of this study was to enhance the general knowledge of endovascular coiling in cerebral aneurysms and its influence on intra-aneurysmal hemodynamics. This goal was accomplished by:

- Elucidating how endovascular coils are distributed inside aneurysms. The quantification of coil density and distribution is a valuable data for clinical understanding of intra-aneurysmal coil structure but also it helps to validate computational techniques. This contribution can be found in chapter 2 and in the reference [90].
- Developing and validating a virtual coiling technique for image-based aneurysm models. This contribution was reached in chapter 3 and in references [86, 100]:
- Investigating how coil configuration and packing density influence intra-aneurysmal hemodynamics. This contribution can be found in chapter 5 and in references [69, 106]

Additionally within this thesis, secondary contributions were achieved by:

- Providing a validation strategy using histological images, for computational models of endovascular devices. This contribution was presented in chapter 3 and in the reference [100].
- Showing the feasibility to perform computational fluid dynamics (CFD) simulation in coiled aneurysm models using a complex and explicit representation of the endovascular devices. This contribution was presented in chapter 3, 4 and 5 and in references [69, 100, 106, 112–114].
- Creating and validating a geometry-hemodynamics image-based CFD simulation. This contribution was presented in chapter 4 and in the reference [92].

6.2 Outlook and Future Work

CFD in combination with the modeling of endovascular devices, has a great potential in cardiovascular interventions and it is called to play the same role as it has in aeronautical engineering, food industry or car design, among others fields. It can support clinicians by understanding the intravascular hemodynamics, by evaluating several treatments before the real intervention takes place, by improving the design of current endovascular devices, by testing new products, etc.

To make this possible, CFD has been applied during last decade in coiled and stented models to investigate their influence on hemodynamics (tables 1.1 and 1.2). However, the validation of endovascular models is challenging and few computational models are actually validated. The difficulty for validation creates skepticism in the clinical community towards the truthfulness of computational

techniques. Nevertheless, the contributions of this thesis should help to unravel this uncertain atmosphere. In particular, the developed technique is the first up-today validated coiling technique for image-based aneurysm models. The validation was done from clinical, geometrical and hemodynamic points of view.

How do these results fit in the state of the art of hemodynamic assessment after coiling? Can we use, for example, a porous medium as it has been adopted by other researchers in this field to simplify the hemodynamic studies after coiling? Yes we can, but neither at this moment nor in all situations.

Why yes. Porous medium modeling is an attractive approach to consider for endovascular coiling. It is generally used by engineers where the geometry being modeled is too complicated or involves relatively small objects. For that, a volume-averaged concept is applied to reformulate the governing equations of flow motion [115]. In the field of coil modeling, there are several studies using this approach to assess postoperative intra-aneurysmal hemodynamics (table 1.1). The porous medium approach has several advantages including faster meshing, implementation and CFD calculation compared to the explicit coil representation.

Why not now. Currently, none of the studies using the porous medium approach has been validated. A reason for that is the lack of experiments to properly derive the permeability and the drag factor, which are important parameters of this approach. To overcome this issue, these parameters are currently based on idealized conditions such as the Kozeny's theory of capillarity [50]. Additionally, porous medium studies in coiled aneurysms have assumed homogeneity and isotropy of the medium (which is not true according to chapter 2) and changing these conditions might difficult the decisions to setup the CFD simulations.

To overcome these limitations, either a validation with experiments or a comparison with a valid model, such as the one proposed in this thesis, can be performed. Recently, a comparison between both coil modeling techniques was done [113]. The results of that study indicate that porous medium modeling tends to underestimate the hemodynamic alterations induced by coils, if the Kozeny's theory is assumed to derive the permeability. This parameter has an important role on intra-aneurysmal hemodynamics after coiling [49]. A comparison with the proposed coiling technique can be used to properly parameterize the porous medium modeling.

Why not always. Due to its mathematical formulation, the porous medium approach can not evaluate the effect of a sole coil in a particular position. Examples of this limitation are the portion of a coil migrating outside the aneurysm cavity in chapter 4 and the study presented in chapter 5, where coil configuration and packing densities were changed.

On the other side, Why not considering a physics-based technique to model the coil insertion as it has been reported by Dequidt et al. in [51] and used by Wei et al. in [53]? A physics-based coiling technique aims different questions. This kind of approach is essential to understand how coils behave during deployment and can be used for clinical training. Besides, it is more difficult to develop since involves the understanding of both solid and fluid mechanics, as well as their complex interaction. Moreover, the validation of a physic-based technique is extremely difficult and is only feasible under simplified and controlled conditions. The di-

fficulties for validation are due to the constrained control during coil deployment and also to the unrepeatable coil configuration. In any case, if all virtual coils would be inserted using a physics-based technique, their distribution should follow what was reported in chapter 2.

Finally to conclude, the developed coiling technique is a fair balance between sophisticated physics-based techniques and simplified porous modeling to investigate intra-aneurysmal hemodynamics after coiling.

6.2.1 Where should we aim?

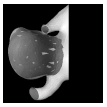

The ultimate goal of computational techniques is to become a practical tool that can be used by clinicians in the diagnosis, therapeutic planning, and postoperative monitoring of patients. Nonetheless, to improve the current CFD modeling of hemodynamics in coiled aneurysm models, several issues should be considered from the clinical and technical points of view:

- **The importance of coil diameter:** Clinicians aim to pack an aneurysm as dense as possible to prevent aneurysm recanalization. To facilitate the procedure, large and thick coils are manufactured. However, the coil diameter has an influence on the postoperative hemodynamics, since the coil surface in contact with blood depends on coil diameters. A previous report indicates that thinner coils decrease more the inflow and intra-aneurysmal velocity, since their surface in contact with blood is higher than with thicker coils if same packing density is used [114]. This report was supported by the developed virtual coiling technique.

- **Stent-assisted coils:** The combination of stenting and coiling is performed when there is a risk of coil migration, especially in wide-neck aneurysms. A clinically-relevant question is whereas or not a high-porosity stent placed at the parent artery to support coils, might also (or not) influence the intra-aneurysmal hemodynamics. A recent study, supported by the work developed in this thesis and a stenting technique [60], found that the addition of high-porosity stents does not add important modifications in the hemodynamics after coiling and might only help to avoid coil migration [112].

- **Non-Newtonian viscous model:** Although there is available a wide set of Non-Newtonian models for blood viscosity (Casson, Herschel-Bulkley or Power law model, etc.), hemodynamic modeling using CFD impose a constant viscosity value, generally ranging between 0.0035 to 0.004 Pa·s. This assumption is due to the stronger influence that other factors of the computational modeling, such as the geometry, have on hemodynamics [39]. However, it is not fully clear the role that the changes in blood viscosity have on intra-aneurysmal hemodynamics in treated aneurysms. Blood viscosity is important to investigate, since hemorheology plays a key role in the success of endovascular therapies by triggering the coagulation cascade.

- **Coil compaction:** Endovascular coils can compact and cause aneurysm recanalization. Coil compaction has been associated to the forces that pulsatile

blood flow applies on coils over time. The use of fluid-structure interaction modeling and an explicit representation of the coils could be a good starting point to understand the mechanisms that produce undesirable outcome of this therapy.

- **Coil preshape:** Although the developed virtual coiling technique does not consider the coil preshape during coil insertion, still the distribution of all coils inside the aneurysm cavity follows what has been found in reality. Nevertheless, the particular coil preshape might have an influence in the response of the whole coil structure against compaction.

- **Arterial wall properties:** In general, cerebral arteries are considered as rigid wall and their mechanical properties are not taken into account. This assumption is based on the facts that the dilatation of cerebral arteries is very small compared to its diameter and that hemodynamics is strongly driven by the morphology of the vasculature [39]. However, this simplification has to be reconsidered and properly studied, specially if endovascular devices modify the vasculature.

- **Blood coagulation:** The goal of endovascular therapies of cerebral aneurysms is to isolate the sac from blood circulation. This can be done by triggering coagulation cascade inside the aneurysm and by keeping a stable thrombus. However, hemorheologic changes after placement of endovascular devices has not been considered yet.

- **Patient-specific hemodynamic condition:** Currently, only the geometry of the vasculature is extracted from the patient though imaging. However, the geometry is just one of the elements that define a CFD simulation. To truly simulate the patient-specific hemodynamics, flow boundary conditions are also required. This information can be extracted either by measuring directly the flow rate or pressure in the patient, or by processing medical images.

References

[1] J. L. Brisman, J. K. Song, and D. W. Newell, "Cerebral aneurysms," *New England Journal of Medicine*, vol. 355, pp. 928–939, Aug 2006.

[2] G. J. E. Rinkel, M. Djibuti, A. Algra, and J. van Gijn, "Prevalence and Risk of Rupture of Intracranial Aneurysms: A Systematic Review," *Stroke*, vol. 29, no. 1, pp. 251–256, 1998.

[3] J. van Gijn, "Subarachnoid haemorrhage: diagnosis, causes and management," *Brain*, vol. 124, pp. 249–278, Feb 2001.

[4] J. W. Hop, G. J. Rinkel, A. Algra, and J. van Gijn, "Case-fatality rates and functional outcome after subarachnoid hemorrhage : A systematic review," *Stroke*, vol. 28, pp. 660–664, Mar 1997.

[5] T. Inagawa and A. Hirano, "Ruptured intracranial aneurysms: An autopsy study of 133 patients," *Surgical Neurology*, vol. 33, pp. 117–123, Feb 1990.

[6] V. V. Menghini, R. D. J. Brown, J. D. Sicks, W. M. O'Fallon, and W. D. O., "Clinical manifestations and survival rates among patients with saccular intracranial aneurysms: population-based study in Olmsted County, Minnesota, 1965 to 1995," *Neurosurgery*, vol. 49, no. 2, pp. 251–256; discussion 256–258, 2001.

[7] E. Grote and W. Hassler, "The critical first minutes after subarachnoid hemorrhage," *Neurosurgery*, vol. 22, no. 4, pp. 654–661, 1988.

[8] J. K. Hope, J. L. Wilson, and F. J. Thomson, "Three-dimensional CT angiography in the detection and characterization of intracranial berry aneurysms," *AJNR Am J Neuroradiol*, vol. 17, pp. 439–445, Mar 1996.

[9] J. M. Wardlaw and P. M. White, "The detection and management of unruptured intracranial aneurysms," *Brain*, vol. 123, pp. 205–221, Feb 2000.

[10] B. Weir, "Unruptured intracranial aneurysms: A review," *J. Neurosurg.*, vol. 96, no. 1, pp. 3–42, 2002.

[11] S. Juvela, "Rebleeding from ruptured intracranial aneurysms," *Surgical Neurology*, vol. 32, pp. 323–326, Nov 1989.

[12] D. O. Wiebers, J. P. Whisnant, J. r. Huston, I. Meissner, R. D. J. Brown, D. G. Piepgras, G. S. Forbes, K. Thielen, D. Nichols, W. M. O'Fallon, J. Peacock, L. Jaeger, N. F. Kassell, G. L. Kongable-Beckman, and J. C. Torner, "Unruptured intracranial aneurysms: Natural history, clinical outcome, and risks of surgical and endovascular treatment," *Lancet*, vol. 362, no. 9378, pp. 103–110, 2003.

[13] A. J. Molyneux, R. S. Kerr, L.-M. Yu, M. Clarke, M. Sneade, J. A. Yarnold, and P. Sandercock, "International subarachnoid aneurysm trial (isat) of neurosurgical clipping versus endovascular coiling in 2143 patients with ruptured intracranial aneurysms: a randomised comparison of effects on survival, dependency, seizures, rebleeding, subgroups, and aneurysm occlusion," *The Lancet*, vol. 366, pp. 809–817, Sep 2005.

[14] M. M. Taha, I. Nakahara, T. Higashi, Y. Iwamuro, M. Iwaasa, Y. Watanabe, K. Tsunetoshi, and T. Munemitsu, "Endovascular embolization vs surgical clipping in treatment of cerebral aneurysms: morbidity and mortality with short-term outcome," *Surgical Neurology*, vol. 66, pp. 277–284, Sep 2006.

[15] S. S. Choi and S. J. Jeon, "Comprehension of two modalities: Endovascular coiling and microsurgical clipping in treatment of intracranial aneurysms," *Neurointervention*, vol. 5, pp. 1–7, Feb 2010.

[16] T. W. M. Raaymakers, G. J. E. Rinkel, M. Limburg, and A. Algra, "Mortality and morbidity of surgery for unruptured intracranial aneurysms : A meta-analysis," *Stroke*, vol. 29, pp. 1531–1538, Aug 1998.

[17] J. Thornton, Q. Bashir, V. A. Aletich, G. M. Debrun, J. I. Ausman, and F. T. Charbel, "What Percentage of Surgically Clipped Intracranial Aneurysms Have Residual Necks?," *Neurosurgery*, vol. 46, pp. 1294–1300, Jun 2000.

[18] B. Lubicz, X. Leclerc, J. Y. Gauvrit, J. P. Lejeune, and J. P. Pruvo, "Giant vertebrobasilar aneurysms: endovascular treatment and long-term follow-up," *Neurosurgery*, vol. 55, pp. 316–323; discussion 323–316, 2004.

[19] K. Choudhari, "Wrapping and coating of cerebral aneurysms: history, evolution and surgical management after a re-bleed," *British Journal of Neurosurgery*, vol. 18, pp. 259–267, Jan 2004.

[20] M. T. Bhatti, K. R. Peters, C. Firment, and R. A. Mericle, "Delayed exacerbation of third nerve palsy due to aneurysmal regrowth after endovascular coil embolization," *Journal of Neuro-Ophthalmology*, vol. 24, pp. 3–10, Mar 2004.

[21] S. Gallas, A. Januel, A. Pasco, J. Drouineau, J. Gabrillargues, A. Gaston, C. Cognard, and D. Herbreteau, "Long-term follow-up of 1036 cerebral aneurysms treated by bare coils: A multicentric cohort treated between 1998 and 2003," *AJNR Am J Neuroradiol*, vol. 30, pp. 1986–1992, Nov 2009.

[22] S.-H. Park, C.-Y. Lee, and M.-B. Yim, "The Merits of Endovascular Coil Surgery for Patients with Unruptured Intracranial Aneurysms," *Journal of Korean Neurosurgical Society*, vol. 43, no. 6, pp. 270–274, 2008.

[23] G. Guglielmi, "History of the genesis of detachable coils, a review," *Journal of Neurosurgery*, vol. 111, pp. 1–8, Jul 2009.

[24] M. Piotin, L. Spelle, C. Mounayer, M. T. Salles-Rezende, D. Giansante-Abud, R. Vanzin-Santos, and J. Moret, "Intracranial aneurysms: Treatment with bare platinum coils–aneurysm packing, complex coils, and angiographic recurrence," *Radiology*, vol. 243, pp. 500–508, May 2007.

[25] H. Henkes, S. Fischer, W. Weber, E. Miloslavski, S. Felber, S. Brew, and D. Kuehne, "Endovascular coil occlusion of 1811 intracranial aneurysms: Early angiographic and clinical results," *Neurosurgery*, vol. 54, no. 2, pp. 268–280, 2004.

[26] M. Sluzewski, W. J. van Rooij, G. J. Rinkel, and W. D, "Endovascular treatment of ruptured intracranial aneurysms with detachable coils: Long-term clinical and serial angiographic results," *Radiology*, vol. 227, pp. 720–724, Jun 2003.

[27] J. K. Hope, J. V. Byrne, and A. J. Molyneux, "Factors influencing successful angiographic occlusion of aneurysms treated by coil embolization," *AJNR Am J Neuroradiol*, vol. 20, pp. 391–399, Mar 1999.

[28] J. Raymond, T. Darsaut, I. Salazkin, G. Gevry, and F. Bouzeghrane, "Mechanisms of occlusion and recanalization in canine carotid bifurcation aneurysms embolized with platinum coils: An alternative concept," *AJNR Am J Neuroradiol*, vol. 29, pp. 745–752, Apr 2008.

[29] G. Lanzino, Y. Kanaan, P. Perrini, H. Dayoub, and K. Fraser, "Emerging concepts in the treatment of intracranial aneurysms: Stents, coated coils, and liquid embolic agents," *Neurosurgery*, vol. 57, pp. 449–459, Sep 2005.

[30] J. Moret, C. Cognard, A. Weill, L. Castaings, and A. Rey, "The 'Remodelling Technique' in the Treatment of Wide Neck Intracranial Aneurysms. Angiographic Results and Clinical Follow-up in 56 Cases," *Interventional neuroradiology: journal of peritherapeutic neuroradiology, surgical procedures and related neurosciences*, vol. 3, no. 1, pp. 21–35, 1997.

[31] G. K. Wong, M. C. Kwan, R. Y. Ng, S. C. Yu, and W. Poon, "Flow diverters for treatment of intracranial aneurysms: Current status and ongoing clinical trials," *Journal of Clinical Neuroscience*, vol. 18, pp. 737–740, Jun 2011.

[32] L. Pierot, "Flow diverter stents in the treatment of intracranial aneurysms: Where are we?," *Journal of Neuroradiology*, vol. 38, pp. 40–46, Mar 2011.

[33] B. Turowski, S. Macht, Z. Kulcsr, D. Hnggi, and W. Stummer, "Early fatal hemorrhage after endovascular cerebral aneurysm treatment with a flow diverter (SILK-Stent), Do we need to rethink our concepts?," *Neuroradiology*, vol. 53, pp. 37–41, Jan 2011.

[34] Y.-H. Ding, D. A. Lewis, R. Kadirvel, D. Dai, and D. F. Kallmes, "The woven endobridge: A new aneurysm occlusion device," *AJNR Am J Neuroradiol*, vol. 32, pp. 607–611, Mar 2011.

[35] A. M. Malek, "Hemodynamic shear stress and its role in atherosclerosis," *JAMA The Journal of the American Medical Association*, vol. 282, pp. 2035–2042, Dec 1999.

[36] R. Kadirvel, Y.-H. Ding, D. Dai, H. Zakaria, A. M. Robertson, M. A. Danielson, D. A. Lewis, H. J. Cloft, and D. F. Kallmes, "The influence of hemodynamic forces on biomarkers in the walls of elastase-induced aneurysms in rabbits," *Neuroradiology*, vol. 49, pp. 1041–1053, Nov 2007.

[37] D. M. Wootton and D. N. Ku, "Fluid mechanics of vascular systems, diseases, and thrombosis," *Annu. Rev. Biomed. Eng.*, vol. 1, pp. 299–329, 1999.

[38] T. Hashimoto, H. Meng, and W. L. Young, "Intracranial aneurysms: links among inflammation, hemodynamics and vascular remodeling," *Neurological Research*, vol. 28, pp. 372–380, Jun 2006.

[39] J. R. Cebral, M. a. Castro, S. Appanaboyina, C. M. Putman, D. Millan, and A. F. Frangi, "Efficient pipeline for image-based patient-specific analysis of cerebral aneurysm hemodynamics: technique and sensitivity," *IEEE transactions on medical imaging*, vol. 24, no. 4, pp. 457–467, 2005.

[40] M.-C. Villa-Uriol, I. Larrabide, J. M. Pozo, M. Kim, M. De Craene, O. Camara, C. Zhang, A. J. Geers, H. Bogunović, H. G. Morales, and A. F. Frangi, "Toward integrated management of cerebral aneurysms," *Philosophical transactions. Series A, Mathematical, physical, and engineering sciences*, vol. 368, no. 1921, pp. 2961–1982, 2010.

[41] J. D. Anderson, *Computational fluid dynamics. The basics with applications*. McGraw Hill, 1995.

[42] J. R. Cebral, M. A. Castro, and N. Alperin, "Flow-area relationship in internal carotid and vertebral arteries," *Physiological Measurement*, vol. 29, pp. 585–594, May 2008.

[43] P. Reymond, F. Merenda, F. Perren, D. Rüfenacht, and N. Stergiopulos, "Validation of a one-dimensional model of the systemic arterial tree," *American journal of physiology. Heart and circulatory physiology*, vol. 297, no. 1, pp. H208–22, 2009.

[44] C. Groden, J. Laudan, S. Gatchell, and H. Zeumer, "Three-dimensional pulsatile flow simulation before and after endovascular coil embolization of a terminal cerebral aneurysm," *J. Cereb. Blood Flow Metab.*, vol. 21, no. 12, pp. 1464–1471, 2001.

[45] L. D. Jou, D. Saloner, and R. Higashida, "Determining intra-aneurysmal flow for coiled cerebral aneurysm with digital fluoroscopy," *Biomedical Engineering Applications Basis and Communications*, vol. 16, no. 2, p. 43, 2004.

[46] H. S. Byun and K. Rhee, "CFD modeling of blood flow following coil embolization of aneurysms," *Medical engineering & physics*, vol. 26, no. 9, pp. 755–761, 2004.

[47] A. Narracott, S. Smith, P. Lawford, H. Liu, R. Himeno, I. Wilkinson, P. Griffiths, and R. Hose, "Development and validation of models for the investigation of blood clotting in idealized stenoses and cerebral aneurysms," *Journal of Artificial Organs*, vol. 8, pp. 56–62, May 2005.

[48] J. R. Cebral and R. Löhner, "Efficient simulation of blood flow past complex endovascular devices using an adaptive embedding technique," *IEEE transactions on medical imaging*, vol. 24, no. 4, pp. 468–476, 2005.

[49] K. S. Cha, E. Balaras, B. B. Lieber, C. Sadasivan, and A. K. Wakhloo, "Modeling the interaction of coils with the local blood flow after coil embolization of intracranial aneurysms," *Journal of Biomechanical Engineering*, vol. 129, no. 6, pp. 873–879, 2007.

[50] N. M. Kakalis, A. P. Mitsos, J. V. Byrne, and Y. P. Ventikos, "The haemodynamics of endovascular aneurysm treatment: a computational modelling approach for estimating the influence of multiple coil deployment," *IEEE transactions on medical imaging*, vol. 27, no. 6, pp. 814–824, 2008.

[51] J. Dequidt, M. Marchal, C. Duriez, E. Kerien, and S. Cotin, "Interactive simulation of embolization coils: modeling and experimental validation," *International Conference on Medical Image Computing and Computer-Assisted Intervention (MICCAI)*, vol. 11, pp. 695–702, 2008.

[52] C. M. Schirmer and A. M. Malek, "Critical influence of framing coil orientation on intra-aneurysmal and neck region hemodynamics in a sidewall aneurysm model," *Neurosurgery*, vol. 67, pp. 1692–1702, Dec 2010.

[53] Y. Wei, S. Cotin, J. Allard, L. Fang, C. Pan, and S. Ma, "Interactive blood-coil simulation in real-time during aneurysm embolization," *Computers & Graphics*, vol. 35, pp. 422–430, Apr 2011.

[54] G. R. Stuhne and D. A. Steinman, "Finite-element modeling of the hemodynamics of stented aneurysms," *Journal of Biomechanical Engineering*, vol. 126, no. 3, p. 382, 2004.

[55] M. Ohta, S. G. Wetzel, P. Dantan, C. Bachelet, and K. O. Lovblad, "Rheological changes after stenting of a cerebral aneurysm: a finite element modeling approach," *Cardiovascular and interventional radiology*, vol. 28, no. 6, pp. 768–772, 2005.

[56] M. Kim, E. I. Levy, H. Meng, and L. N. Hopkins, "Quantification of Hemodynamic Changes Induced by Virtual Placement of Multiple Stents across a Wide-Necked Basilar Trunk Aneurysm," *Neurosurgery*, vol. 61, pp. 1305–1313, Dec 2007.

[57] T.-M. Liou and Y.-C. Li, "Effects of stent porosity on hemodynamics in a sidewall aneurysm model," *Journal of Biomechanics*, vol. 41, pp. 1174–1183, Jan 2008.

[58] S. Appanaboyina, F. Mut, R. Löhner, C. Putman, and J. R. Cebral, "Simulation of intracranial aneurysm stenting: Techniques and challenges," *Computer Methods in Applied Mechanics and Engineering*, vol. 198, pp. 3567–3582, Sep 2009.

[59] W. Fu, Z. Gu, X. Meng, B. Chu, and A. Qiao, "Numerical simulation of hemodynamics in stented internal carotid aneurysm based on patient-specific model," *Journal of Biomechanics*, vol. 43, pp. 1337–1342, May 2010.

[60] I. Larrabide, M. Kim, L. Augsburger, M.-C. Villa-Uriol, D. A. Rüfenacht, and A. F. Frangi, "Fast virtual deployment of self-expandable stents: Method and in vitro evaluation for intracranial aneurysmal stenting," *Medical Image Analysis*, vol. 16, pp. 721–730, Apr 2012.

[61] L. Augsburger, P. Reymond, D. A. Rüfenacht, and N. Stergiopulos, "Intracranial stents being modeled as a porous medium: Flow simulation in stented cerebral aneurysms," *Annals of Biomedical Engineering*, vol. 39, pp. 850–863, Feb 2011.

[62] A. Bernardini, I. Larrabide, H. G. Morales, G. Pennati, L. Petrini, S. Cito, and A. F. Frangi, "Influence of different computational approaches for stent deployment on cerebral aneurysm hemodynamics," *Interface Focus*, vol. 1, no. 3, pp. 338–348, 2011.

[63] M. H. Babiker, L. F. Gonzalez, J. Ryan, F. Albuquerque, D. Collins, A. Elvikis, and D. H. Frakes, "Influence of stent configuration on cerebral aneurysm fluid dynamics," *Journal of Biomechanics*, vol. 45, no. 3, pp. 440–447, 2012.

[64] M.-H. Li, B.-L. Gao, C. Fang, B.-X. Gu, Y.-S. Cheng, W. Wang, and G. Scotti, "Angiographic follow-up of cerebral aneurysms treated with Guglielmi detachable coils: an analysis of 162 cases with 173 aneurysms," *AJNR Am J Neuroradiol*, vol. 27, pp. 1107–1112, May 2006.

[65] J.-P. Pruvo, X. Leclerc, G. Soto Ares, J.-P. Lejeune, and D. Leys, "Endovascular treatment of ruptured intracranial aneurysms," *Journal of Neurology*, vol. 246, pp. 244–249, Apr 1999.

[66] J.-N. Vallée, L. Pierot, F. Mont'alverne, F. Turjman, A. Bonafé, S. Bracard, D. Lo, S. Crozier, H. Duffau, H. M. Barragan-Campos, B. Jean, R. Guillevin, and J. Chiras, "Unruptured intracranial aneurysms treated by three-dimensional coil embolization: evaluation of the postoperative aneurysm occlusion volume," *Neuroradiology*, vol. 47, pp. 438–445, Jun 2005.

[67] B. Lubicz, X. Leclerc, J.-Y. Gauvrit, J.-P. Lejeune, and J.-P. Pruvo, "Three-dimensional packing with complex orbit coils for the endovascular treatment of intracranial aneurysms," *AJNR Am J Neuroradiol*, vol. 26, pp. 1342–1348, Jun-Jul 2005.

[68] M. Piotin, A. Iijima, H. Wada, and J. Moret, "Increasing the packing of small aneurysms with complex-shaped coils: an in vitro study," *AJNR Am J Neuroradiol*, vol. 24, pp. 1446–1448, Aug 2003.

[69] H. G. Morales, M. Kim, E. E. Vivas, M.-C. Villa-Uriol, I. Larrabide, T. Sola, L. Guimaraens, and A. F. Frangi, "How Do Coil Configuration and Packing Density Influence Intra-Aneurysmal Hemodynamics?," *AJNR Am J Neuroradiol*, vol. 32, pp. 1935–1941, Nov 2011.

[70] L. Goubergrits, B. Thamsen, a. Berthe, J. Poethke, U. Kertzscher, K. Affeld, C. Petz, H.-C. Hege, H. Hoch, and a. Spuler, "In vitro study of near-wall flow in a cerebral aneurysm model with and without coils," *AJNR Am J Neuroradiol*, vol. 31, pp. 1521–1528, Sep 2010.

[71] A. P. Mitsos, N. M. Kakalis, Y. P. Ventikos, and J. V. Byrne, "Haemodynamic simulation of aneurysm coiling in an anatomically accurate computational fluid dynamics model: technical note," *Neuroradiology*, vol. 50, pp. 341–347, Apr 2008.

[72] D. F. Kallmes, G. A. Helm, S. B. Hudson, T. A. Altes, H. M. Do, J. W. Mandell, and H. J. Cloft, "Histologic Evaluation of Platinum Coil Embolization in an Aneurysm Model in Rabbits," *Radiology*, vol. 213, pp. 217–222, 1999.

[73] T. A. Altes, H. J. Cloft, J. G. Short, A. DeGast, H. M. Do, G. A. Helm, and D. F. Kallmes, "Creation of saccular aneurysms in the rabbit: a model suitable for testing endovascular devices," *AJR Americal Journal of Roentgenology*, vol. 174, pp. 349–354, 2000.

[74] D. Dai, Y.-H. Ding, M. a. Danielson, R. Kadirvel, D. A. Lewis, H. J. Cloft, and D. F. Kallmes, "Modified histologic technique for processing metallic coil-bearing tissue," *AJNR Am J Neuroradiol*, vol. 26, pp. 1932–1936, Sep 2005.

[75] Z. Zeng, D. F. Kallmes, M. J. Durka, Y.-H. Ding, D. A. Lewis, R. Kadirvel, and a. M. Robertson, "Hemodynamics and Anatomy of Elastase-Induced Rabbit Aneurysm Models: Similarity to Human Cerebral Aneurysms?," *AJNR Am J Neuroradiol*, vol. 32, pp. 595–601, Mar 2011.

[76] N. H. Fujiwara, H. J. Cloft, W. F. Marx, J. G. Short, M. E. Jensen, and D. F. Kallmes, "Serial angiography in an elastase-induced aneurysm model in rabbits: evidence for progressive aneurysm enlargement after creation," *AJNR Am J Neuroradiol*, vol. 22, pp. 698–703, Apr 2001.

[77] M. Sluzewski, W. J. van Rooij, M. J. Slob, J. O. Bescós, C. H. Slump, and D. Wijnalda, "Relation between aneurysm volume, packing, and compaction in 145 cerebral aneurysms treated with coils," *Radiology*, vol. 231, pp. 653–658, Jun 2004.

[78] Y. Kawanabe, a. Sadato, W. Taki, and N. Hashimoto, "Endovascular occlusion of intracranial aneurysms with guglielmi detachable coils: Correlation between coil packing density and coil compaction," *Acta Neurochirurgica*, vol. 143, pp. 451–455, Jun 2001.

[79] S. Tamatani, Y. Ito, H. Abe, T. Koike, S. Takeuchi, and R. Tanaka, "Evaluation of the stability of aneurysms after embolization using detachable coils: Correlation between stability of aneurysms and embolized volume of aneurysms," *AJNR Am J Neuroradiol*, vol. 23, pp. 762–767, 2002.

[80] M. J. Slob, M. Sluzewski, and W. J. van Rooij, "The relation between packing and reopening in coiled intracranial aneurysms: a prospective study," *Neuroradiology*, vol. 47, pp. 942–945, Dec 2005.

[81] C. Sherif, H. Plenk, K. Grossschmidt, F. Kanz, and G. Bavinzski, "Computer-assisted quantification of occlusion and coil densities on angiographic and histological images of experimental aneurysms," *Neurosurgery*, vol. 58, no. 3, pp. 559–566; discussion 559–66, 2006.

[82] D. Lopes and S. Sani, "Histological postmortem study of an internal carotid artery aneurysm treated with the neuroform stent," *Neurosurgery*, vol. 56, p. E416, Feb 2005.

[83] C. Sadasivan, L. Cesar, J. Seong, A. Rakian, Q. Hao, F. Tio, A. K. Wakhloo, and B. B. Lieber, "An original flow diversion device for the treatment of intracranial aneurysms: Evaluation in the rabbit elastase-induced model," *Stroke*, vol. 40, pp. 952–958, Mar 2009.

[84] M. Mehra, M. C. Hurley, M. J. Gounis, R. M. King, A. Shaibani, G. Dabus, F. E. Labdag, E. I. Levy, and B. R. Bendok, "The impact of coil shape design on angiographic occlusion, packing density and coil mass uniformity in aneurysm embolization: an in vitro study," *Journal of NeuroInterventional Surgery*, vol. 3, pp. 131–136, Jun 2011.

[85] D. Roy, G. Milot, and J. Raymond, "Endovascular treatment of unruptured aneurysms," *Stroke*, vol. 32, pp. 1998–2004, Sep 2001.

[86] H. G. Morales, I. Larrabide, M. Kim, M.-C. Villa-Uriol, J. M. Macho, J. Blasco, L. San Roman, and A. F. Frangi, "Virtual Coiling of Intracranial Aneurysms Based on Dynamic Path Planning," in *International Conference on Medical Image Computing and Computer-Assisted Intervention (MICCAI). Toronto, Canada*, pp. 355–362, 2011.

[87] H. Bogunović, J. M. Pozo, M. C. Villa-Uriol, C. B. L. M. Majoie, R. van den Berg, H. A. F. Gratama van Andel, J. M. Macho, J. Blasco, L. S. Román, and A. F. Frangi, "Automated segmentation of cerebral vasculature with aneurysms in 3dra and tof-mra using geodesic active regions: An evaluation study," *Medical Physics*, vol. 38, no. 1, pp. 210–222, 2011.

[88] S. Dhar, M. Tremmel, J. Mocco, M. Kim, J. Yamamoto, A. H. Siddiqui, L. N. Hopkins, and H. Meng, "Morphology parameters for intracranial aneurysm rupture risk assessment," *Neurosurgery*, vol. 63, pp. 185–197, Aug 2008.

[89] M. L. Raghavan, B. S. Ma, and R. E. Harbaugh, "Quantified aneurysm shape and aneurysm rupture," *J. Neurosurg.*, vol. 102, pp. 355–362, 2005.

[90] H. G. Morales, I. Larrabide, A. J. Geers, D. Dai, D. F. Kallmes, and A. F. Frangi, "Analysis and quantification of endovascular coils distribution inside saccular aneurysms using histological images," *Journal of NeuroInterventional Surgery*, in press, 2012.

[91] A. Sorteberg, W. Sorteberg, B. D. L. Aagaard, A. Rappe, and C. M. Strother, "Hemodynamic versus hydrodynamic effect of guglielmi detachable coils on intra-aneurysmal pressure and flow at varying pulse rate and systemic pressure," *AJNR Am J Neuroradiol*, vol. 25, pp. 1049–1057, Jun-Jul 2004.

[92] H. G. Morales, I. Larrabide, M.-C. Villa-Uriol, A. J. Geers, and A. F. Frangi, "Towards the validation of a virtual coiling technique using a real versus simulated bolus injection," in *2nd International Conference on Mathematical and Computational Biomedical Engineering (CMBE). Washington, USA*, pp. 513–515, 2011.

[93] A. R. Dehdashti, L. Thines, R. a. Willinsky, and M. Tymianski, "Symptomatic enlargement of an occluded giant carotido-ophthalmic aneurysm after endovascular treatment: the vasa vasorum theory," *Acta Neurochirurgica*, vol. 151, pp. 1153–1158, Sep 2009.

[94] M. H. Babiker, L. F. Gonzalez, F. Albuquerque, D. Collins, A. Elvikis, and D. H. Frakes, "Quantitative effects of coil packing density on cerebral aneurysm fluid dynamics: An in vitro steady flow study," *Annals of Biomedical Engineering*, vol. 38, pp. 2293–2301, Jul 2010.

[95] S. G. Imbesi and C. W. Kerber, "Analysis of slipstream flow in a wide-necked basilar artery aneurysm: evaluation of potential treatment regimens," *AJNR Am J Neuroradiol*, vol. 22, pp. 721–724, Apr 2001.

[96] S. Rudin, Z. Wang, I. Kyprianou, K. R. Hoffmann, Y. Wu, H. Meng, L. R. Guterman, B. Nemes, D. R. Bednarek, J. Dmochowski, and L. N. Hopkins, "Measurement of flow modification in phantom aneurysm model: Comparison of coils and a longitudinally and axially asymmetric stent–initial findings," *Radiology*, vol. 231, pp. 272–276, Apr 2004.

[97] M. D. Ford, G. R. Stuhne, H. N. Nikolov, D. F. Habets, S. P. Lownie, D. W. Holdsworth, and D. A. Steinman, "Virtual angiography for visualization and validation of computational models of aneurysm hemodynamics," *IEEE transactions on medical imaging*, vol. 24, no. 12, pp. 1586–1592, 2005.

[98] Q. Sun, A. Groth, M. Bertram, I. Waechter, T. Bruijns, R. Hermans, and T. Aach, "Phantom-based experimental validation of computational fluid dynamics simulations on cerebral aneurysms," *Medical Physics*, vol. 37, no. 9, pp. 5054–5065, 2010.

[99] I. Larrabide, P. Omedas, Y. Martelli, X. Planes, M. Nieber, J. Moya, C. Butakoff, R. Sebastián, O. Camara, M. D. Craene, B. Bijnens, and A. F. Frangi, "Gimias: An open source framework for efficient development of research tools and clinical prototypes," in *Functional Imaging and Modeling of the Heart*, vol. 5528 of *Lecture Notes in Computer Science*, pp. 417–426, www.gimias.org, Springer Berlin Heidelberg, 2009.

[100] H. G. Morales, I. Larrabide, A. J. Geers, L. San Roman, J. Blasco, J. M. Macho, , and A. F. Frangi, "A Virtual Coiling Technique for Cerebral Aneurysm Models Based on Dynamic Path Planning: Algorithm, Validation and Application using CFD," *Submitted, under review*, 2012.

[101] H. Bogunović and S. Loncarić, "Blood flow and velocity estimation based on vessel transit time by combining 2D and 3D X-ray angiography," in *International Conference on Medical Image Computing and Computer-Assisted Intervention (MICCAI)*, vol. 9, pp. 117–124, 2006.

[102] J. R. Cebral, R. S. Pergolizzi, and C. M. Putman, "Computational fluid dynamics modeling of intracranial aneurysms: Qualitative comparison with cerebral angiography," *Academic Radiology*, vol. 14, pp. 804–813, Jul 2007.

[103] J. Raymond, F. Guilbert, A. Weill, S. a. Georganos, L. Juravsky, A. Lambert, J. Lamoureux, M. Chagnon, and D. Roy, "Long-term angiographic recurrences after selective endovascular treatment of aneurysms with detachable coils," *Stroke*, vol. 34, no. 6, pp. 1398–1403, 2003.

[104] M. S. Alnaes, J. r. Isaksen, K.-A. Mardal, B. Romner, M. K. Morgan, and T. Ingebrigtsen, "Computation of hemodynamics in the circle of willis," *Stroke*, vol. 38, pp. 2500–2505, Aug 2007.

[105] J. B. White, C. G. M. Ken, H. J. Cloft, and D. F. Kallmes, "Coils in a nutshell: A review of coil physical properties," *AJNR Am J Neuroradiol*, vol. 29, pp. 1242–1246, Jan 2008.

[106] H. G. Morales, M. Kim, E. E. Vivas, and A. F. Frangi, "Influence of Coil Packing Rate and Configuration on Intracranial Aneurysm Hemodynamics," in *World Congress on Medical Physics and Biomedical Engineering, 11th International Congress of the IUPESM. Munich, Germany*, pp. 2291–2294, 2009.

[107] A. Sorteberg, W. Sorteberg, A. Rappe, and C. M. Strother, "Effect of guglielmi detachable coil placement on intra-aneueysmal flow: Experimental study in canines," *AJNR Am J Neuroradiol*, vol. 23, pp. 288–294, Apr 2002.

[108] K. Mori, Y. Nakao, N. Horinaka, R. Wada, A. Hirano, and M. Maeda, "Cerebral aneurysm regrowth and coil unraveling after incomplete guglielmi detachable coil embolization: Serial angiographical and histological findings-case report," *Neurologia medico-chirurgica*, vol. 43, no. 6, pp. 293–297, 2003.

[109] J. Jiang and C. Strother, "Computational Fluid Dynamics Simulations of Intracranial Aneurysms at Varying Heart Rates: A "patient-specific" Study," *Journal of Biomechanical Engineering*, vol. 131, no. 9, p. 091001, 2009.

[110] M. Piotin, S. Mandai, K. J. Murphy, K. Sugiu, P. Gailloud, J. B. Martin, and D. A. Rüfenacht, "Dense packing of cerebral aneurysms: an in vitro study with detachable platinum coils," *AJNR Am J Neuroradiol*, vol. 21, pp. 757–760, Apr 2000.

[111] J. R. Cebral, F. Mut, M. Raschi, E. Scrivano, R. Ceratto, P. Lylyk, and C. M. Putman, "Aneurysm rupture following treatment with flow-diverting stents: computational hemodynamics analysis of treatment," *AJNR Am J Neuroradiol*, vol. 32, pp. 27–33, Jan 2011.

[112] H. G. Morales, I. Larrabide, J. M. Macho, J. Blasco, L. San Roman, and A. F. Frangi, "Evaluation of Patient-Specific Intra-Aneurysmal Hemodynamics after Endovascular Treatments by CFD Models," in *SCATh Joint Workshop on New Technologies for Computer/Robot Assisted Surgery. Graz, Austria*, pp. 513–515, 2011.

[113] H. G. Morales, I. Larrabide, M. L. Aguilar, A. J. Geers, J. M. Macho, L. S. Roman, and A. F. Frangi, "Comparison of Two Techniques of Endovascular Coil Modeling in Cerebral Aneurysms using CFD," in *IEEE International Symposium on Biomedical Imaging (ISBI). Barcelona, Spain*, pp. 1216–1219, 2012.

[114] M. L. Aguilar, H. G. Morales, I. Larrabide, J. M. Macho, L. San Roman, and A. F. Frangi, "Effect of coil surface area on the hemodynamics of a patient-specific intracranial aneurysm: a computational study," in *IEEE International Symposium on Biomedical Imaging (ISBI). Barcelona, Spain*, pp. 1180–1183, 2012.

[115] M. Kaviany, *Principles of Heat Transfer in Porous Media.* Mechanical Engineering Series, Springer New York, 2nd ed., 1995.

Publications During PhD Thesis

International Journal

1. A. Bernardini, I. Larrabide, **H.G. Morales**, G. Pennati, L. Petrini, S. Cito, A.F. Frangi. Influence of different computational approaches for stent deployment on cerebral aneurysm hemodynamics. Interface Focus. 1(3):338-348, 2011.
2. **H.G. Morales**, M. Kim, E.E. Vivas, M.-C. Villa-Uriol, I. Larrabide, T. Sola L. Guimaraens, A.F. Frangi. How Do Coil Configuration and Packing Density Influence Intra-Aneurysmal Hemodynamics? AJNR Am J Neuroradiol. 32(10):1935–1941, 2011.
3. M.-C. Villa-Uriol, I. Larrabide, J.M. Pozo, M. Kim, M. De Craene, O. Camara, C. Zhang, A.J. Geers, **H.G. Morales**, H. Bogunović, R. Cardenes, A.F. Frangi. Toward integrated management of cerebral aneurysms. Philosophical Transactions of the Royal Society Series A. 368(1921):2961-1982. 2010.
4. I. Larrabide, M.-C. Villa-Uriol, R. Cardenes, V. Barbarito, L. Carotenuto, A. J. Geers, **H.G. Morales**, J. M. Pozo, M. Mazzeo, H. Bogunović, P. Omedas, C. Riccobene, J.M. Macho, A.F. Frangi. AngioLab A software tool for morphological analysis and endovascular treatment planning of intracranial aneurysms. Computer Methods and Programs in Biomedicine. *In press.* 2012.
5. **H.G. Morales**, I. Larrabide, A.J. Geers, D. Dai, D.F. Kallmes, A.F. Frangi. Analysis and Quantification of Endovascular Coils Distribution Inside Saccular Aneurysms Using Histological Images. Journal of NeuroInterventional Surgery. *In press.* 2012.
6. **H.G. Morales**, I. Larrabide, A.J. Geers, J.M. Macho and A.F. Frangi. A Virtual Coiling Technique of Cerebral Aneurysm Models Based on Dynamic Path Planning. Submitted 2012 - Under review.
7. I. Larrabide, M.L. Aguilar, **H.G. Morales**, A.J. Geers, Z. Kulczar, D. Rüfenacht and A.F. Frangi. Intra-aneurysmal pressure and flow changes induced by flow diverters: relation to aneurysm size and shape. AJNR Am J Neuroradiol. *In press.* 2012.

Book Chapter

1. M.-C. Villa-Uriol, I. Larrabide, J.M. Pozo, M. Kim, M. De Craene, O. Camara, C. Zhang, A.J. Geers, H. Bogunović, **H.G. Morales** and A.F. Frangi. Cerebral aneurysms: A patient-specific and image-based management pipeline. J.M. Tavares, R.M. Jorge, editors.: Computational Vision and Medical Image Processing - Recent Trends. Springer book series Computational Method in Applied Sciences, 327-349,2011.

Peer-reviewed International Conference

1. **H.G. Morales**, M. Kim, E.E. Vivas, A.F. Frangi. Influence of Coil Packing Rate and Configuration on Intracranial Aneurysm Hemodynamics. In *World Congress on Medical Physics and Biomedical Engineering, 11th International Congress of the IUPESM. Munich, Germany.* pp. 2291-2294, 2009.

2. A. Bernardini, I. Larrabide, **H.G. Morales**, G. Pennati, L. Petrini, A.F. Frangi. Hemodynamics in Stented Aneurysmatic Cerebral Vessel: Comparison of Different Computational Approaches for Stent Deployment. In *Virtual Physiological Human Network of Excellence (VPH NoE). Brussels, Belgium.* pp. 240–242, 2010.
3. A.J. Geers, I. Larrabide, **H.G. Morales**, A.F. Frangi. Comparison of steady-state and transient blood flow simulations of intracranial aneurysms. In *IEEE Engineering in Medicine and Biology Society (EMBS). Buenos Aires, Argentina.* pp. 2622–2625, 2010.
4. **H.G. Morales**, I. Larrabide, M.-C. Villa-Uriol, A.J. Geers, A.F. Frangi. Towards the validation of a virtual coiling technique using a real versus simulated bolus injection. In *2nd International Conference on Mathematical and Computational Biomedical Engineering (CMBE). Washington, USA.* pp. 513-515, 2011.
5. I. Larrabide, M.L. Aguilar, **H.G. Morales**, S. Cito, D.A. Rfenacht, Z. Kulcsar, S. Wetzel, A.F. Frangi. Effect of flow diverters on IA flow dynamics: assessment in 23 aneurysms. In *2nd International Conference on Mathematical and Computational Biomedical Engineering (CMBE). Washington, USA.* pp. 67–70, 2011.
6. A.J. Geers, I. Larrabide, **H.G. Morales**, A.F. Frangi. Comparing Geometry and Hemodynamics of MCA. In *2nd International Conference on Mathematical and Computational Biomedical Engineering (CMBE). Washington, USA.* pp. 83–86, 2011.
7. **H.G. Morales**, I. Larrabide, J.M. Macho, J. Blasco, L. San Roman, A.F. Frangi. Evaluation of Patient-Specific Intra-Aneurysmal Hemodynamics after Endovascular Treatments by CFD Models. In *SCATh Joint Workshop on New Technologies for Computer/Robot Assisted Surgery. Graz, Austria.* 2011.
8. I. Larrabide, M.L. Aguilar, **H.G. Morales**, S. Cito, D.A. Rfenacht, Z. Kulcsar, S. Wetzel, A.F. Frangi. Endovascular treatment of intracranial aneurysms with flow-diverter stents: a CFD study. In *SCATh Joint Workshop on New Technologies for Computer/Robot Assisted Surgery. Graz, Austria.* 2011.
9. **H.G. Morales**, I. Larrabide, M. Kim, M.-C. Villa-Uriol, J.M. Macho, J. Blasco,L. San Roman, A.F. Frangi. Virtual Coiling of Intracranial Aneurysms Based on Dynamic Path Planning. In *International Conference on Medical Image Computing and Computer Assisted Intervention (MICCAI). Toronto, Canada.* pp. 355-362, 2011. Winner of a Student Travel Award.
10. **H.G. Morales**, I. Larrabide, M.L. Aguilar, A.J. Geers, J.M. Macho, L. San Roman and A.F. Frangi. Comparison of Two Technique of Endovascular Coil Modeling in Cerebral Aneurysms Using CFD. In *IEEE International Symposium on Biomedical Imaging (ISBI). Barcelona, Spain.* pp. 1216–1219, 2012.
11. M.L. Aguilar, **H.G. Morales**, I. Larrabide, J.M.Macho, L. San Roman and A.F. Frangi. Effect of Coil Diameter on the Hemodynamics of a Patient-Specific Intracranial Aneurysm: A Computational Study. In *IEEE International Symposium on Biomedical Imaging (ISBI). Barcelona, Spain.* pp. 1180–1183, 2012.

International Conference Abstract

1. M. De Craene, E.E. Vivas, J.M. Pozo, M.-C. Villa-Uriol, T. Sola, L. Guimaraens, J. Blasco, J.M. Macho, **H.G. Morales**, A. Radaelli, A.F. Frangi. L, et al. Coil compaction and aneurysm growth: image-based quantification using non-rigid registration. In *5th International Intracranial Stent Symposium (ICS). Ankara, Turkey.* 2008.
2. A.J. Geers, I. Larrabide, **H.G. Morales**, S. Cito, M.-C. Villa-Uriol, A.F. Frangi. Steady-state and transient hemodynamic simulations of virtually treated intracranial aneurysms. In *Live Interventional Neuroradiology Conference (LINC) & Intracranial Stent Meeting (ICS). Houston, USA.* 2010.
3. **H.G. Morales**, M. Kim, E.E. Vivas, M.-C. Villa-Uriol, I. Larrabide, T. Sola, L. Guimaraens, A.F. Frangi. Effects of Coil Configuration and Packing Density on Intra-aneurysmal Hemodynamics. In *Live Interventional Neuroradiology Conference (LINC) & Intracranial Stent Meeting (ICS). Houston, USA.* 2010.

4. A.J. Geers, I. Larrabide, **H.G. Morales**, A.F. Frangi. Relationship between geometry and hemodynamics of MCA aneurysms. In *8th International Interdisciplinary Cerebrovascular Symposium (ICS). Shanghai, China.* 2011.

5. **H.G. Morales**, I. Larrabide, A.J. Geers, D.F. Kallmes, D. Dai, Y.H. Ding, A.F. Frangi. Histological Analysis of Endovascular Coil Distribution. In *8th International Interdisciplinary Cerebrovascular Symposium (ICS). Shanghai, China.* 2011.

6. I. Larrabide, M.L. Aguilar, **H.G. Morales**, A.J. Geers, D.A. Rfenacht, A.F. Frangi. Hemodynamic quantification of aneurysms after treatment with flow diversion device. In *8th International Interdisciplinary Cerebrovascular Symposium (ICS). Shanghai, China.* 2011.

Curriculum Vitae

Hernán Morales was born in the city of La Serena, Chile. He graduated of Mechanical Engineering at the University of Chile in 2006. Afterwards, he worked developing mining industry projects focused on piping. Since February 2008, he joined the Center for Computational Imaging and Simulation Technologies in Biomedicine (CISTIB) at the Universitat Pompeu Fabra (UPF), Barcelona as PhD student. His research fields are biomechanics and biomedical computing.
Currently, his main research interests are focused on understanding vascular hemodynamics, especially in cerebral aneurysms with endovascular therapies, by image processing and computational fluid dynamic modeling.

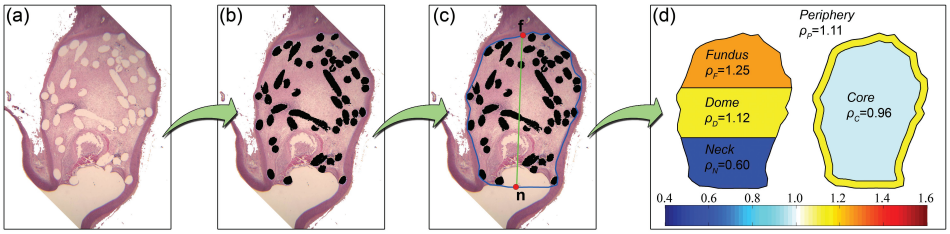

Figure 2.2, page 22: Processing of a histological image. (a) Original histological image. (b) Coil segmentation. (c) Aneurysm wall and neck delineation (blue contour) and longitudinal axis (green line) defined by f and n (red dots). (d) Automatic partitioning and calculation of normalized densities.

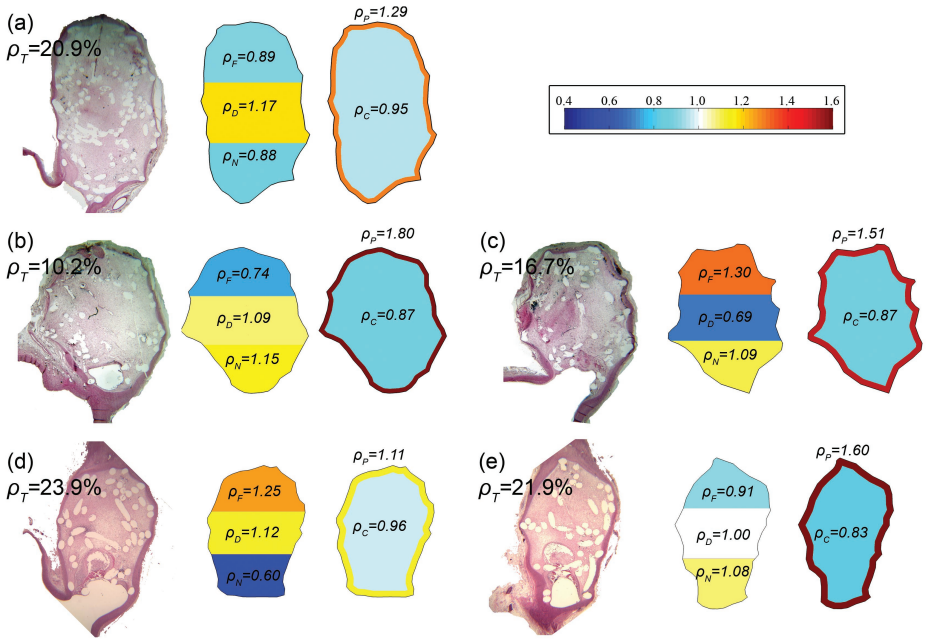

Figure 2.3, page 23: Color maps of normalized coil densities for five histological images (three aneurysms).

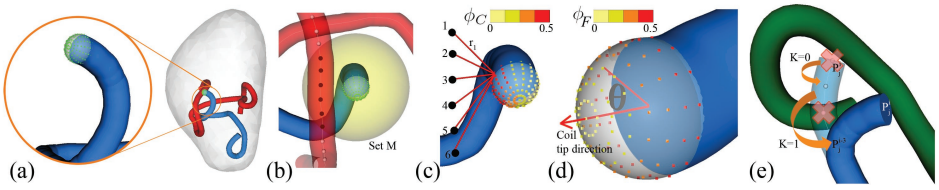

Figure 3.1, page 35: Schematic description of potential fields. (a) Coil being inserted (blue), candidate locations (green dots) at coil tip and the coiling domain, which is represented by the aneurysm model (close volume) and an inserted coil (red). (b) The set M_j^i (black dots) defined by the yellow sphere of radius $\alpha \cdot r_j$ around the coil tip. (c). Representation of the field ϕ_C for one of the candidate locations. (d) Representation of the field ϕ_F and coil tip direction (red arrow). (e) An scheme of coil pull-back field ϕ_{PB}.

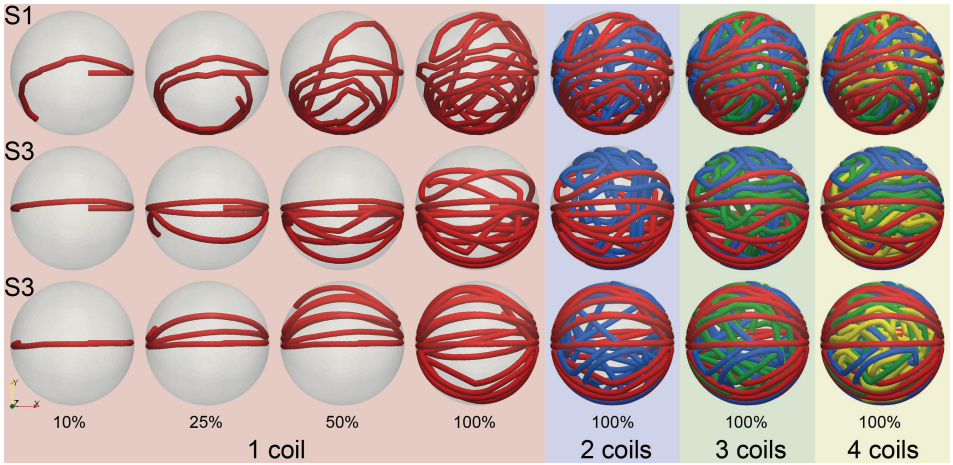

Figure 3.2, page 37: Three tests performed on the sphere increasing number of candidates from S1 to S3. Columns present the percentage of insertion for each coil.

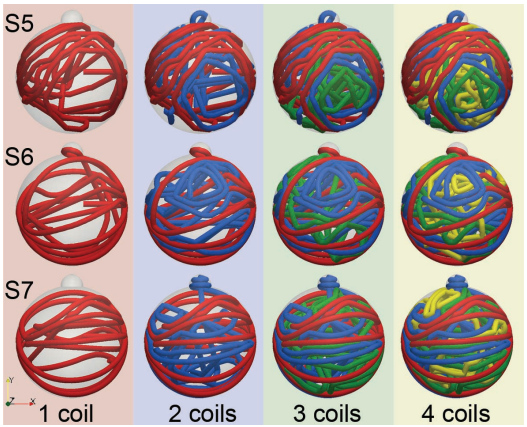

Figure 3.3, page 38: Three tests performed in a sphere with a bleb. Here, the number candidates was incremented from S5 to S7. Initial coil direction was $\hat{x}$

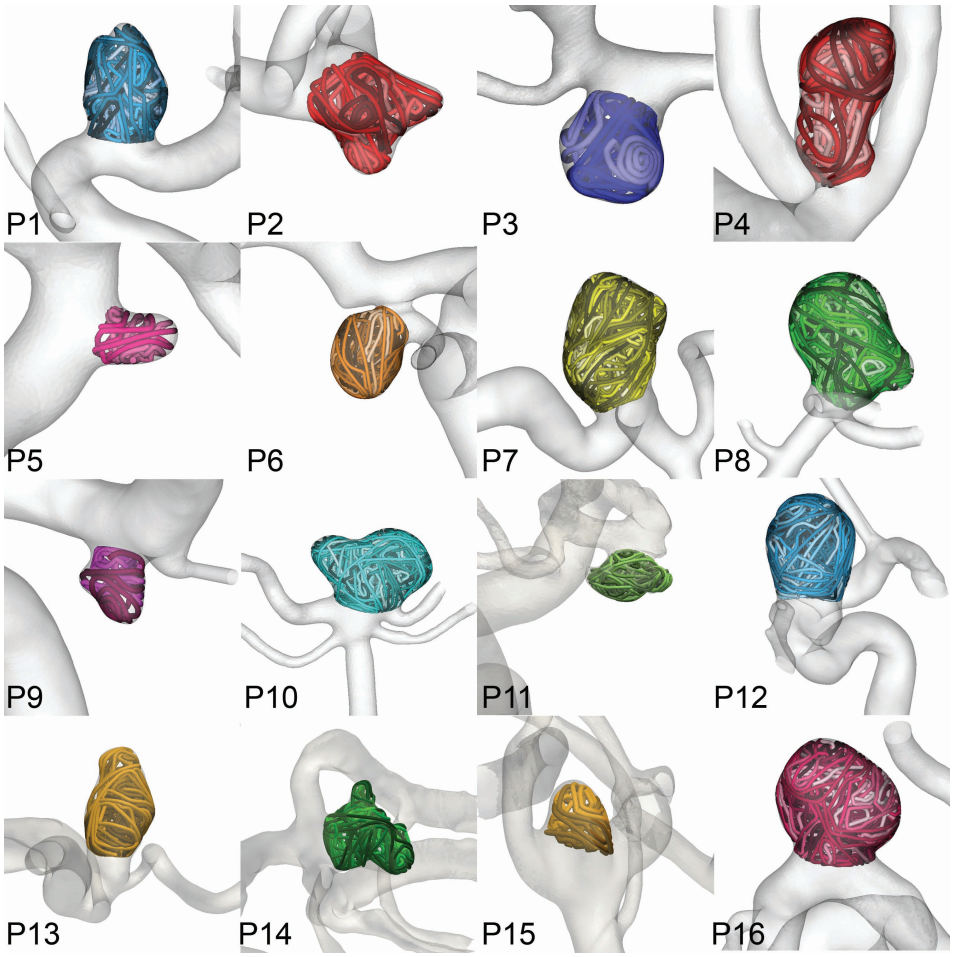

Figure 3.4, page 40: Virtual coiling technique applied on sixteen image-based aneurysm models. Coils were colored to differentiate them from each other.

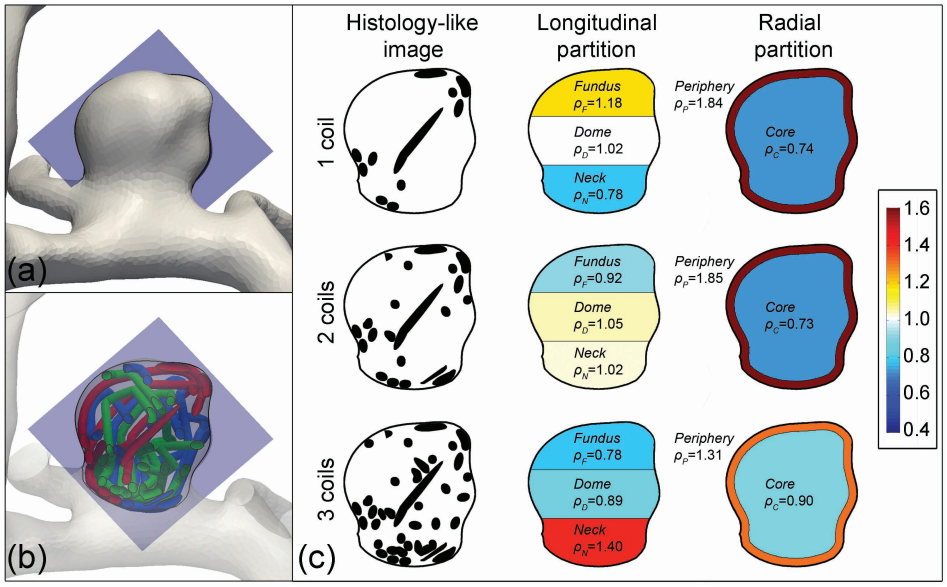

Figure 3.7, page 45: Histology-like image generation and processing for three coils inserted in case P3, produced with initial direction $\hat{x}$. (a) Definition of the cut plane. (b) Intersection of the cut plane and the aneurysm model and coils. (c) Histology-like image with one to three coils, with their partitions and calculated normalized in-slice densities at each region.

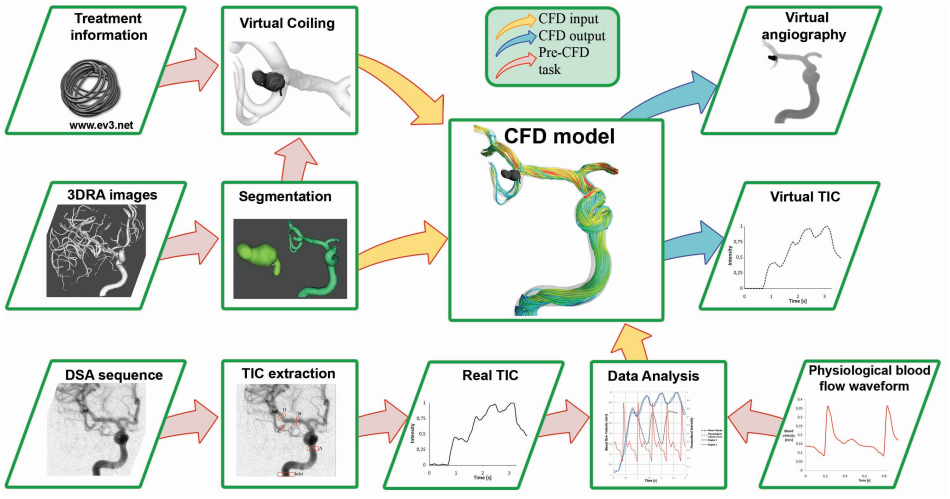

Figure 4.1, page 59: Pipeline for CFD setup using geometrical and flow information from medical images.

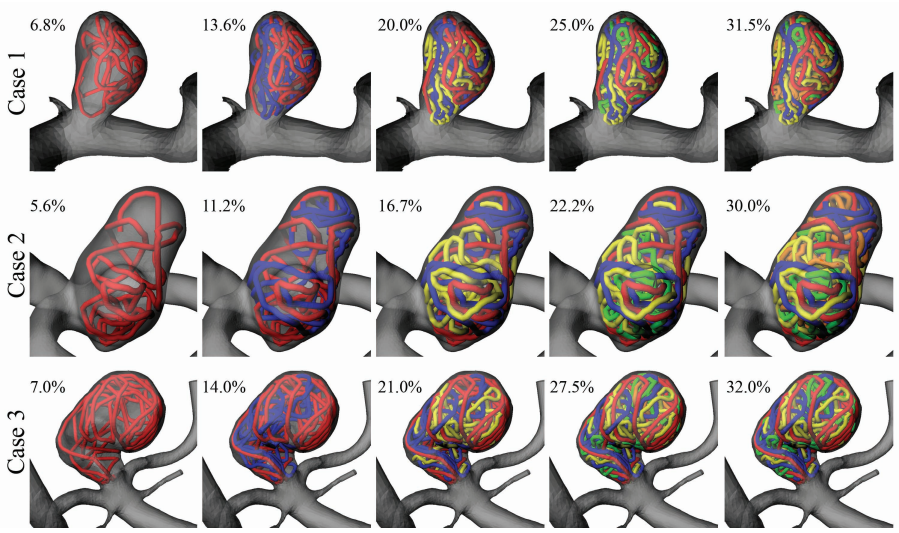

Figure 5.1, page 68: Results of virtual coiling in all cases. Percentages indicate coil packing densities.

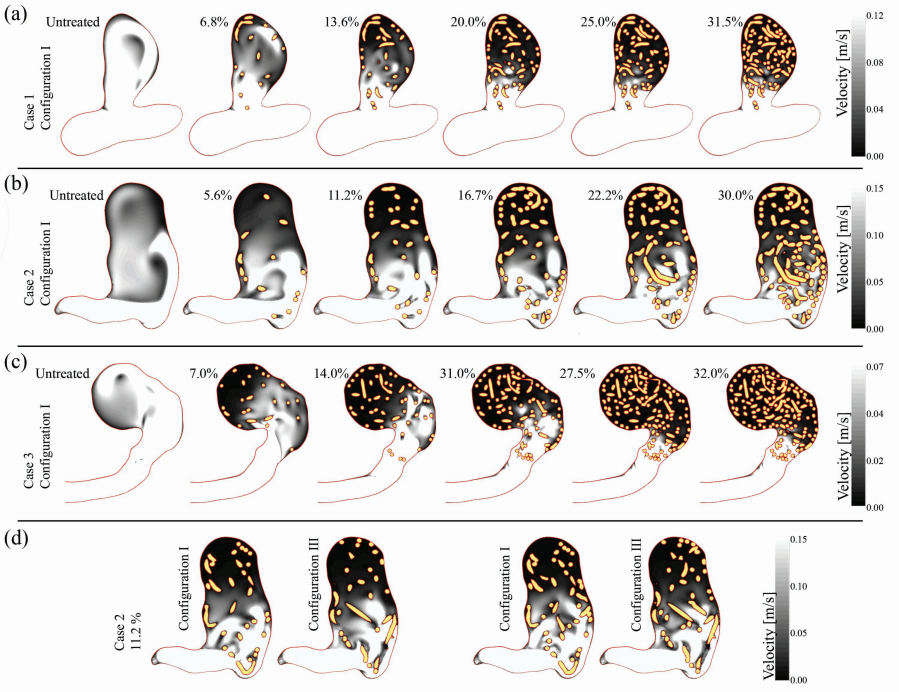

Figure 5.2, page 70: Blood flow velocity magnitudes in grayscale for an aneurysm-cross section at peak systole for all cases. (a-c) Changes in the velocity are presented with a fixed coil configuration and increasing packing density for all cases. In (d) two coil configurations are compared for packing densities of 11.2% and 16.7% of case 2. The coils are presented in yellow and the percentages represent the packing densities achieved for each model.

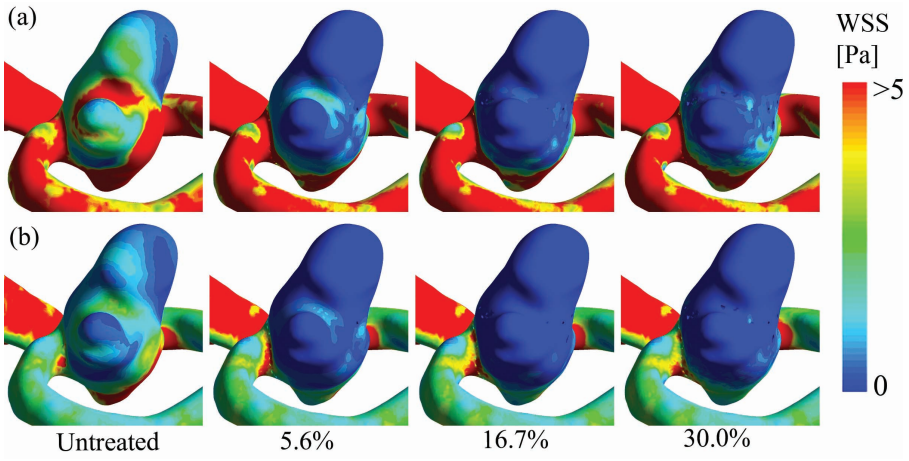

Figure 5.3, page 70: WSS distributions for the untreated and several treated models for case 2, calculated at peak systole (a) and end-diastole (b).

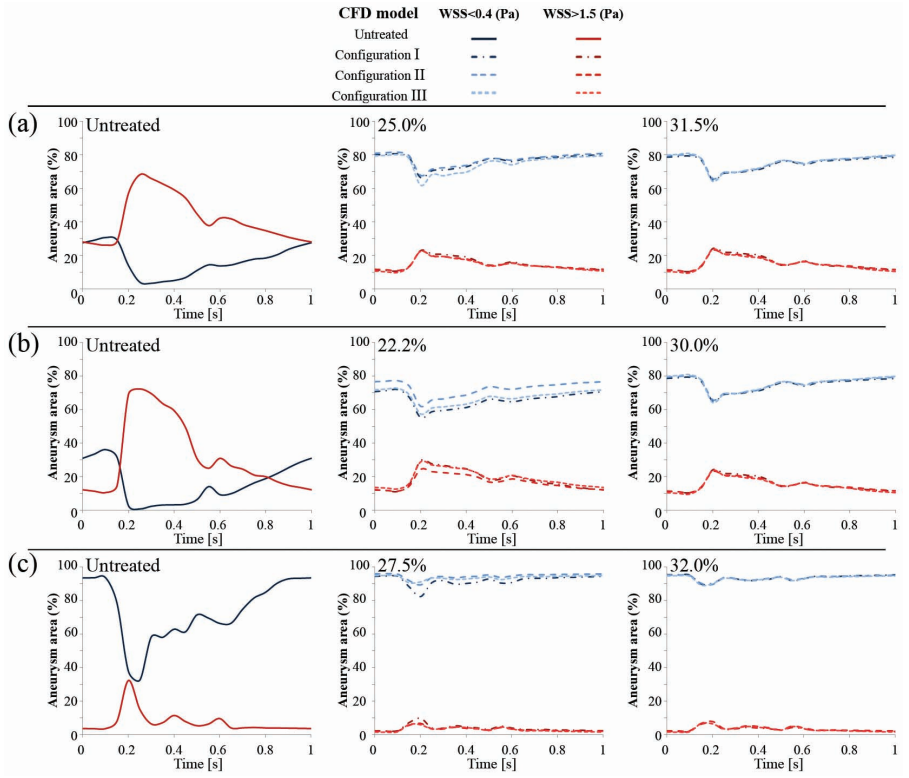

Figure 5.5, page 72: Variation of aneurysm areas with low and high WSS expressed as a percentage of the whole aneurysm dome (%) during one cardiac cycle for all cases. (a) case 1, (b) case 2 and (c) case 3.